Relaxation methods for gauge field equilibrium equations

Stephen L. Adler

The Institute for Advanced Study, Princeton, New Jersey 08540

Tsvi Piran

The Institute for Advanced Study, Princeton, New Jersey 08540
and Racah Institute of Physics, The Hebrew University, Jerusalem, Israel

This article gives a pedagogical introduction to relaxation methods for the numerical solution of elliptic partial differential equations, with particular emphasis on treating nonlinear problems with δ-function source terms and axial symmetry, which arise in the context of effective Lagrangian approximations to the dynamics of quantized gauge fields. The authors present a detailed theoretical analysis of three models which are used as numerical examples: the classical Abelian Higgs model (illustrating charge screening), the semiclassical leading logarithm model (illustrating flux confinement within a free boundary or "bag"), and the axially symmetric Bogomol'nyi-Prasad-Sommerfield monopoles (illustrating the occurrence of topological quantum numbers in non-Abelian gauge fields). They then proceed to a self-contained introduction to the theory of relaxation methods and allied iterative numerical methods and to the practical aspects of their implementation, with attention to general issues which arise in the three examples. The authors conclude with a brief discussion of details of the numerical solution of the models, presenting sample numerical results.

CONTENTS

I. INTRODUCTION

Over the last few years, numerical methods have played an increasingly important role in theoretical physics. Their prominence is attributable both to improvements in computers and decreased computational costs, and to the increased attention of theorists to nonlinear, nonperturbative problems in quantum field theory, for which purely analytical methods are inadequate. In treating quantum field theories computationally, two strategies are possible. The first, which has been intensively pursued recently, is to set up a discrete lattice analog of the full quantum field theory, and then to numerically evaluate the Feynman path integral by Monte Carlo techniques. This method has the advantage of giving results which can in principle be made as accurate as desired. Nonetheless, the necessity of using a four-dimensional computational lattice and of generating a large ensemble of field configurations makes simulation very costly, and in practice this has been a severe limiting factor. A second strategy is to first make analytic approximations, which replace the field theoretic problem by a classical variational problem involving an effective Lagrangian functional, leading to a system of partial differential equations which are then solved numerically. This approach is necessarily approximate, since exact knowledge of the effective Lagrangian is not possible without an exact evaluation of the Feynman path integral. However, the second strategy has the advantages that symmetries of the physical problem can be exploited to reduce the dimensionality of the computational problem, and that only a single equilibrium field configuration need be generated, permitting the study of very large computational lattices even on small computers. We believe that the two strategies are, in a sense, complementary; eventually, simulations may be used to infer the form of effective Lagrangians, which can then be used to analyze large classes of problems of physical interest.

Our aim in this article is to give a pedagogical review of the numerical analysis methods required by the second strategy. Assuming that an approximate nonlinear classical effective Lagrangian has been given, we show how relaxation methods can be used to solve the partial differential equations which govern the equilibrium field configurations. We focus on problems which arise in gauge field theories of current interest and in Sec. II introduce and

analytically characterize three nonlinear models which will be studied as illustrative examples. In Sec. III we give a self-contained introduction to the theory of relaxation methods and to practical aspects of their implementation, with special emphasis on treating nonlinear problems with singular (δ-function) source terms. Readers primarily interested in numerical analysis can proceed directly to Sec. III, after reading only the brief survey and theoretical discussion of Secs. II.A and II.B. In Sec. IV we give specific details of the application of the methods of Sec. III to the models of Secs. II.C, II.D, and II.E, together with a small sampling of numerical results. Certain technical details of the analytical structure of the three models are described in the Appendixes.

II. THEORETICAL ANALYSIS OF MODELS TO BE STUDIED

A. Introduction

In this section, we give a self-contained theoretical analysis of the models which later on will be studied numerically. All of the models discussed below describe time-independent three-dimensional problems with a rotational symmetry axis, and hence lead to two-dimensional computational problems in cylindrical coordinates. Our primary focus will be on the statics of classical charges in nonlinear Abelian and non-Abelian gauge field theories, as formulated by using classical action functional methods. In Sec. II.B we give the basic formalism for classical Lagrangian statics and illustrate it by briefly considering the case of classical electrostatics. In Sec. II.C we discuss the statics of classical sources in the Abelian Higgs model, in which external source charges are screened. In Sec. II.D we discuss the statics of classical sources using the leading logarithm semiclassical effective action functional for an SU(n) non-Abelian gauge theory, and show analytically that this model describes flux and charge confinement. As a secondary topic we consider non-Abelian gauge field configurations with topological quantum numbers, as exemplified by the axially-symmetric SU(2) topological monopole solutions, the theory of which is discussed in Sec. II.E. In the analyses of Secs. II.C–II.E, we place particular emphasis on identifying special features of the models under study which must be taken into account when solving them numerically.

B. Classical Lagrangian statics

Consider a classical dynamical system described by the action

$$S=\int dtL, \tag{2.1a}$$

$$L=\sum_i{}' p_i\dot{q}_i - H(p,q),\ \dot{q}=\frac{dq}{dt}\ , \tag{2.1b}$$

where q_i and p_i are the canonical coordinates and momenta, where H is the Hamiltonian, and where the prime indicates that those coordinates which have identically vanishing canonical momenta are omitted from the sum. We will be specifically interested in systems for which the equations of motion implied by extremizing S have nontrivial time-independent solutions, and want to find a variational principle for calculating the energy

$$V_{\text{static}}=H(p,q) \tag{2.2}$$

associated with such static solutions. For time-independent solutions, extremizing S is equivalent to extremizing $L(q;\dot{q}=0)$, and so evaluating Eq. (2.1b) at $\dot{q}=0$ gives

$$\begin{aligned} L_{\text{ext}} &= \text{ext}_q L(q;\dot{q}=0) \\ &= -H=-V_{\text{static}}\ . \end{aligned} \tag{2.3}$$

Equation (2.3) gives a variational formulation of the problem of calculating V_{static} and is the fundamental equation of classical Lagrangian statics.

As an illustration of Eq. (2.3), let us consider the familiar example of classical electrostatics. The Lagrangian for the Maxwell field coupled to an external static source density j^0 is[1]

$$L=\int d^3x[\tfrac{1}{2}(\mathbf{E}^2-\mathbf{B}^2)-j^0A^0]\ , \tag{2.4}$$

where the fields $\mathbf{E}$ and $\mathbf{B}$ are related to the scalar potential A^0 and the vector potential $\mathbf{A}$ by

$$\mathbf{E}=-\nabla A^0-\dot{\mathbf{A}},\ \mathbf{B}=\nabla\times\mathbf{A}\ . \tag{2.5}$$

Specializing to static solutions with $\dot{\mathbf{A}}=0$, we have

$$L[A^0,\mathbf{A};\dot{\mathbf{A}}=0]=\int d^3x\{\tfrac{1}{2}[(\nabla A^0)^2-(\nabla\times\mathbf{A})^2]-j^0A^0\}\ , \tag{2.6}$$

which is stationary when the potentials satisfy

$$\nabla\cdot\mathbf{E}=-\nabla^2A^0=j^0\ , \tag{2.7a}$$

$$\nabla\times\mathbf{B}=\nabla\times(\nabla\times\mathbf{A})=0\ . \tag{2.7b}$$

If the potentials are required to vanish at infinity, the general solution to Eq. (2.7) is

$$\begin{aligned} A^0(\mathbf{x}) &= \int d^3x'\frac{j^0(\mathbf{x}')}{4\pi|\mathbf{x}-\mathbf{x}'|}\ , \\ \mathbf{A}(\mathbf{x}) &= \nabla\Psi(\mathbf{x})\ , \end{aligned} \tag{2.8}$$

with Ψ an arbitrary gauge function. Substituting Eqs. (2.7) and (2.8) back into Eq. (2.6), we get, after an integration by parts,

$$\begin{aligned} L_{\text{ext}} &= \int d^3x(-\tfrac{1}{2}A^0\nabla^2A^0-j^0A^0)=-\tfrac{1}{2}\int d^3x\, j^0A^0 \\ &= -\tfrac{1}{2}\int d^3xd^3x'\frac{j^0(\mathbf{x})j^0(\mathbf{x}')}{4\pi|\mathbf{x}-\mathbf{x}'|}=-V_{\text{static}}\ , \end{aligned} \tag{2.9}$$

[1]Boldface will be used throughout to denote spatial vector indices.

in agreement with the general formula of Eq. (2.3). As a final remark, we note that this example shows that Eq. (2.3) is not a minimum principle; although Eq. (2.6) is stationary at $\mathbf{B}=\nabla\times\mathbf{A}=0$, this value of $\mathbf{B}$ maximizes, rather than minimizes,[2] the Lagrangian L.

C. The Abelian Higgs model

The first, and simplest nonlinear model which we shall discuss is the Abelian Higgs model, coupled to an external source charge density. The fields of this model are an Abelian gauge potential A^μ together with a complex scalar field φ of charge e. The Lagrangian is[3]

$$\begin{aligned} L&=\int d^3x\,\mathscr{L}\ , \\ \mathscr{L}&=\tfrac{1}{2}(\mathbf{E}^2-\mathbf{B}^2)-j^0A^0+\left|\left[i\frac{\partial}{\partial t}-eA^0\right]\varphi\right|^2 \\ &\quad-|(i\nabla+e\mathbf{A})\varphi|^2-\tfrac{1}{2}C(|\varphi|^2-\kappa^2)^2\ , \end{aligned} \tag{2.10}$$

with $\mathbf{E}$ and $\mathbf{B}$ constructed from the potentials $\mathbf{A}$ and A^0 as in Eq. (2.5), and with $|\varphi|^2=\varphi\varphi^*$, where φ^* is the complex conjugate of φ. When specialized to time-independent fields by setting $\dot{\mathbf{A}}$ and $\dot{\varphi}$ to zero, Eq. (2.10) simplifies to

$$\begin{aligned} \mathscr{L}&=\tfrac{1}{2}[(\nabla A^0)^2-(\nabla\times\mathbf{A})^2]-j^0A^0 \\ &\quad+e^2(A^0)^2|\varphi|^2-|(i\nabla+e\mathbf{A})\varphi|^2 \\ &\quad-\tfrac{1}{2}C(|\varphi|^2-\kappa^2)^2\ , \end{aligned} \tag{2.11}$$

which is invariant under the time-independent gauge transformation

$$\begin{aligned} &\varphi\to\varphi e^{i\psi}\ , \\ &\mathbf{A}\to\mathbf{A}+e^{-1}\nabla\psi\ . \end{aligned} \tag{2.12}$$

By a suitable choice of gauge[3] we can make the scalar field φ real, so that Eq. (2.11) becomes

$$\begin{aligned} \mathscr{L}&=\tfrac{1}{2}[(\nabla A^0)^2-(\nabla\times\mathbf{A})^2]-j^0A^0 \\ &\quad+e^2(A^0)^2\varphi^2-(\nabla\varphi)^2-e^2\mathbf{A}^2\varphi^2-\tfrac{1}{2}C(\varphi^2-\kappa^2)^2\ . \end{aligned} \tag{2.13}$$

As our final simplification, we note that since Eq. (2.13) has no source term coupled to $\mathbf{A}$, it is stationary with respect to variations of $\mathbf{A}$ around $\mathbf{A}=0$. Hence to calculate V_{static} it suffices to consider the $\mathbf{A}=0$ specialization of Eq. (2.13), giving

$$\begin{aligned} L[A^0,\varphi]&=\int d^3x\{\tfrac{1}{2}(\nabla A^0)^2-j^0A^0+e^2(A^0)^2\varphi^2 \\ &\quad-(\nabla\varphi)^2-\tfrac{1}{2}C(\varphi^2-\kappa^2)^2\}\ , \\ V_{\text{static}}&=-\text{ext}_{A^0,\varphi}L[A^0,\varphi]\ . \end{aligned} \tag{2.14}$$

Varying the action of Eq. (2.14), we get the Euler-Lagrange equations

$$\begin{aligned} &\nabla^2A^0=2e^2A^0\varphi^2-j^0\ , \\ &\nabla^2\varphi=-e^2(A^0)^2\varphi+C\varphi(\varphi^2-\kappa^2)\ . \end{aligned} \tag{2.15}$$

These equations will be solved numerically in Sec. IV.B for a source j^0 describing point charges located symmetrically on the z axis,

$$j^0=Q\delta(x)\delta(y)[\delta(z-a)-\delta(z+a)]\ , \tag{2.16}$$

for which A^0 is an even function and φ is an odd function of z. A straightforward analysis[3] shows that the leading behavior of A^0 and φ, at infinity and in the neighborhood of the source charges, is given by the following formulas.

At ∞:

$$\begin{aligned} &\varphi\sim\kappa+\frac{\varphi^{(\infty)}}{r}\exp[-r(2C\kappa^2)^{1/2}]\ , \\ &A^0\sim A^{0(\infty)}\left[\frac{1}{r_1}-\frac{1}{r_2}\right]\exp[-r(2e^2\kappa^2)^{1/2}]\ . \end{aligned} \tag{2.17a}$$

At $r_{\left[\begin{smallmatrix}1\\2\end{smallmatrix}\right]}\sim 0$:

$$\begin{aligned} &\varphi\sim\varphi^{(0)}r_{\left[\begin{smallmatrix}1\\2\end{smallmatrix}\right]}^{\lambda},\quad \lambda=-\tfrac{1}{2}+\left[\tfrac{1}{4}-\left[\frac{eQ}{4\pi}\right]^2\right]^{1/2}\ , \\ &A^0\sim(\pm)\left[\frac{Q}{4\pi r_{\left[\begin{smallmatrix}1\\2\end{smallmatrix}\right]}}+A^{0(0)}\right]\ , \end{aligned} \tag{2.17b}$$

with $\varphi^{(\infty)}$, $A^{0(\infty)}$, $\varphi^{(0)}$, $A^{0(0)}$ constants and with

$$\begin{aligned} r&=(x^2+y^2+z^2)^{1/2}\ , \\ r_{\left[\begin{smallmatrix}1\\2\end{smallmatrix}\right]}&=[x^2+y^2+(z\mp a)^2]^{1/2}\ . \end{aligned} \tag{2.18}$$

At large distances, the Higgs field φ approaches the constant κ (there is a second solution to the equations with $\varphi\to-\varphi$) and the scalar potential A^0 shows the characteristic exponential decay expected in a Higgs phase, which arises from the screening of the source j^0 by the charged Higgs field. Close to the source charges, the Higgs field becomes infinite as $r_{\left[\begin{smallmatrix}1\\2\end{smallmatrix}\right]}^{\lambda}$ with $-\frac{1}{2}<\lambda<0$ for

---

[2]For neutral charge distributions (with $\int d^3j^0=0$) the variational principle $\delta L[A^0,\mathbf{A};\dot{\mathbf{A}}=0]=0$ is minimax: the fields of classical electrostatics minimize L with respect to variations in A^0, while maximizing L with respect to variations in $\mathbf{A}$. A functional which (for neutral charge distributions) is minimized by the fields of classical electrostatics is

$$\tilde{L}[A^0,\mathbf{A}]=\int d^3x\{\tfrac{1}{2}[(\nabla A^0)^2+(\nabla\times\mathbf{A})^2]-j^0A^0\}\ .$$

Functionals of this form can be useful for mathematical purposes [see, e.g., Adler (1981a, 1981b) and Footnote 13 below], but unlike L have no direct physical interpretation.

[3]For a pedagogical discussion of the Abelian Higgs model, see Bernstein (1974). The analysis described in Sec. II.C was carried out by Adler and Pearson (1978, and unpublished); see Appendix B of Adler (1978a).

weak source charges Q satisfying the inequality[4]

$$\left[\frac{eQ}{4\pi}\right]^2 < \tfrac{1}{4} , \tag{2.19}$$

and the scalar potential has Coulomb-type singularities. The removal of the infinite Coulomb self-energies from the formula for V_{static} will be discussed in detail later on, in Sec. III.E of the text and in Appendix C.

D. Non-Abelian statics in the leading logarithm model

The second nonlinear model which we shall discuss is constructed from an SU(n) non-Abelian gauge theory coupled to an external source charge density. The fields of this model are an SU(n) non-Abelian gauge potential $A^{b\mu}$, with $b=1,\ldots,n^2-1$ the internal symmetry index. Making the conventional rescaling of the gauge potentials by the coupling constant g, the action and Lagrangian for this theory are

$$\begin{aligned} &S=\int L dt,\ L=\int d^3x \mathscr{L} , \\ &\mathscr{L}=\frac{1}{2g^2}(\mathbf{E}^a\cdot\mathbf{E}^a-\mathbf{B}^a\cdot\mathbf{B}^a)-j^{a0}A^{a0} , \end{aligned} \tag{2.20}$$

with the field-potential relations given now by

$$\begin{aligned} &E^{aj}=-\mathscr{D}_j A^{a0}-\frac{\partial}{\partial t}A^{aj} , \\ &B^{aj}=\varepsilon^{jkl}\left[\frac{\partial}{\partial x^k}A^{al}+\tfrac{1}{2}f^{abc}A^{bk}A^{cl}\right] . \end{aligned} \tag{2.21}$$

In Eq. (2.21), ε^{jkl} denotes the usual three-index antisymmetric tensor defined by

$$\varepsilon^{jkl}=\varepsilon^{ljk}=\varepsilon^{klj} ,\ \varepsilon^{jkl}=-\varepsilon^{kjl},\ \varepsilon^{123}=1 , \tag{2.22}$$

f^{abc} are the SU(n) group structure constants [for SU(2), $f^{abc}=\varepsilon^{abc}$], and $\mathscr{D}_j$ is the covariant derivative defined (for arbitrary w^a) by

$$\mathscr{D}_j w^a=\frac{\partial}{\partial x^j}w^a+f^{abc}A^{bj}w^c . \tag{2.23}$$

Static (and nonstatic) extrema of the action of Eq. (2.20) have been extensively discussed in the literature,[5] and can be found numerically by the same algorithm which we use later on to solve the topological monopole model. Hence instead of basing a numerical example on Eq. (2.20), we consider instead the much more interesting model in which L is replaced by an effective action L_{eff}, which (for slowly varying fields) incorporates the effect of radiative corrections to leading logarithm order, while keeping j^{a0} a classical[6] source. Both explicit one-loop calculations for the special case of constant field-strengths,[7] and more general renormalization-group arguments,[8] show that the action L_{eff} is obtained by replacing the coupling constant g^2 in Eq. (2.20) by a field-strength-dependent "running" coupling constant $g^2(\mathscr{F})$,

[4]The fact that λ becomes complex for large Q is an indication that, for large Q, pair production is important and that a field-theoretic discussion is needed. In a full field-theory treatment of the Abelian Higgs model, Eq. (2.14) is replaced by

$$V_{\text{static}}=-\text{ext}_{A^0,\varphi}L_{\text{eff}}[A^0,\varphi] ,$$

with L_{eff} an effective action functional which includes the effects of virtual quanta. When radiative corrections are ignored, L_{eff} reduces to the Lagrangian of Eq. (2.14).

[5]For an exhaustive survey, see Actor (1979).

[6]Two types of approximation schemes have been discussed in the literature for reducing SU(n) quantum chromodynamics with quantized source charges to classical source charge models. For methods involving a direct replacement of the SU(3) color charges by quasi-Abelian effective charges which respect the triality selection rules for color singlet states, see Mandula (1976) and Adler (1982). For methods involving a study of the algebraic properties of the SU(n) color charges, see Khriplovich (1978); Adler (1978b); Giles and McLerran (1978); Cvitanović, Gonsalves, and Neville (1978); Rittenberg and Wyler (1978); Lee (1979); Adler (1979); Lee (1980); Adler (1980); Bender, Gromes, and Rothe (1980); Adler (1981a); Milton, Palmer, and Pinsky (1982); and Milton, Wilcox, Palmer, and Pinsky (1982).

[7]The one-loop Yang-Mills effective action functional for constant field strengths has been calculated by a number of authors. See, for an early calculation, Batalin, Matinyan, and Savvidy (1977), and for recent discussions and references, Schanbacher (1982) and Anishetty (1982). Methods for constructing gauge-invariant effective action functionals beyond one-loop order have been given by 't Hooft (1975a), DeWitt (1981), Boulware (1981), and Abbott (1981).

[8]Matinyan and Savvidy (1978) and Pagels and Tomboulis (1978) have shown how the structure of the renormalization-group improved effective action can be inferred from the conformal trace anomaly. Renormalization-group arguments give an expression for $\mathscr{L}(\mathscr{F})$ of the form

$$\mathscr{L}(\mathscr{F})=\tfrac{1}{8}b_0\mathscr{F}\log(\mathscr{F}/e\kappa^2)\left[1+\frac{8b_1}{b_0^2}\frac{\log\log(\mathscr{F}/e\kappa^2)}{\log(\mathscr{F}/e\kappa^2)}\right]+O(\mathscr{F}) ,$$

with b_0 and b_1 the usual β-function coefficients defined in one- and two-loop orders. Adler (1981b) has argued that this expression may give the leading two terms in the effective action for *weak* fields $|\mathscr{F}/e\kappa^2|\ll 1$ as well as for strong fields $|\mathscr{F}/e\kappa^2|\gg 1$, because the magnitude of the running coupling constant of Eq. (2.24) is small in both regions. This argument suggests that, very generally, the effective dielectric constant changes sign between the strong and weak field regions, which is the essential feature responsible for confinement in the leading logarithm model.

The corrections of order $\mathscr{F}$ are not determined by renormalization-group arguments and in general are highly nonlocal (i.e., they depend on derivatives of the field strengths). Adler (1983) gives arguments indicating that the nonlocal terms in L_{eff} become important in the ultraviolet (short-distance) limit, but are unimportant relative to the local terms in the infrared (long-distance, or confining) limit. The order-$\mathscr{F}$ terms also can have imaginary parts; for example, if κ^2 in Eq. (2.28) is replaced by $-\kappa^2$, an additional imaginary term appears in $\mathscr{L}(\mathscr{F})$ at the order-$\mathscr{F}$ level. Hence even the sign of $\mathscr{F}$ at the extremum of $\mathscr{L}$ cannot be determined by a renormalization-group argument.

$$g^2(\mathscr{F})=\frac{g^2}{1+\frac{1}{4}b_0 g^2\log(\mathscr{F}/\mu^4)}\ , \tag{2.24}$$

with $\mathscr{F}$ the field-strength invariant

$$\mathscr{F}=\mathbf{E}^a\cdot\mathbf{E}^a-\mathbf{B}^a\cdot\mathbf{B}^a, \tag{2.25}$$

which appears in the classical action. The constant b_0 in Eq. (2.24) is the asymptotic freedom constant[9]

$$b_0=\frac{1}{8\pi^2}\frac{11}{3}C_2[\mathrm{SU}(n)]=\frac{1}{8\pi^2}\frac{11}{3}n\ , \tag{2.26}$$

while the mass μ is the renormalization point and g^2 is the value of the running coupling constant at $\mathscr{F}=\mu^4$. Combining Eqs. (2.20)—(2.25) and defining the one-loop renormalization-group-invariant parameter

$$\kappa^2=\frac{\mu^4}{e}e^{-4/(b_0 g^2)}\ , \tag{2.27}$$

we get the effective action for the leading logarithm model,[8]

$$L_{\mathrm{eff}}=\int d^3x\,\mathscr{L}_{\mathrm{eff}}=\int d^3x[\mathscr{L}(\mathscr{F})-j^{a0}A^{a0}]\ , \tag{2.28a}$$

$$\mathscr{L}(\mathscr{F})=\tfrac{1}{8}b_0\mathscr{F}\log(\mathscr{F}/e\kappa^2)\ . \tag{2.28b}$$

When specialized to time-independent fields,[10] Eq. (2.21) for E^{aj} becomes

$$E^{aj}=-\mathscr{D}_j A^{a0}\ , \tag{2.29}$$

and Eq. (2.3) for V_{static} yields the variational problem

$$V_{\mathrm{static}}=-\mathrm{ext}_{A^{a0},A^{aj}}\{L_{\mathrm{eff}}[A^{a0},A^{aj}]\}\ . \tag{2.30}$$

The Euler-Lagrange equations for Eq. (2.30) are

$$\mathscr{D}_j(\varepsilon E^{aj})=j^{a0}\ , \tag{2.31a}$$

$$\varepsilon^{kjm}\mathscr{D}_j(\varepsilon B^{am})=-f^{abc}A^{b0}\varepsilon E^{ck}\ , \tag{2.31b}$$

where we have introduced a field-strength-dependent effective dielectric constant ε defined by

$$\varepsilon=\frac{\partial\mathscr{L}(\mathscr{F})}{\partial(\frac{1}{2}\mathscr{F})}=\tfrac{1}{4}b_0\log(\mathscr{F}/\kappa^2)\ . \tag{2.32}$$

Applying a covariant derivative $\mathscr{D}_k$ to Eq. (2.31b) gives the equation

$$\tfrac{1}{2}\varepsilon^{kjm}[\mathscr{D}_k,\mathscr{D}_j](\varepsilon B^{am})=-f^{abc}(\mathscr{D}_k A^{b0})\varepsilon E^{ck}-f^{abc}A^{b0}\mathscr{D}_k(\varepsilon E^{ck})\ . \tag{2.33}$$

Using the easily verified identity (which holds for arbitrary w^a),

$$[\mathscr{D}_k,\mathscr{D}_j]w^a=\varepsilon^{kjl}f^{abc}B^{bl}w^c\ , \tag{2.34}$$

we find that the left-hand side of Eq. (2.33) is

$$\tfrac{1}{2}\varepsilon^{kjm}\varepsilon^{kjl}f^{abc}B^{bl}\varepsilon B^{cm}=0\ , \tag{2.35a}$$

while on substituting Eq. (2.29) the first term on the right-hand side of Eq. (2.33) becomes

$$f^{abc}\varepsilon E^{bk}E^{ck}=0\ . \tag{2.35b}$$

Hence the second term on the right-hand side of Eq. (2.33) must also vanish. After substitution of Eq. (2.31a), this gives the constraint

$$f^{abc}A^{b0}j^{c0}=0\ , \tag{2.36}$$

which states that to get a static solution, the scalar potential and the source charge density must locally lie in commuting directions in internal symmetry space.

In particular, for a source density j^{c0} describing a particle with effective classical charge Q^c at $\mathbf{x}_1$ and an antiparticle with effective classical charge $\bar{Q}^c$ at $\mathbf{x}_2$,

$$j^{c0}=Q^c\delta^3(\mathbf{x}-\mathbf{x}_1)+\bar{Q}^c\delta^3(\mathbf{x}-\mathbf{x}_2)\ , \tag{2.37}$$

the constraint of Eq. (2.36) becomes

$$\begin{aligned} &f^{abc}A^{b0}(\mathbf{x}_1)Q^c=0\ ,\\ &f^{abc}A^{b0}(\mathbf{x}_2)\bar{Q}^c=0\ . \end{aligned} \tag{2.38}$$

By making a suitable time-independent gauge transformation, we can align Q^c and $\bar{Q}^c$ to lie in antiparallel directions in internal symmetry space,

$$Q^c=\hat{q}^cQ\ ,\quad \bar{Q}^c=-\hat{q}^cQ\ , \tag{2.39}$$

with $\hat{q}$ a fixed internal symmetry unit vector. The constraints of Eq. (2.38) can then be satisfied by making the quasi-Abelian ansatz

$$\begin{aligned} &A^{a0}=\hat{q}^aA^0\ ,\\ &A^{aj}=\hat{q}^aA^j,\ \ (A^1,A^2,A^3)\equiv\mathbf{A}\ , \end{aligned} \tag{2.40}$$

which describes a conserved electric flux of magnitude Q running between the two point sources, as is appropriate to a model for the quark-antiquark confinement problem.[11] For the potentials of Eq. (2.40), the field-potential relations of Eq. (2.21) become

---

[9]In SU(3) quantum chromodynamics (QCD) with N_f massless fermion flavors, Eq. (2.26) for b_0 becomes

$$b_0=\frac{1}{8\pi^2}(11-\tfrac{2}{3}N_f)\ .$$

[10]Since the physically relevant extrema of the effective action are the *mean* potentials induced when a source j^{a0} is added to the standard functional integration quantization formalism [see, for example, Abers and Lee (1973)], they must be time independent when the source is time independent.

[11]The quasi-Abelian ansatz of Eq. (2.40) excludes "charge-screening" solutions of the type discussed by Sikivie and Weiss (1978, 1979), Kiskis (1980a), Jackiw and Rossi (1980), and Hilf and Polley (1981). Such solutions may be relevant as models for the behavior of an SU(n) gauge field with *adjoint* representation sources. *Fundamental* representation sources, such as quarks and antiquarks, cannot be screened by the gauge gluon field.

$$E^{aj}=\hat{q}^a E^j,\ (E^1,E^2,E^3)\equiv\mathbf{E}=-\nabla A^0\ ,$$
$$B^{aj}=\hat{q}^a B^j,\ (B^1,B^2,B^3)\equiv\mathbf{B}=\nabla\times\mathbf{A}\ . \tag{2.41}$$

The internal symmetry structure of the problem can now be completely factored away. Equations (2.30) and (2.28) simplify to

$$\begin{aligned} &V_{\text{static}}=-\text{ext}_{A^0,\,A^j}\{L_{\text{eff}}[A^0,A^j]\}\ ,\\ &L_{\text{eff}}=\int d^3x[\mathscr{L}(\mathscr{F})-j^0A^0]\ ,\\ &\mathscr{F}=(\nabla A^0)^2-(\nabla\times\mathbf{A})^2\ ,\\ &j^0=Q\delta(x)\delta(y)[\delta(z-a)-\delta(z+a)]\ , \end{aligned} \tag{2.42}$$

where we have again located the source charges symmetrically on the z axis, and the Euler-Lagrange equations of Eq. (2.31) become

$$\nabla\cdot(\varepsilon\mathbf{E})=j^0\ , \tag{2.43a}$$

$$\nabla\times(\varepsilon\mathbf{B})=0\ , \tag{2.43b}$$

with the dependence on $\mathscr{F}$ of $\mathscr{L}$ and ε given by Eq. (2.28b) and Eq. (2.32), respectively. We have thus reduced our model to a problem in nonlinear Abelian electrostatics.[12,13]

As in the discussion of classical electrostatics in Sec. II.B, the extremum over the vector potential in Eq. (2.42) can be carried out by inspection. From Eq. (2.43b) we get

$$\begin{aligned} 0&=\int d^3x\,\mathbf{A}\cdot\nabla\times(\varepsilon\mathbf{B})\\ &=\int d^3x\,\varepsilon\mathbf{B}^2-\int_{\text{surface at }\infty}d\mathbf{S}\cdot\varepsilon(\mathbf{A}\times\mathbf{B})\ , \end{aligned} \tag{2.44}$$

and so if we restrict ourselves to solutions with a vanishing surface integral at infinity, we must have

$$\varepsilon\mathbf{B}^2=0\ , \tag{2.45a}$$

giving three branches (Ia, Ib, and II, respectively),

$$\begin{aligned} &\mathbf{B}=0\ ,\ \mathbf{E}^2>\kappa^2\ ,\\ &\mathbf{B}=0\ ,\ \mathbf{E}^2<\kappa^2\ ,\\ &\varepsilon=0\implies\mathbf{B}^2=\mathbf{E}^2-\kappa^2\ . \end{aligned} \tag{2.45b}$$

In the strong-field region near the source charges, the asymptotic freedom of non-Abelian gauge theories requires that the solution of Eqs. (2.43) approach a Coulomb-type solution with $\mathbf{E}$ large and $\mathbf{B}$ vanishing; together with continuity, this implies that a finite domain containing the source charges lies on branch Ia. Specializing the analysis, for the time being, to this branch, we set $\mathbf{B}=\mathbf{A}=0$ and rewrite Eqs. (2.41) and (2.43a) as

$$\begin{aligned} &\nabla\cdot\mathbf{D}=j^0\ ,\ \nabla\times\mathbf{E}=0\ ,\\ &\mathbf{D}=\varepsilon(E)\mathbf{E}\ ,\\ &\varepsilon(E)=\tfrac{1}{4}b_0\log(E^2/\kappa^2)\ ,\ E=|\,\mathbf{E}\,|\ . \end{aligned} \tag{2.46}$$

A graph of the nonlinear dielectric constant $\varepsilon(E)$, showing its intersection (for $\mathbf{B}=0$) with the three branches of Eq. (2.45b), is shown in Fig. 1.

Equations (2.46) are the basic statement of the problem which will be studied numerically in Sec. IV.C. In order to get a tractable numerical method, it is necessary (for reasons discussed in Appendix A) to rewrite the equations in manifestly flux-conserving form. To exploit the axial symmetry of the problem, let us work henceforth in cylindrical coordinates ρ,z,ϕ defined by

$$\rho=(x^2+y^2)^{1/2},\ \ \phi=\tan^{-1}(y/x)\ , \tag{2.47}$$

in which the coordinates of the point sources of Eq. (2.42) are $\rho=0$, $z=\pm a$. We then note that $\mathbf{D}$ can be parametrized in terms of a single scalar function $\Phi(\rho,z)$ by writing[14]

$$\mathbf{D}=-\frac{1}{2\pi}\nabla\phi\times\nabla\Phi=-\frac{\hat{\phi}}{2\pi\rho}\times\nabla\Phi=\nabla\times\left[\frac{\hat{\phi}}{2\pi\rho}\Phi\right]\ . \tag{2.48}$$

The representation of Eq. (2.48) automatically satisfies $\nabla\cdot\mathbf{D}=0$ at points off the axis, and at points on the axis where Φ is sufficiently smooth. The physical interpretation of Φ follows from calculating the total flux through a surface of revolution S (with element of area $d\mathbf{A}$) bounded by a circle C of radius ρ (with element of arc length $d\mathbf{l}=dl\hat{\phi}$), as shown in Fig. 2. We get

$$\begin{aligned} \text{flux through } S&=\int_S d\mathbf{A}\cdot\mathbf{D}=\int_S d\mathbf{A}\cdot\nabla\times\left[\frac{\hat{\phi}}{2\pi\rho}\Phi\right]\\ &=\int_C d\mathbf{l}\cdot\left[\frac{\hat{\phi}}{2\pi\rho}\Phi\right]=\Phi\ , \end{aligned} \tag{2.49}$$

showing that Φ is simply the flux through S. If we draw the surface S so that it always intersects the z axis on the segment $z>a$, as shown in Fig. 2, the flux function Φ as-

[12]Dielectric models for confinement in QCD have been discussed in a qualitative way by a number of authors; see, for example, Kogut and Susskind (1974), 't Hooft (1975b), Pagels and Tomboulis (1978), Friedberg and Lee (1978), Callan, Dashen, and Gross (1979), and Nambu (1981).

[13]Pagels and Tomboulis (1978) and Mills (1979) showed that when a single isolated charge is present, the leading logarithm model gives a linearly divergent infrared energy. A proof that the model of Eq. (2.42) gives a linear static potential for large source separations was first given by Adler (1981a), using the related minimum principle in which $\mathscr{F}$ is replaced by $(\nabla A^0)^2+(\nabla\times\mathbf{A})^2$. (See the comments in Footnote 2 above.)

[14]The flux function formulation was introduced in Adler (1981b). The analysis of the characteristic form of the flux function equation, and its numerical solution, were given by Adler and Piran (1982a).

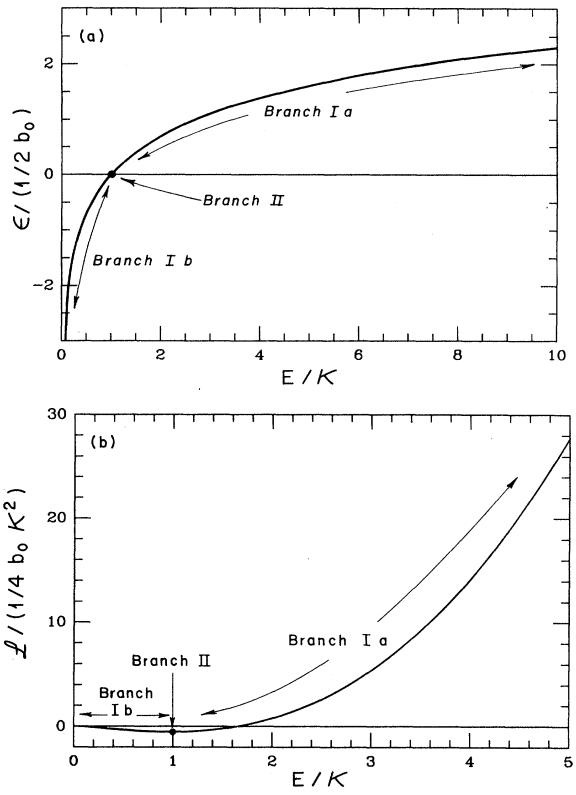

FIG. 1. (a) Plot of $\varepsilon(E)$ of Eq. (2.46), showing its intersection (for $\mathbf{B}=0$) with the three branches of Eq. (2.45b). (b) Corresponding plot of $\mathscr{L}(\mathscr{F}=E^2)$ of Eq. (2.28b).

sumes the following boundary values on the axis of rotation and at infinity:

$$\Phi=0,\ \rho=0,\ |z|>a\ ,$$
$$\Phi=Q,\ \rho=0,\ |z|<a\ , \tag{2.50}$$
$$\Phi\to 0 \text{ as } \rho^2+z^2\to\infty\ .$$

To verify these, we note that Φ is an even function of z, and that on the segment $\rho=0$, $z>a$, the surface S degenerates to a point and intercepts no flux. Similarly, on the segment $\rho=0$, $|z|<a$, the surface S intercepts all of the flux in a positive sense, as illustrated in Fig. 3. The requirement that Φ should vanish on the sphere at infinity

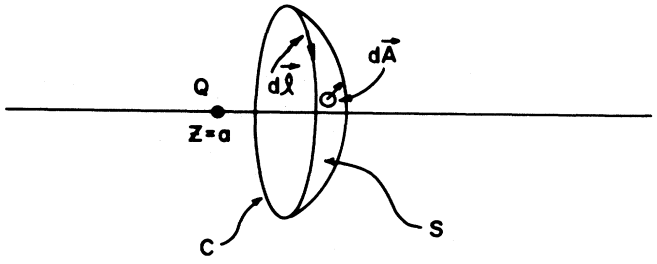

FIG. 2. Surface of revolution S with circular boundary C used in Eq. (2.49) to evaluate the flux function Φ.

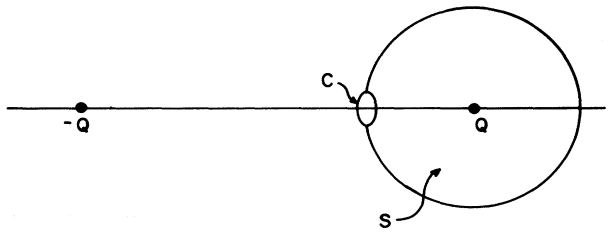

FIG. 3. Surface S (bounded by an infinitesimal circle C) used to evaluate Φ on the axis at $|z|<a$.

ensures that no additional flux sources or sinks lie at spatial infinity.

The dynamical equation for Φ is obtained from

$$\nabla\times\mathbf{E}=\nabla\times\left[\frac{\mathbf{D}}{\varepsilon}\right]=0\ . \tag{2.51}$$

Defining $D=|\mathbf{D}|$, we can algebraically invert the constitutive equation $D=\varepsilon(E)E$ to get

$$\varepsilon(E(D))\equiv\varepsilon[D]\ , \tag{2.52}$$

so that Eq. (2.51) becomes a differential equation for $\mathbf{D}$,

$$\nabla\times\left[\frac{\mathbf{D}}{\varepsilon[D]}\right]=0\ . \tag{2.53}$$

This equation can be rewritten by using the vector identity

$$\nabla\cdot(\mathbf{V}_1\times\mathbf{V}_2)=\mathbf{V}_2\cdot(\nabla\times\mathbf{V}_1)-\mathbf{V}_1\cdot(\nabla\times\mathbf{V}_2)\ , \tag{2.54}$$

with

$$\mathbf{V}_1=\frac{\mathbf{D}}{\varepsilon}\ ,\quad \mathbf{V}_2=\frac{\hat{\phi}}{\rho}\ ,$$
$$\nabla\times\mathbf{V}_1=0=\nabla\times\mathbf{V}_2\ , \tag{2.55}$$

which when simplified by using $\hat{\phi}\cdot\nabla\Phi=0$ gives

$$\nabla\cdot[\sigma(\rho,|\nabla\Phi|)\nabla\Phi]=0\ ,$$
$$\sigma(\rho,|\nabla\Phi|)\equiv\frac{1}{\rho^2\varepsilon[D]}\ ,\quad D=\frac{|\nabla\Phi|}{2\pi\rho}\ . \tag{2.56}$$

Equation (2.56) is the formulation of the leading logarithm model which will be studied numerically in Sec. IV.C. As a check, we note that in the case of classical electrostatics, where $\varepsilon[D]\equiv 1$, Eq. (2.56) and the boundary conditions of Eq. (2.50) are satisfied by

$$\Phi=\tfrac{1}{2}Q(\cos\vartheta_2-\cos\vartheta_1)\ ,$$
$$\vartheta_1=\tan^{-1}\left[\frac{\rho}{z-a}\right]\ ,\quad \vartheta_2=\tan^{-1}\left[\frac{\rho}{z+a}\right]\ ,\quad 0\le\vartheta_{1,2}<\pi\ , \tag{2.57}$$

which, when substituted into Eq. (2.48), gives the expected result

$$\mathbf{D}=\frac{Q\hat{r}_1}{4\pi r_1^2}-\frac{Q\hat{r}_2}{4\pi r_2^2}\ ,$$
$$\hat{r}_{\left[\begin{smallmatrix}1\\2\end{smallmatrix}\right]}=(\mathbf{x}-\mathbf{x}_{\left[\begin{smallmatrix}1\\2\end{smallmatrix}\right]})/r_{\left[\begin{smallmatrix}1\\2\end{smallmatrix}\right]}\ , \tag{2.58}$$
$$r_{\left[\begin{smallmatrix}1\\2\end{smallmatrix}\right]}=[x^2+y^2+(z\mp a)^2]^{1/2}\ .$$

In the case where $\varepsilon(E)$ is given by Eq. (2.46), the coefficient function σ is given on branch Ia by

$$\sigma(\rho,|\nabla\Phi|)=\frac{2\pi\kappa}{\rho|\nabla\Phi|}f\left[\frac{|\nabla\Phi|}{\pi b_0\kappa\rho}\right], \tag{2.59}$$

with $f(w)$ implicitly defined by the transcendental equation

$$w=f\log f,\quad f\geq 1\ . \tag{2.60}$$

For small w and large w, the behavior of $f(w)$ is given by

$$f=1+w-\tfrac{1}{2}w^2+O(w^3)\ ,\quad |w|\ll 1\ , \tag{2.61a}$$
$$f=\frac{w}{\log w}\left\{1+\frac{\log\log w}{\log w}+O\left[\left(\frac{\log\log w}{\log w}\right)^2\right]\right\},\quad w\gg 1\ , \tag{2.61b}$$

as shown in Fig. 4(a), giving σ the behavior graphed in Fig. 4(b). The fact that σ becomes infinite as $f=E/\kappa$ approaches 1 from above (i.e., as $w\propto D$ approaches 0) means that a solution which is initially on branch Ia can approach branch II only as a degenerate limit and cannot cross back and forth between branch Ia and branch Ib. In the vicinity of the source charge at $\rho=0$, $z=a$, Eqs. (2.50), (2.56), and (2.59)—(2.61) can be integrated to give the leading behavior[15]

$$\mathbf{D}=\frac{Q\hat{r}_1}{4\pi r_1^2}+O(1)\ ,$$
$$\mathbf{E}=\hat{r}_1\kappa f\left[\frac{Q}{2\pi\kappa b_0 r_1^2}\right]+O(1)\ ,$$
$$A^0=\kappa\int_{r_1}^{\text{const}}dr_1' f\left[\frac{Q}{2\pi\kappa b_0(r_1')^2}\right]+O(r_1)\ , \tag{2.62}$$
$$\Phi=Q\tfrac{1}{2}(1-\cos\vartheta_1)+O(r_1^2\sin^2\vartheta_1)\ ,$$

where the structure of the subdominant terms $O(\ )$ has been indicated up to powers of $\log r_1$. The corresponding behavior at $\rho=0$, $z=-a$ is obtained by reflecting the formulas of Eq. (2.62) in the $z=0$ plane.

Once Φ has been determined by solving the boundary value problem formulated above, the static potential can be calculated by substituting $\nabla\cdot\mathbf{D}=j^0$ into Eq. (2.42) and integrating by parts. This gives

$$V_{\text{static}}=\int d^3x\{ED-\mathscr{L}[E(D)^2]+\mathscr{L}[E(0)^2=\kappa^2]\}\ , \tag{2.63}$$

where an infinite constant $\int d^3x\,\mathscr{L}(\kappa^2)$ has been added to Eq. (2.63) to render the integral convergent at spatial infinity. A little algebra shows that Eq. (2.63) is equivalent to the following computationally convenient formula:

$$V_{\text{static}}=\int d^3x\tfrac{1}{2}\sigma\left[\frac{\nabla\Phi}{2\pi}\right]^2(1+\xi)\ ,$$
$$\xi=(f^2-1)/(2fw)\ , \tag{2.64}$$

with σ, f, and w as defined above. A second useful expression for V_{static} is obtained by using the identity

$$\mathscr{L}[E(D)^2]-\mathscr{L}[E(0)^2]=\int_{E(0)}^{E(D)}dE'\frac{\partial\mathscr{L}(E'^2)}{\partial E'}$$
$$=\int_{E(0)}^{E(D)}dE'D(E')$$
$$=ED-\int_0^D dD'E(D')\ , \tag{2.65}$$

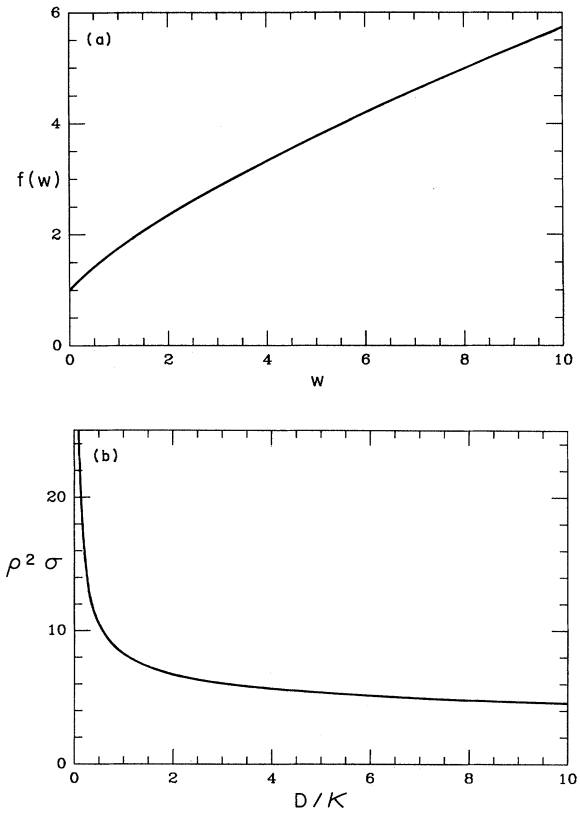

FIG. 4. (a) Plot of the function $f(w)$ defined in Eq. (2.60). (b) Plot of $\rho^2\sigma$, defined in Eqs. (2.59)—(2.61), as a function of D/κ.

[15]Since $Q\frac{1}{2}(1-\cos\vartheta_1)$ exactly satisfies the boundary conditions of Eq. (2.50) around $z=a$, the leading subdominant term in Φ must vanish at $\vartheta_1=0,\vartheta_1=\pi$. This boundary condition eliminates a possible term in Φ behaving as $O[r_1(a+b\cos\vartheta_1)]$, giving the structure shown in Eq. (2.62).

which when substituted into Eq. (2.63) gives the familiar formula

$$V_{\text{static}} = \int d^3x \mathscr{H} , \tag{2.66a}$$

with $\mathscr{H}$ the field energy density

$$\mathscr{H} = \int_0^D dD' E(D') . \tag{2.66b}$$

Since we have noted above (and will see in greater detail below) that the region of support of D is confined to branch Ia, where $E(D) \geq \kappa$, Eq. (2.66) gives the inequality

$$V_{\text{static}} \geq \kappa \int d^3x D . \tag{2.67}$$

To turn Eq. (2.67) into a useful lower bound on the large distance behavior of V_{static}, we must exclude the infinite Coulomb self-energies. This is most easily done by excluding from the x integration small spheres of radius ε around the source charges, motivating the definitions

$$\begin{aligned} &\Omega = \text{domain}\{ |\mathbf{x}-\mathbf{x}_1| \geq \varepsilon , |\mathbf{x}-\mathbf{x}_2| \geq \varepsilon \} , \\ &V^{(\varepsilon)}_{\text{static}} = \int_\Omega d^3x \mathscr{H}(x) \geq \kappa \int_\Omega d^3x D . \end{aligned} \tag{2.68}$$

When we write $d^3x = dl dA$, with l the length along and dA the element of area perpendicular to the flux lines of D, Eq. (2.67) then yields the lower bound[16]

$$\begin{aligned} &V_{\text{static}}(R) \geq \kappa \int_\Omega dA D \int dl \geq \kappa Q l_{\min} = \kappa Q (R - 2\varepsilon) , \\ &R = |\mathbf{x}_1 - \mathbf{x}_2| = 2a , \end{aligned} \tag{2.69}$$

showing that V_{static} increases at least linearly for large source separations. A more detailed discussion of the removal of the Coulomb self-energies from the formula for V_{static} is given in Sec. III.E below.

A great deal of insight into the behavior of Eq. (2.56) is obtained by putting it into the standard form for a second-order, quasilinear differential equation,

$$a^{kl}(x,\Phi,\nabla\Phi)\partial_k\partial_l\Phi + c(x,\Phi,\nabla\Phi) = 0 , \tag{2.70}$$

and analyzing the structure of its characteristics. Defining the inward directed unit normal $\hat{n}$ and the corresponding normal derivative ∂_n,

$$\hat{n} = \frac{\nabla\Phi}{|\nabla\Phi|} , \quad \partial_n = \hat{n}\cdot\nabla , \tag{2.71}$$

we can see through a straightforward calculation given in Appendix A that Eq. (2.56) is equivalent to

$$[(\partial_\rho^2 + \partial_z^2 - \partial_n^2) + \alpha\partial_n^2]\Phi - \alpha\rho^{-1}\partial_\rho\Phi = 0 . \tag{2.72}$$

The coefficient α is given by

$$\begin{aligned} &\alpha = 1 + \frac{\partial \log\sigma}{\partial \log|\nabla\Phi|} = \frac{d(\log f)}{d(\log w)} = \frac{w f'(w)}{f(w)} = \frac{w}{w + f(w)} , \\ &w = \frac{\partial_n\Phi}{\pi b_0 \kappa \rho} = \frac{2D}{b_0\kappa} ; \end{aligned} \tag{2.73}$$

[16]The flux estimate of Eq. (2.69) is due to 't Hooft (1975b).

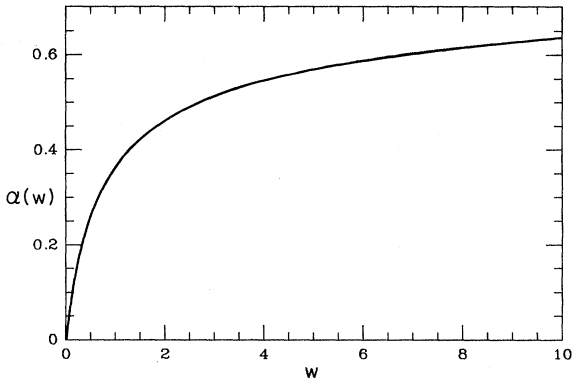

FIG. 5. Plot of the function $\alpha(w)$ defined in Eq. (2.73).

the function $\alpha(w)$ is graphed in Fig. 5 and [from Eq. (2.61)] has the following approximate forms for small and large w:

$$\begin{aligned} &\alpha = w + O(w^2) , \quad |w| \ll 1 , \\ &\alpha = 1 - \frac{1}{\log w} + O\left[\frac{\log\log w}{(\log w)^2}\right] , \quad w \gg 1 . \end{aligned} \tag{2.74}$$

From Eqs. (2.73) and (2.74) and Fig. 5 we see that α lies between 0 and 1 for $D > 0$, but vanishes when $D = 0$. Hence Eq. (2.72) is of degenerating elliptic type,[17] and has a real characteristic at a surface of constant Φ, where $|\nabla\Phi| = 0$. The second normal derivative $\partial_n^2\Phi$ is discontinuous across this characteristic, which acts as a free boundary, dividing space into two causally disconnected regions. From the boundary condition of Eq. (2.50), we learn that the exterior of the free boundary is completely surrounded by surfaces on which $\Phi = 0$. Hence $\Phi \equiv 0$ outside the characteristic, giving the solution the qualitative form graphed in Fig. 6. In the vicinity of a point B on the free boundary where $\rho = \rho_B$ and where the radius of curvature of the free boundary is R_B, a simple analysis given in Appendix A shows that Φ has the leading behavior

$$\Phi \approx \tfrac{1}{2}\frac{\pi b_0 \kappa \rho_B}{R_B}\left[\left[n - \tfrac{1}{2}\frac{l^2}{R_B}\right]^2 + O(n^2, l^4)\right] , \tag{2.75}$$

with n and l normal and tangential Cartesian coordinates at B (see Fig. 7). Since Φ is increasing towards the interior, we must have $R_B > 0$, and so the free boundary is everywhere convex. As indicated in Fig. 6, the free boun-

[17]The theory of equations of this type, and extensive references, are given in Oleĭnik and Radkevič (1973). This book treats only the linear case [see Eq. (A18)], rather than the quasilinear case encountered in the leading logarithm model. An important difference found in the quasilinear case is that the location of the characteristic depends on the solution to the equation, rather than being *a priori* known. This is why the real characteristic of Eq. (2.72) behaves as a free, as opposed to a fixed, boundary.

dary intersects the axis of rotation at a point $\rho=0, z=z_A$; in Appendix A it is shown that $z_A > a$, with the possibility $z_A = a$ excluded. Apart from this statement, we have been unable to characterize analytically the structure of the free-boundary–rotation axis intersection.[18] Once Φ and $\mathbf{D}$ have been determined in the interior region, A^0 can be calculated from the formula

$$A^0(\rho,z) = -\int_0^z dz' \frac{\hat{z}\cdot\mathbf{D}(\rho,z')}{\varepsilon[D(\rho,z')]} . \tag{2.76}$$

An interesting alternative method, discussed in Appendix A, is to determine A^0 from the known solution for ε by solving the linear differential equation

$$\nabla\cdot(\varepsilon\nabla A^0) = -j^0 \tag{2.77}$$

within the free boundary.

Since Φ and $\mathbf{D}$ vanish identically outside the free boundary, continuity requires that ε remain zero in the whole of the exterior region. Thus the exterior scalar and vector potentials are constrained only by the requirement that the electric and magnetic fields satisfy the branch II condition

$$\mathbf{E}^2 - \mathbf{B}^2 = \kappa^2 , \tag{2.78}$$

but are otherwise undetermined. In other words, the functional L_{eff} has an infinite equivalence class of C^1 extrema $A^0, \mathbf{A}$, corresponding to all possible ways of satisfying Eq. (2.78) outside the free boundary. All members of this equivalence class[19] give the same A^0, Φ inside the free boundary, and make the same physical predictions.

The solution to the leading logarithm model is clearly qualitatively similar to the confinement domain found in the MIT "bag" model,[20] but there are important differences. At the boundary of an MIT "bag" the fields (the first derivatives of the potentials) are discontinuous, corresponding to the presence of a step function in the variational principle formulation. In the leading logarithm model, the boundary is a characteristic across which the fields are continuous, with only the first derivatives of the fields (the second derivatives of the potentials) having discontinuities. This behavior corresponds to the fact that the variational formulation of the leading logarithm model involves a smooth action functional L_{eff}.

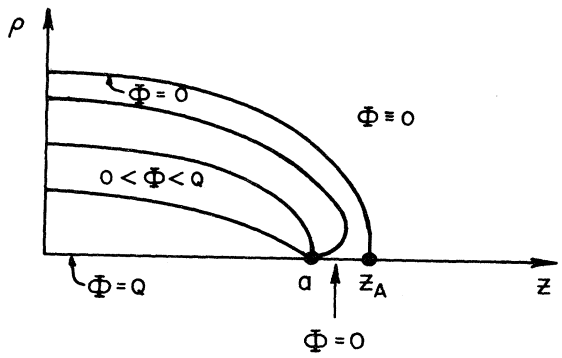

FIG. 6. Qualitative appearance of the solution of Eqs. (2.50), (2.56), and (2.59)–(2.61).

E. Axially symmetric Bogomol'nyi-Prasad-Sommerfield monopoles

As our final nonlinear example, let us consider a non-Abelian generalization of the Abelian Higgs model of Eq. (2.10), in which an SU(2) non-Abelian gauge field is coupled to a real scalar field φ^a, $a=1,2,3$, in the adjoint representation. The Lagrangian is

$$\begin{aligned} L &= \int d^3x \mathscr{L} , \\ \mathscr{L} &= \tfrac{1}{2}(\mathbf{E}^a\cdot\mathbf{E}^a - \mathbf{B}^a\cdot\mathbf{B}^a) \\ &\quad + \tfrac{1}{2}(\mathscr{D}_0\varphi^a)^2 - \tfrac{1}{2}(\mathscr{D}_j\varphi^a)^2 - \tfrac{1}{2}C[(\varphi^a)^2-\kappa^2]^2 , \end{aligned} \tag{2.79}$$

with the field strengths and covariant derivatives given by

$$E^{aj} = -\mathscr{D}_j A^{a0} - \frac{\partial}{\partial t}A^{aj}, \tag{2.80a}$$

$$B^{aj} = \varepsilon^{jkl}\left[\frac{\partial}{\partial x^k}A^{al} + \tfrac{1}{2}\varepsilon^{abc}A^{bk}A^{cl}\right] ,$$

$$\mathscr{D}_0\varphi^a = \frac{\partial}{\partial t}\varphi^a - \varepsilon^{abc}A^{b0}\varphi^c , \tag{2.80b}$$

$$\mathscr{D}_j w^a = \frac{\partial}{\partial x^j}w^a + \varepsilon^{abc}A^{bj}w^c \text{ for } w^a = \varphi^a \text{ or } A^{a0} ,$$

$$[\mathscr{D}_k, \mathscr{D}_j]w^a = \varepsilon^{kjl}\varepsilon^{abc}B^{bl}w^c . \tag{2.80c}$$

In writing Eqs. (2.79) and (2.80), we have for simplicity taken the gauge field coupling g to be unity. We will

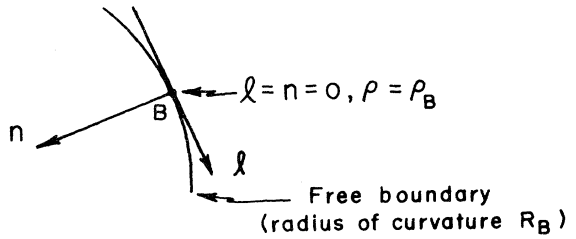

FIG. 7. Geometry near the free boundary used in Eqs. (2.75) and (A10)–(A12).

[18]The numerical results given below suggest that the free boundary intersects the rotation axis at a right angle (rather than at a cusp), but we have no proof of this.

[19]A question which remains to be clarified in the field-theoretic context is whether the degenerate exterior solutions should be interpreted as vacuum structure. For articles advocating this view see, for example, Savvidy (1977), Pagels and Tomboulis (1978), and Nielsen (1981); for possible problems with this interpretation, see Kiskis (1980b) and Cabo and Shabad (1980).

[20]The MIT "bag" model was introduced by Chodos *et al.* (1974); for a review, see Hasenfratz and Kuti (1978), and for a reinterpretation within QCD, see Johnson (1978).

again be interested in static solutions for which all time derivatives vanish, but this time (since no external source charge-density coupling to A^{a0} has been included) we will take $A^{a0}=0$. After making these simplifications we have

$$-L=H=\int d^3x\mathscr{H}\ , \tag{2.81}$$

with $\mathscr{H}$ the field energy density

$$\mathscr{H}=\tfrac{1}{2}\mathbf{B}^a\cdot\mathbf{B}^a+\tfrac{1}{2}(\mathscr{D}_j\varphi^a)^2+\tfrac{1}{2}C[(\varphi^a)^2-\kappa^2]^2\ . \tag{2.82}$$

We will be interested in what follows in the finite energy extrema of Eq. (2.81), which clearly must satisfy

$$\lim_{r\to\infty}(\varphi^a)^2=\kappa^2\ . \tag{2.83}$$

Defining a unit SU(2) internal symmetry vector $\hat{n}^a(\hat{r})$ on the sphere at spatial infinity by

$$\begin{aligned}&\hat{n}^a(\hat{r})=\lim_{r\to\infty}\varphi^a(r\hat{r})/\kappa\ ,\\ &\hat{r}=\mathbf{x}/r\ ,\end{aligned} \tag{2.84}$$

we see that the complete specification of the boundary condition for φ^a requires specifying the number of times the two-sphere on which $\hat{n}^a$ lies is covered, when the two-sphere on which $\hat{r}$ lies is traversed once. This number (which must be an integer when $\hat{n}^a$ is a continuous function of $\hat{r}$) is the winding number or topological quantum number

$$n=\lim_{r\to\infty}\frac{1}{8\pi}\int_{\text{sphere at }\infty}d^2S^i\varepsilon^{ijk}\varepsilon^{abc}\hat{n}^a\frac{\partial}{\partial x^j}\hat{n}^b\frac{\partial}{\partial x^k}\hat{n}^c\ . \tag{2.85}$$

Hence the problem of finding finite energy extrema of H breaks up into discrete topological sectors.

Extrema of H for $C\neq 0$ are called 't Hooft (1974)—Polyakov (1974) monopoles. A very interesting special case, introduced by Prasad and Sommerfield (1975) and Bogomol'nyi (1976) and extensively studied since then,[21] is obtained by setting $C=0$ but retaining the boundary conditions of Eqs. (2.83)—(2.85), giving

$$\begin{aligned}&H=\int d^3x\tfrac{1}{2}(B^{aj}B^{aj}+\mathscr{D}_j\varphi^a\mathscr{D}_j\varphi^a)\ ,\\ &\lim_{r\to\infty}\varphi^a=\kappa\hat{n}^a\ ,\\ &\text{winding number of }\hat{n}^a=n\ .\end{aligned} \tag{2.86}$$

The Euler-Lagrange equations obtained by varying the functional H of Eq. (2.86) are

$$\begin{aligned}&\mathscr{D}_j\mathscr{D}_j\varphi^a=0\ ,\\ &\varepsilon^{kjm}\mathscr{D}_jB^{am}=-\varepsilon^{abc}\varphi^b\mathscr{D}_k\varphi^c\ ,\end{aligned} \tag{2.87}$$

while the field-potential relations of Eq.(2.80) imply that

$$\begin{aligned}&\mathscr{D}_jB^{aj}=0\ ,\\ &\varepsilon^{kjm}\mathscr{D}_j\mathscr{D}_m\varphi^a=-\varepsilon^{abc}\varphi^bB^{ck}\ .\end{aligned} \tag{2.88}$$

Although Eqs. (2.87) are complicated second-order differential equations, they are satisfied by any φ^a, A^{aj} satisfying the first-order differential equations

$$-\mathscr{D}_j\varphi^a=\xi B^{aj}\ ,\quad \xi=\pm 1\ , \tag{2.89}$$

with the cases $\xi=1$ (-1) termed, respectively, self-dual (anti-self-dual).[22] To see that Eq. (2.89) suffices, we note that by Eq. (2.88) we have

$$\mathscr{D}_j\mathscr{D}_j\varphi^a=-\xi\mathscr{D}_jB^{aj}=0\ , \tag{2.90a}$$

while by using Eq. (2.80c) we get

$$\begin{aligned}\varepsilon^{kjm}\mathscr{D}_jB^{am}&=-\xi\varepsilon^{kjm}\mathscr{D}_j\mathscr{D}_m\varphi^a\\ &=\xi\varepsilon^{abc}\varphi^bB^{ck}=-\xi^2\varepsilon^{abc}\varphi^b\mathscr{D}_k\varphi^c\ .\end{aligned} \tag{2.90b}$$

Remarkably, Eq. (2.89) is also a necessary condition for a minimum of H, as may be seen by the following[23] rearrangement of Eq. (2.86),

$$\begin{aligned}H&=H_1+H_2\ ,\\ H_1&=\int d^3x\tfrac{1}{2}(B^{aj}+\xi\mathscr{D}_j\varphi^a)^2\ ,\\ H_2&=-\xi\int d^3xB^{aj}\mathscr{D}_j\varphi^a\\ &=-\xi\int d^3x\mathscr{D}_j(B^{aj}\varphi^a)\\ &=-\xi\int_{\text{sphere at }\infty}d^2S^jB^{aj}\varphi^a\ .\end{aligned} \tag{2.91}$$

Since H_2 reduces to a surface term, the functional H can be extremal only for fields for which H_1 vanishes, giving the condition of Eq. (2.89). The surface term H_2 can be evaluated by noting that in order for the integral of Eq. (2.86) to converge, $\mathscr{D}_j\hat{n}^a$ must vanish at large r, giving the following relation between A^{aj} and $\hat{n}^a$ on the sphere at infinity,

$$A^{aj}=\hat{n}^a\hat{n}^bA^{bj}-\varepsilon^{abc}\hat{n}^b\frac{\partial}{\partial x^j}\hat{n}^c\ . \tag{2.92}$$

Combining Eqs. (2.80a) and (2.92), one finds, after some algebra,

$$B^{aj}\hat{n}^a=\frac{\partial}{\partial x^k}(\varepsilon^{jkl}\hat{n}^aA^{al})-\tfrac{1}{2}\varepsilon^{jkl}\varepsilon^{abc}\hat{n}^a\frac{\partial}{\partial x^k}\hat{n}^b\frac{\partial}{\partial x^l}\hat{n}^c\ . \tag{2.93}$$

---

[21]For recent reviews on monopoles, see Jaffe and Taubes (1980) and O'Raifeartaigh and Rouhani (1981).

[22]This terminology stems from the fact that $-\mathscr{D}_j\varphi^a$ can be formally reinterpreted as a static Euclidean electric field strength $E^{aj}_{(E)}\equiv -\mathscr{D}_jA^{a0}_{(E)}$, $A^{a0}_{(E)}\equiv\varphi^a$, in terms of which $\mathscr{L}=-\tfrac{1}{2}(\mathbf{B}^a\cdot\mathbf{B}^a+\mathbf{E}^a_{(E)}\cdot\mathbf{E}^a_{(E)})$. The self-dual ($\xi=1$) solutions satisfy $E^{aj}_{(E)}=B^{aj}$, while the anti-self-dual ($\xi=-1$) solutions satisfy $E^{aj}_{(E)}=-B^{aj}$. Clearly, a $\xi=1$ solution can be converted to a $\xi=-1$ solution simply by changing the sign of φ^a.

[23]This argument is due to Bogomol'nyi (1976) and to Coleman, Parke, Neveu, and Sommerfield (1977).

The surface integral of the first term on the right-hand side of Eq. (2.93) vanishes; and so, referring back to Eq. (2.85), we get

$$H_2=4\pi\kappa\xi n \ . \tag{2.94}$$

Since the positivity of H implies that H_2 is positive when H_1 vanishes, we conclude that

$$H_2=4\pi\kappa\,|\,n\,|\ , \quad \xi=n/|\,n\,|\ . \tag{2.95}$$

Hence the minimum of H in each topological sector is determined solely by the topological quantum number.

The minimum of H in the $n=1$ topological sector is given by the simple expression

$$\begin{aligned}\varphi^a&=-\frac{x^a}{r^2}(1-\kappa r\coth\kappa r)\ ,\\ A^{aj}&=\frac{\varepsilon^{ajl}x^l}{r^2}\left[1-\frac{\kappa r}{\sinh\kappa r}\right]\ ,\end{aligned} \tag{2.96}$$

which satisfies Eqs. (2.89) with $\xi=1$. This solution is the simplest of a family of solutions of Eq. (2.89), in which the Higgs field φ^a and the potentials A^{aj} are axially symmetric and reflection symmetric, as described by the following ansatz:

$$\begin{aligned}&\varphi^a=h_1\hat{z}^a+h_2\hat{\rho}_n^a\ ,\\ &A^{aj}=\hat{\phi}^j\left[\frac{f_1-n}{\rho}\hat{z}^a+\frac{f_2}{\rho}\hat{\rho}_n^a\right]-(\hat{z}^j a_1+\hat{\rho}^j a_2)\hat{\phi}_n^a\ ,\\ &\rho=(x^2+y^2)^{1/2},\quad \phi=\tan^{-1}(y/x)\ ,\\ &\hat{z}=(0,0,1)\ ,\\ &\hat{\rho}_n=(\cos n\phi,\sin n\phi,0),\quad \hat{\rho}=\hat{\rho}_1\ ,\\ &\hat{\phi}_n=(-\sin n\phi,\cos n\phi,0),\quad \hat{\phi}=\hat{\phi}_1\ .\end{aligned} \tag{2.97}$$

The potentials $h_{1,2}$, $f_{1,2}$, and $a_{1,2}$ are functions of ρ and z, with $z\leftrightarrow -z$ reflection symmetry and behavior on the $z=0$ and $\rho=0$ axes as follows:

$$\begin{aligned}&h_2,f_1,a_1 \text{ even in } z\ ,\\ &h_1,f_2,a_2 \text{ odd in } z\ ,\\ &h_1=f_2=a_2=0 \text{ at } z=0\ ,\\ &a_1=f_2=h_2=0,\ f_1=n \text{ at } \rho=0,\ n\geq 1\ .\end{aligned} \tag{2.98}$$

Although analytic forms for the solutions of Eq. (2.89) within the ansatz of Eqs. (2.97) and (2.98) are now known,[24] we will treat the problem of finding the axially symmetric, reflection-symmetric minima of H as a numerical example in Sec. IV.D. In Appendix B we give explicit expressions for the functional H when expressed in terms of the potentials $h_{1,2},\ldots,$ and discuss the residual Abelian gauge invariance of the six-function ansatz and the choice of a gauge-fixing term for numerical work. From the equations given in Appendix B, a straightforward calculation shows that the leading behavior of the potentials at infinity[25] is given by the following formulas (in which terms of order $e^{-\kappa r}$ are omitted):

$$\begin{aligned}&h_1=h\cos\vartheta,\ h_2=h\sin\vartheta\ ,\\ &a_1=-\frac{\sin\vartheta}{r},\ a_2=\frac{\cos\vartheta}{r}\ ,\\ &f_1=f\cos\vartheta,\ f_2=f\sin\vartheta\ ,\\ &h=\kappa-\frac{n}{r}+\sum_{\substack{l=2\\ l\text{ even}}}^{\infty}\frac{a_l^{(\infty)}P_l(\cos\vartheta)}{r^{l+1}}\ ,\\ &f=n\cos\vartheta+\rho\sum_{\substack{l=2\\ l\text{ even}}}^{\infty}\frac{a_l^{(\infty)}P_{l1}(\cos\vartheta)}{l r^{l+1}}\ ,\\ &r=(\rho^2+z^2)^{1/2},\ \vartheta=\tan^{-1}(\rho/z)\ .\end{aligned} \tag{2.99}$$

The leading behavior at the origin[25] is also calculated in Appendix B, where it is shown that even in the higher topological sectors $n>1$, the Higgs field φ^a has only a first-order zero at $r=0$.

III. RELAXATION METHODS FOR THE NUMERICAL SOLUTION OF ELLIPTIC PARTIAL DIFFERENTIAL EQUATIONS

A. Introduction

In this section we give a detailed introduction to both the theoretical and practical aspects of the numerical solution of elliptic partial differential equations of the type encountered in Sec. II. We assume that the reader has read Sec. II.A and especially Sec. II.B, and has at least glanced over Secs. II.C–II.E. However, the discussion of numerical methods which follows is essentially self-contained, and makes only minimal references back to the formulas in Sec. II. Motivated by the fact that the numerical solution of the models of Secs. II.C–II.E can be reduced to a sequence of solutions to linear differential

[24]For the analytic construction of axially symmetric multimonopole solutions and references, see Prasad and Rossi (1981).

[25]Equations (2.99) and (B11) are the expansions calculated in the gauge $\partial_z a_1+\partial_\rho a_2=0$. For $n=1$, this gauge condition does not uniquely fix the order r terms in $a_{1,2}$ near $r=0$; the general solution for $n=1$ is $a_1=-b\rho(\frac{1}{2}+\alpha)+O(r^2), a_2=bz(\frac{1}{2}-\alpha)+O(r^2)$, with α a free parameter. The $n=1$ case of Eq. (B11) corresponds to $\alpha=\frac{1}{2}$, while the standard form of the single monopole solution given in Eq. (2.96) corresponds to $\alpha=0$. [To put Eq. (2.96) in the form of Eq. (2.97), one uses $\hat{r}^a=\hat{z}^a\cos\vartheta+\hat{\rho}^a\sin\vartheta$, $\varepsilon^{ajl}\hat{r}^l=(\hat{\rho}^a\hat{\varphi}^j-\hat{\rho}^j\hat{\varphi}^a)\cos\vartheta+(\hat{\varphi}^a\hat{z}^j-\hat{\varphi}^j\hat{z}^a)\times\sin\vartheta$.] The expansions of Eqs. (2.99) and (B11) were derived by Adler (unpublished), Rebbi and Rossi (1980), and Houston and O'Raifeartaigh (1981).

equation problems combined with Newton iterations, we base most of our exposition on the simple linear problem of calculating the static potential V_{static} of external test charges Q, $-Q$ immersed in a dielectric medium, with an axially symmetric position-dependent dielectric constant $\varepsilon(x)=\varepsilon(\rho,z)>0$. According to the general Lagrangian statics formalism of Sec. II.B, this problem has the variational formulation

$$V_{\text{static}}=-\text{ext}_{\varphi}\int d^3x[\tfrac{1}{2}\varepsilon(x)(\nabla\varphi)^2-j^0\varphi]\ ,$$
$$j^0=Q\delta(x)\delta(y)[\delta(z-a)-\delta(z+a)]\ , \tag{3.1}$$

where we have positioned the test charges at $z=\pm a$ on the z axis. When restricted to axially symmetric scalar potentials $\varphi=\varphi(\rho,z)$, the Euler-Lagrange equation corresponding to the extremum in Eq. (3.1) takes the form

$$\nabla\cdot(\varepsilon\nabla\varphi)=\frac{1}{\rho}\frac{\partial}{\partial\rho}\left[\rho\varepsilon\frac{\partial\varphi}{\partial\rho}\right]+\frac{\partial}{\partial z}\left[\varepsilon\frac{\partial\varphi}{\partial z}\right]=-j^0\ , \tag{3.2}$$

and has the boundary condition

$$\varphi\to 0 \text{ as } r=(\rho^2+z^2)^{1/2}\to\infty\ . \tag{3.3}$$

Most of the features encountered in the numerical solution of the nonlinear models of Secs. II.C—II.E already appear in the numerical solution of the model of Eqs. (3.1)—(3.3).

In the succeeding sections we describe the steps involved in formulating this model for numerical solution, digressing briefly where needed to give additional techniques required in the analysis of the models of Sec. II. In Sec. III.B we discuss the reduction of Eqs. (3.1)—(3.3) to discrete form and give a simple method for treating the boundary of the computational mesh. In Sec. III.C we describe the basic theory of iterative methods for the solution of the discretized equations. In Sec. III.D we introduce Jacobian "stretching" transformations of the ρ,z axes, and in Sec. III.E we discuss the removal of the infinite Coulomb self-energies from V_{static}. In Sec. III.F we show how nonlinear problems can be reduced to a sequence of quasilinear problems, to which the discussion of Secs. III.B—III.E applies, and in Sec. III.G we discuss some relevant programming considerations. Although the sections just enumerated are deliberately concise, they cover all of the major issues which we have encountered in programming the models of Sec. II. Readers seeking a more detailed discussion of the numerical solution of elliptic partial differential equations should consult the books of Ames (1977), Bauer, Betancourt, and Garabedian (1978), Hockney and Eastwood (1981), and Roache (1976).

B. Discretization of the continuum problem and treatment of the boundary of the computational mesh

In order to formulate the continuum problem of Eqs. (3.1)—(3.3) for numerical analysis, we must approximate it by a similar problem defined on a discrete computational lattice.[26] Before proceeding to the three-dimensional, axially symmetric case, let us consider first the even simpler one-dimensional model defined by

$$V_{\text{static}}=-\text{ext}_{\varphi}\int dz\left[\tfrac{1}{2}\varepsilon(z)\left[\frac{\partial\varphi}{\partial z}\right]^2-j^0\varphi\right]\ , \tag{3.4}$$

with the Euler-Lagrange equation

$$\frac{\partial}{\partial z}\left[\varepsilon(z)\frac{\partial\varphi}{\partial z}\right]=-j^0(z)\ . \tag{3.5}$$

To introduce the computational lattice for Eqs. (3.4) and (3.5), we replace the continuous variable z by a discrete one

$$z_i=z_0+i\Delta z,\ i=\ldots,-2,-1,0,1,2,\ldots, \tag{3.6a}$$

and let ε_i,φ_i denote the values of the continuous functions $\varepsilon(z),\varphi(z)$ on the discrete points of Eq. (3.6a),

$$\varepsilon_i=\varepsilon(z_i),\quad \varphi_i=\varphi(z_i)\ . \tag{3.6b}$$

Working to second-order accuracy in $(\Delta z)^2$, we can then replace differential operators by finite difference operators—for example,

$$\left.\frac{\partial\varphi}{\partial z}\right|_i\to\frac{\varphi_{i+1}-\varphi_{i-1}}{2\Delta z}=\frac{\varphi_{i+1/2}-\varphi_{i-1/2}}{\Delta z}\ , \tag{3.7a}$$

where $\varphi_{i+1/2}$ is defined by

$$\varphi_{i+1/2}=\tfrac{1}{2}(\varphi_{i+1}+\varphi_i)\ , \tag{3.7b}$$

and

$$\left.\frac{\partial^2\varphi}{\partial z^2}\right|_i\to\frac{\varphi_{i+1}-2\varphi_i+\varphi_{i-1}}{(\Delta z)^2}\ . \tag{3.7c}$$

Because terms of order $(\Delta z)^2$ are neglected when the continuum problem is represented in finite difference form on the computational lattice, the finite differencing procedure is necessarily ambiguous. Thus the differential operator $(\partial/\partial z)(\varepsilon\partial\varphi/\partial z)$ appearing in Eq. (3.5) can be represented either as

$$\frac{\varepsilon_{i+1/2}(\varphi_{i+1}-\varphi_i)-\varepsilon_{i-1/2}(\varphi_i-\varphi_{i-1})}{(\Delta z)^2}\ , \tag{3.8a}$$

[26]There is an important difference, however, between the formulation of a field theory as a lattice gauge theory [see Creutz (1978)] and the discretization of a classical action functional. In the case of a full-fledged field theory it is essential to have a discrete analog of the full gauge group to avoid picking up spurious radiative corrections in one- or higher-loop order. In the case of a classical action functional, which may be thought of as a tree-approximation field theory, the discretization need not have an intrinsic gauge invariance, and it is in fact desirable to add gauge-fixing terms to the action [as in Eqs. (B5) and (B6)] to make the extremum unique and the differential equations elliptic.

or as

$$\varepsilon_i \frac{(\varphi_{i+1}-2\varphi_i+\varphi_{i-1})}{(\Delta z)^2}+\frac{(\varepsilon_{i+1}-\varepsilon_{i-1})(\varphi_{i+1}-\varphi_{i-1})}{4(\Delta z)^2}\ , \tag{3.8b}$$

both of which are second-order accurate. The difference between Eq. (3.8a) and Eq. (3.8b) is in fact

$$\frac{(\varepsilon_{i+1}-2\varepsilon_i+\varepsilon_{i-1})(\varphi_{i+1}-2\varphi_i+\varphi_{i-1})}{4(\Delta z)^2} \tag{3.9}$$

and corresponds to a continuum term

$$\tfrac{1}{4}(\Delta z)^2\frac{\partial^2\varepsilon}{\partial z^2}\frac{\partial^2\varphi}{\partial z^2}\ , \tag{3.10}$$

which vanishes as $\Delta z\to 0$. Although either Eq. (3.8a) or Eq. (3.8b) can in principle be used as the basis for a finite difference scheme, the form of Eq. (3.8a) has the advantage, unlike Eq. (3.8b), of satisfying an exact summation by parts formula

$$\sum_{i=i_1}^{i_2}\Delta z(\Delta z)^{-2}[\varepsilon_{i+1/2}(\varphi_{i+1}-\varphi_i)-\varepsilon_{i-1/2}(\varphi_i-\varphi_{i-1})]$$
$$=(\Delta z)^{-1}[\varepsilon_{i_2+1/2}(\varphi_{i_2+1}-\varphi_{i_2})-\varepsilon_{i_1-1/2}(\varphi_{i_1}-\varphi_{i_1-1})]\ , \tag{3.11a}$$

which is the counterpart of the continuum integration by parts formula

$$\int_{z_1}^{z_2}dz\frac{\partial}{\partial z}\left[\varepsilon(z)\frac{\partial\varphi}{\partial z}\right]=\varepsilon(z_2)\left.\frac{\partial\varphi}{\partial z}\right|_{z_2}-\varepsilon(z_1)\left.\frac{\partial\varphi}{\partial z}\right|_{z_1}\ . \tag{3.11b}$$

The analog of Eq. (3.8a) in higher dimensions guarantees that Gauss's law (or a similar conservation law) is automatically satisfied, and so Eq. (3.8a) is called the conservation form of $(\partial/\partial z)(\varepsilon\,\partial\varphi/\partial z)$, and we will always use it in preference to Eq. (3.8b).

A procedure which in most cases automatically generates the conservation form of the equations of motion is first to discretize the Lagrangian functional by the second-order accurate replacement

$$L=\int dz\left[\tfrac{1}{2}\varepsilon(z)\left(\frac{\partial\varphi}{\partial z}\right)^2-j^0\varphi\right]$$
$$\to\sum_i\left[\tfrac{1}{2}\varepsilon_{i+1/2}\left(\frac{\varphi_{i+1}-\varphi_i}{\Delta z}\right)^2-j_i^0\varphi_i\right]\Delta z\ , \tag{3.12}$$

where we have used

$$\left.\frac{\partial\varphi}{\partial z}\right|_{i+1/2}\to\left[\frac{\varphi_{i+1}-\varphi_i}{\Delta z}\right]^2\ . \tag{3.13}$$

Equating to zero the derivative of L with respect to the nodal value φ_i then gives

$$0=\frac{\partial L}{\partial\varphi_i}=\varepsilon_{i+1/2}\frac{\varphi_i-\varphi_{i+1}}{(\Delta z)^2}+\varepsilon_{i-1/2}\frac{\varphi_i-\varphi_{i-1}}{(\Delta z)^2}-j_i^0$$
$$\Rightarrow\frac{\varepsilon_{i+1/2}(\varphi_{i+1}-\varphi_i)-\varepsilon_{i-1/2}(\varphi_i-\varphi_{i-1})}{(\Delta z)^2}=-j_i^0\ , \tag{3.14}$$

yielding the desired form of the finite difference equation. This method is particularly advantageous in dealing with variational problems, such as those of Sec. II, which have more than one field variable, since it guarantees that the members of the resulting set of finite difference equations for these dependent variables are mutually consistent. In the special case in which $\varepsilon(z)$ is a constant and j^0 is a sum of point sources at the lattice nodes, the procedure of Eqs. (3.12)—(3.14) can be viewed as an application of the Rayleigh-Ritz variational method with a trial function $\tilde{\varphi}(z)$ which is trapezoidal in form,

$$\tilde{\varphi}(z)=\sum_i\psi_{i+1/2}(z)\ ,$$
$$\psi_{i+1/2}(z)=0,\ z<z_i \text{ or } z>z_{i+1}\ , \tag{3.15}$$
$$\psi_{i+1/2}(z)=\frac{\varphi_i(z_{i+1}-z)+\varphi_{i+1}(z-z_i)}{\Delta z}\ ,\quad z_i<z<z_{i+1}\ .$$

Returning to the general case in which $\varepsilon(z)$ is spatially varying, we find that the half-node value $\varepsilon_{i+1/2}$ appearing in Eq. (3.12) can be computed, to second-order accuracy, from either the analog of Eq. (3.7b),

$$\varepsilon_{i+1/2}=\tfrac{1}{2}[\varepsilon(z_{i+1})+\varepsilon(z_i)]\ , \tag{3.16}$$

or from the alternate formula

$$\varepsilon_{i+1/2}=\varepsilon(z_{i+1/2})\ , \tag{3.17a}$$

where $z_{i+1/2}$ is a point on the half-node lattice defined by

$$z_{i+1/2}=z_0+(i+\tfrac{1}{2})\Delta z,\quad i=\ldots,-2,-1,0,1,2,\ldots\ . \tag{3.17b}$$

The definition of Eq. (3.17) is superior when (as in the model of Sec. II.D) ε is a function of $|\nabla\varphi|$ rather than being given *a priori* . To see this, let us consider the one-dimensional case with $\varepsilon=F(\partial\varphi/\partial z)$, for which Eq. (3.16) gives

$$\varepsilon_{i+1/2}=\tfrac{1}{2}\left[F\left[\frac{\varphi_{i+2}-\varphi_i}{2\Delta z}\right]+F\left[\frac{\varphi_{i+1}-\varphi_{i-1}}{2\Delta z}\right]\right]$$
$$=F[\varphi'(z_{i+1/2})]+(\Delta z)^2\{\tfrac{7}{24}\varphi'''(z_{i+1/2})F'[\varphi'(z_{i+1/2})]+\tfrac{1}{8}[\varphi''(z_{i+1/2})]^2F''[\varphi'(z_{i+1/2})]\}+\cdots\ , \tag{3.18a}$$

while Eq. (3.17) instead yields

$$\varepsilon_{i+1/2}=F\left[\frac{\varphi_{i+1}-\varphi_i}{\Delta z}\right]$$
$$=F[\varphi'(z_{i+1/2})]+\tfrac{1}{24}(\Delta z)^2\varphi'''(z_{i+1/2})F'[\varphi'(z_{i+1/2})]$$
$$+\cdots\ , \tag{3.18b}$$

a form which is both computationally simpler than Eq. (3.18a) and which gives $F[\varphi'(z_{i+1/2})]$ with a smaller error term. A second reason for preferring Eq. (3.17), connected with the axial symmetry of the models under study, will be discussed shortly.

We are now ready to turn our attention to the axially symmetric example of Eqs. (3.1)—(3.3). The continuum variational principle for this problem is

$$V_{\text{static}}=-\text{ext}_{\varphi}L, \tag{3.19}$$
$$L=2\pi\int_0^\infty \rho d\rho\int_{-\infty}^{\infty}dz\tfrac{1}{2}\varepsilon(\rho,z)\left[\left[\frac{\partial\varphi}{\partial\rho}\right]^2+\left[\frac{\partial\varphi}{\partial z}\right]^2\right]$$
$$-Q\varphi(\rho=0,z=a)+Q\varphi(\rho=0,z=-a)\ ,$$

where we have explicitly integrated out the delta functions in the source term. We proceed by first reducing the Lagrangian functional L to discrete form, and then differentiating with respect to the nodal value $\varphi_{i,j}$ to get the discrete form of the equations of motion. We introduce the computational lattice[27]

$$\rho_i=i\Delta\rho,\quad i=0,1,2,\ldots\ ,$$
$$z_j=j\Delta z,\quad j=\ldots,-2,-1,0,1,2,\ldots\ , \tag{3.20a}$$

and the corresponding half-node lattice

$$\rho_{i+1/2}=(i+\tfrac{1}{2})\Delta\rho,\quad i=0,1,2,\ldots\ ,$$
$$z_{j+1/2}=(j+\tfrac{1}{2})\Delta z,\quad j=\ldots,-2,-1,0,1,2,\ldots\ , \tag{3.20b}$$

and express the discrete form of L in terms of the values of φ on the lattice of Eq. (3.20a) and the values of the prefactors ε and ρ on the half-node lattice of Eq. (3.20b),

$$\text{dependent variable: } \varphi_{i,j}=\varphi(\rho_i,z_j)\ ,$$
$$\text{prefactors: } \varepsilon_{i+1/2,j+1/2}=\varepsilon(\rho_{i+1/2},z_{j+1/2})\ , \tag{3.21}$$
$$\rho_{i+1/2}\ .$$

The advantage of putting explicit factors of ρ on the half-node lattice is that the smallest value of ρ which appears in the discrete problem is then $\rho_{1/2}=\frac{1}{2}\Delta\rho\neq 0$, giving a procedure which applies to functionals (such as those associated with the models of Secs. II.D and II.E) which contain explicit factors ρ^{-1}. We shall assume that the source charges lie on points of the computational lattice, so that

$$a=n_Q\Delta z\ , \tag{3.22}$$

with n_Q a positive integer. If we proceed by direct analogy with Eq. (3.12), the discrete form of L is then

$$L=2\pi\sum_{i=0}^{\infty}\sum_{j=-\infty}^{\infty}\left[\tfrac{1}{2}\rho_{i+1/2}\varepsilon_{i+1/2,j}\left[\frac{\varphi_{i+1,j}-\varphi_{i,j}}{\Delta\rho}\right]^2+\tfrac{1}{2}\rho_i\varepsilon_{i,j+1/2}\left[\frac{\varphi_{i,j+1}-\varphi_{i,j}}{\Delta z}\right]^2\right]\Delta\rho\Delta z$$
$$-Q\varphi_{0,n_Q}+Q\varphi_{0,-n_Q}\ , \tag{3.23}$$

where the prefactors $\varepsilon_{i+1/2,j}$ and $\rho_i\varepsilon_{i,j+1/2}$ are to be computed as averages of the neighboring half-node values,

$$\varepsilon_{i+1/2,j}\equiv\tfrac{1}{2}(\varepsilon_{i+1/2,j-1/2}+\varepsilon_{i+1/2,j+1/2})\ ,$$
$$\rho_i\varepsilon_{i,j+1/2}\equiv\tfrac{1}{2}(\rho_{i-1/2}\varepsilon_{i-1/2,j+1/2}+\rho_{i+1/2}\varepsilon_{i+1/2,j+1/2}),$$
$$\rho_{-1/2}\varepsilon_{-1/2,j+1/2}\equiv 0\ . \tag{3.24}$$

Differentiating Eq. (3.23) with respect to $\varphi_{i,j}$ then gives the discrete form of the field equation,

$$0=\frac{\partial L}{\partial\varphi_{i,j}}\Rightarrow 2\pi\left[\frac{\Delta z}{\Delta\rho}\right][\rho_{i+1/2}\varepsilon_{i+1/2,j}(\varphi_{i+1,j}-\varphi_{i,j})-\rho_{i-1/2}\varepsilon_{i-1/2,j}(\varphi_{i,j}-\varphi_{i-1,j})]$$
$$+2\pi\left[\frac{\Delta\rho}{\Delta z}\right][\rho_i\varepsilon_{i,j+1/2}(\varphi_{i,j+1}-\varphi_{i,j})-\rho_i\varepsilon_{i,j-1/2}(\varphi_{i,j}-\varphi_{i,j-1})]$$
$$=-Q\delta_{i,0}\delta_{j,n_Q}+Q\delta_{i,0}\delta_{j,-n_Q}\ . \tag{3.25}$$

To see that this equation is in conservation form, we note that the first square bracket on the left-hand side is an exact difference with respect to i, while the second square bracket is an exact difference with respect to j. Hence, when summed over i and j with arbitrary limits, Eq. (3.25) yields a sum of surface terms which are a discrete, second-order accurate version of the continuum flux conservation law

[27] In principle, one could use variable grid spacings by taking

$$\rho_i=\sum_{k=1}^{i}\Delta\rho_k,\quad z_j=\sum_{k=1}^{j}\Delta z_k\ ,$$

with $\Delta\rho_k$ and Δz_k having a dependence on k. However, the same effect can be achieved by using a computational lattice with fixed grid spacings, together with a Jacobian transformation from the computational to the physical coordinates, as discussed in Sec. III.D below. When extremely complicated geometries are encountered, for which it is hard to find suitable Jacobian transformations, the use of finite element methods may be appropriate; see Ames (1977) for a discussion.

$$\int d\mathbf{S}\cdot\varepsilon\nabla\varphi=\int_{V \text{ enclosed by } S} d^3x(-j^0) \ . \tag{3.26}$$

For example, from the sum

$$\sum_{i=0}^{\infty}\sum_{j=j_A}^{j_B}\mathscr{E} \ , \tag{3.27a}$$

where $\mathscr{E}$ represents Eq. (3.25), we learn that

$$2\pi\sum_{i=0}^{\infty}\rho_i\Delta\rho\varepsilon_{i,j_B+1/2}\left[\frac{\varphi_{i,j_B+1}-\varphi_{i,j_B}}{\Delta z}\right] -2\pi\sum_{i=0}^{\infty}\rho_i\Delta\rho\varepsilon_{i,j_A-1/2}\left[\frac{\varphi_{i,j_A}-\varphi_{i,j_A-1}}{\Delta z}\right] =\sum_{j=j_A}^{j_B}(Q\delta_{j,-n_Q}-Q\delta_{j,n_Q})=-\mathscr{N} \ , \tag{3.27b}$$

where $\mathscr{N}$ is the net charge between the plane $z=\Delta z(j_A-\frac{1}{2})$ and the plane $z=\Delta z(j_B+\frac{1}{2})$, in agreement with the form taken by Eq. (3.26) when V is chosen as the slice of three-space bounded by the planes $z=\Delta z(j_A-\frac{1}{2}),z=\Delta z(j_B+\frac{1}{2})$.

The reduction to discrete form of the example of Eqs. (3.1)—(3.3) illustrates a number of principles which apply in general in constructing a second-order accurate discretization of a Lagrangian functional [cf. the excellent discussion of Bauer, Betancourt, and Garabedian (1978), pp. 23—26].

(i) In general, one should average over the largest possible collection of terms, rather than averaging over each individual factor. For example, the expression in Eq. (3.24) for $\rho_i\varepsilon_{i,j+1/2}$ is clearly superior to the longer expression

$$\tfrac{1}{4}(\rho_{i-1/2}+\rho_{i+1/2})(\varepsilon_{i-1/2,j+1/2}+\varepsilon_{i+1/2,j+1/2}) \ , \tag{3.28}$$

which also represents $\rho_i\varepsilon_{i,j+1/2}$ to second-order accuracy.

(ii) In approximating the square of first derivatives, one should always square first and then average. For example, in Eq. (3.23), the ρ-derivative terms which contain a prefactor $\rho_{i+1/2}\varepsilon_{i+1/2,j-1/2}$ are

$$2\pi\frac{\Delta z}{\Delta\rho}\tfrac{1}{4}\rho_{i+1/2}\varepsilon_{i+1/2,j-1/2}[(\varphi_{i+1,j}-\varphi_{i,j})^2 +(\varphi_{i+1,j-1}-\varphi_{i,j-1})^2] \ , \tag{3.29a}$$

with the square bracket arising from the average of $(\partial\varphi/\partial\rho)^2$ over the unit cell with center at $(\rho,z)=(\rho_{i+1/2},z_{j-1/2})$. An alternative, second-order accurate representation for this average, obtained by averaging before squaring, would be

$$\frac{1}{(2\Delta\rho)^2}(\varphi_{i+1,j}-\varphi_{i,j}+\varphi_{i+1,j-1}-\varphi_{i,j-1})^2 \ . \tag{3.29b}$$

The advantage of squaring before averaging [Eq. (3.29a)] is that it couples the node i,j only to the nearest-neighbor nodes $i\pm1,j$ and $i,j\pm1$ in which a single index has been changed, as shown in Fig. 8. If, on the other hand, one averages before squaring [Eq. (3.29b)], one gets additional couplings of the node i,j to the nodes $i+1,j-1,\ldots,$ which are not nearest neighbors on the computational lattice. These non-nearest-neighbor couplings lead to more complicated computer codes.

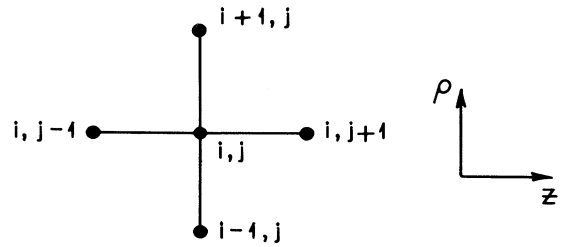

FIG. 8. Computational lattice node i,j with the nearest neighbors $i+1,j;i-1,j;i,j+1;i,j-1$, to which it is coupled when derivative-squared terms in the Lagrangian are discretized by squaring before averaging.

(iii) When the discretized Lagrangian L is written in the form

$$L=\sum_i\sum_j K_{i,j} \ , \tag{3.30}$$

the simplest kernel $K_{i,j}$ is obtained by using different unit-cell coverings of the computational lattice for different terms in the continuum action. For example, to discretize the ρ-derivative term

$$2\pi\int\rho d\rho\int dz\tfrac{1}{2}\varepsilon(\rho,z)\left[\frac{\partial\varphi}{\partial\rho}\right]^2 \ , \tag{3.31a}$$

one uses the "ρ-derivative covering" shown in Fig. 9(a), in which the unit cell contains two lattice nodes differing in their i index, and from which one gets

$$K_{i,j}^{(\rho)}=2\pi\tfrac{1}{2}\rho_{i+1/2}\varepsilon_{i+1/2,j}\left[\frac{\varphi_{i+1,j}-\varphi_{i,j}}{\Delta\rho}\right]^2 \ . \tag{3.31b}$$

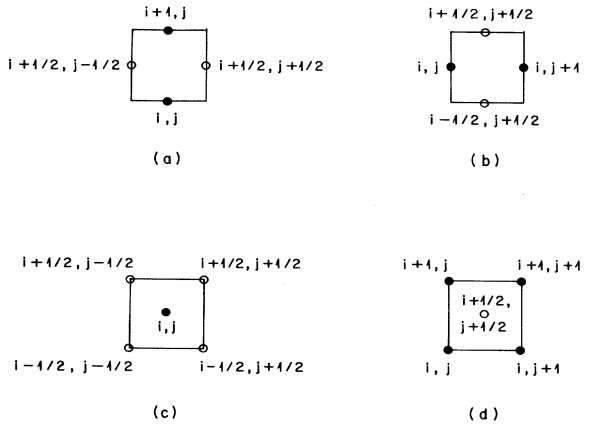

FIG. 9. The unit cells for (a) the "ρ-derivative covering," (b) the "z-derivative covering," (c) the "nonderivative covering," and (d) the "ρ,z derivative covering." Darkened circles (●) denote points of the computational lattice; open circles (○) denote points of the half-node lattice. See the discussion in Sec. III.B and Table I.

Similarly, to discretize the z-derivative term

$$2\pi \int \rho d\rho \int dz \tfrac{1}{2}\varepsilon(\rho,z)\left[\frac{\partial\varphi}{\partial z}\right]^2, \tag{3.32a}$$

one uses the "z-derivative covering" shown in Fig. 9(b), in which the unit cell contains two lattice nodes differing in their j index, and which yields

$$K^{(z)}_{i,j}=2\pi\tfrac{1}{2}\rho_i\varepsilon_{i,j+1/2}\left[\frac{\varphi_{i,j+1}-\varphi_{i,j}}{\Delta z}\right]^2. \tag{3.32b}$$

In discretizing the examples of Sec. II, we will also encounter nonderivative terms, for which one uses the "nonderivative covering" of Fig. 9(c), and an antisymmetrized mixed ρ,z derivative term, for which one uses the "ρ,z derivative covering" of Fig. 9(d). The results of using these four unit-cell choices to discretize the various continuum Lagrangian terms which appear in this paper are summarized in Table I, in which the abbreviated notation h denotes a collection of factors which are defined on the half-node lattice.

Up to this point we have ignored the question of what happens when a nodal variable $\varphi_{i,j}$ in Eq. (3.30) lies on the boundary of the computational mesh. In this case either one nearest neighbor (for i,j on an edge of the mesh) or two nearest neighbors (for i,j at a corner of the mesh) can lie outside the computational mesh proper, and the kernels $K_{i,j}$ linking these exterior neighbors to $\varphi_{i,j}$ are to be omitted from Eq. (3.30). Rather than separately programming these special cases of $K_{i,j}$, it is simpler to extend the computational mesh by one cell at the edges, giving the "bordered" mesh shown in Fig. 10, with the h factors of Table I defined to be zero at the half nodes within the border. Equation (3.30) can then be used over all of the original computational mesh (which lies within the inner edge of the border), irrespective of the values as-

TABLE I. Use of the coverings of Fig. 9 to reduce continuum Lagrangian terms to discrete form. In the following, f,f_1,f_2 denote field variables defined on the computational lattice, while h denotes a collection of factors defined on the half-node lattice.

Continuum Lagrangian term	Unit cell	Discrete form
$\int d\rho \int dz\, h\left[\frac{\partial f}{\partial \rho}\right]^2$	Fig. 9(a)	$\sum_i \sum_j \Delta\rho\Delta z\,\frac{1}{2}(h_{i+1/2,j+1/2}+h_{i+1/2,j-1/2}) \times (f_{i+1,j}-f_{i,j})^2/(\Delta\rho)^2$
$\int d\rho \int dz\, h f_1 \frac{\partial f_2}{\partial \rho}$	Fig. 9(a)	$\sum_i \sum_j \Delta\rho\Delta z\,\frac{1}{2}(h_{i+1/2,j+1/2}+h_{i+1/2,j-1/2}) \times \frac{1}{2}(f_{1i+1,j}+f_{1i,j})(f_{2i+1,j}-f_{2i,j})/\Delta\rho$
$\int d\rho \int dz\, h\left[\frac{\partial f}{\partial z}\right]^2$	Fig. 9(b)	$\sum_i \sum_j \Delta\rho\Delta z\,\frac{1}{2}(h_{i+1/2,j+1/2}+h_{i-1/2,j+1/2}) \times (f_{i,j+1}-f_{i,j})^2/(\Delta z)^2$
$\int d\rho \int dz\, h f_1 \frac{\partial f_2}{\partial z}$	Fig. 9(b)	$\sum_i \sum_j \Delta\rho\Delta z\,\frac{1}{2}(h_{i+1/2,j+1/2}+h_{i-1/2,j+1/2}) \times \frac{1}{2}(f_{1i,j+1}+f_{1i,j})(f_{2i,j+1}-f_{2i,j})/\Delta z$
$\int d\rho \int dz\, hf$	Fig. 9(c)	$\sum_i \sum_j \Delta\rho\Delta z \times \frac{1}{4}(h_{i+1/2,j+1/2}+h_{i+1/2,j-1/2} +h_{i-1/2,j-1/2}+h_{i-1/2,j+1/2})f_{i,j}$
$\int d\rho \int dz\, h \times\left[\frac{\partial f_1}{\partial\rho}\frac{\partial f_2}{\partial z}-\frac{\partial f_1}{\partial z}\frac{\partial f_2}{\partial\rho}\right]$	Fig. 9(d)	$\sum_i \sum_j \Delta\rho\Delta z h_{i+1/2,j+1/2} \times \frac{1}{2}[(f_{1i+1,j}-f_{1i,j+1})(f_{2i+1,j+1}-f_{2i,j}) -(f_{1i+1,j+1}-f_{1i,j})(f_{2i+1,j}-f_{2i,j+1})]/(\Delta\rho\Delta z)$

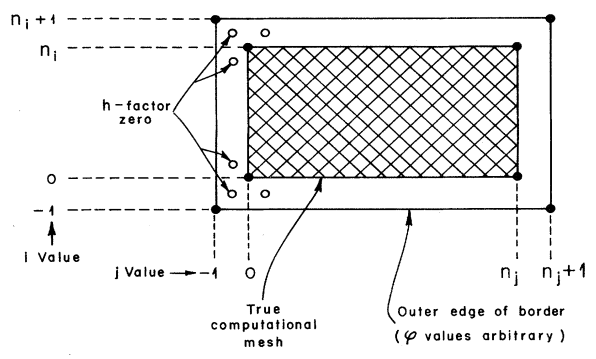

FIG. 10. Computational mesh extended by one unit cell to form a border. At the half nodes within the border, the h factors of Table I are assigned the value zero. The corresponding summation limits for the four coverings of Fig. 9 are given in Table II.

signed to φ at nodes on the outer edge of the border, since these nodes automatically appear multiplied by an h factor of zero. When this procedure is used, the summation limits for the four coverings of Figs. 9(a)—9(d) are as given in Table II.

C. Iterative methods of solution

Let us now suppose that the discretization procedure of the preceding section has been carried out on a computational lattice with n_i+1, n_j+1 nodes in the ρ,z directions, respectively. Equation (3.25) then gives us a set of $N=(n_i+1)(n_j+1)$ linear equations in the N unknown variables $\varphi_{i,j}$. Since N is typically a very large number (up to $\approx 4\times 10^4$ in the computations described in Sec. IV), the direct solution of this set of equations by matrix inversion is not feasible, and we must resort instead to an iterative method of solution.

Before describing the specific algorithms used to solve Eq. (3.25), let us first discuss a simple and familiar iterative method which will also be needed in the applications of Sec. IV. This is the Newton iteration for finding the roots of the equation

$$f(w)=0\ , \tag{3.33}$$

which is constructed as follows. Given an estimate $w^{(n)}$ of a root w^* of Eq. (3.33), we Taylor expand $f(w)$ around $w^{(n)}$, giving

$$f(w)=f(w^{(n)})+(w-w^{(n)})f'(w^{(n)}) +\tfrac{1}{2}(w-w^{(n)})^2 f''(w^{(n)})+\cdots\ . \tag{3.34}$$

When substituted into Eq. (3.33), Eq. (3.34) gives an exact power-series equation for w^*. When Eq. (3.34) is approximated by the first two terms in the series expansion, it gives a new approximation to w^*,

$$w^*\approx w^{(n+1)}=w^{(n)}-\frac{f(w^{(n)})}{f'(w^{(n)})}\ . \tag{3.35}$$

The error of the new approximation can be estimated by subtracting the two equations

$$0=f(w^{(n)})+(w^{(n+1)}-w^{(n)})f'(w^{(n)})\ , \tag{3.36a}$$

$$0=f(w^{(n)})+(w^*-w^{(n)})f'(w^{(n)})+\tfrac{1}{2}(w^*-w^{(n)})^2 f''(w^{(n)}) +O[(w^*-w^{(n)})^3]\ ,$$

giving

$$w^{(n+1)}-w^*\approx \tfrac{1}{2}(w^{(n)}-w^*)^2\frac{f''(w^{(n)})}{f'(w^{(n)})}+O[(w^{(n)}-w^*)^3] \approx \tfrac{1}{2}(w^{(n)}-w^*)^2\frac{f''(w^*)}{f'(w^*)}+O[(w^{(n)}-w^*)^3]\ . \tag{3.36b}$$

Hence the error after $n+1$ iterations is of order the square of the error after n iterations, and convergence proceeds very rapidly to w^*, provided that the initial guess $w^{(0)}$ lies close enough to w^*. Rewriting Eq. (3.36b) as

$$\frac{|w^{(1)}-w^*|}{|w^{(0)}-w^*|}\approx \tfrac{1}{2}|w^{(0)}-w^*|\left|\frac{f''(w^*)}{f'(w^*)}\right| +O[(w^{(0)}-w^*)^2]\ , \tag{3.37a}$$

we see that a sufficient condition on $w^{(0)}$ to guarantee that the Newton iteration converges to the root w^* is

TABLE II. Summation limits for the coverings of Fig. 9, using the "bordered" mesh of Fig. 10.

Unit cell	Lower i,j limits	Upper i limit	Upper j limit
"ρ-derivative covering" Fig. 9(a)	0	n_i-1	n_j
"z-derivative covering" Fig. 9(b)	0	n_i	n_j-1
"nonderivative covering" Fig. 9(c)	0	n_i	n_j
"ρ,z derivative covering" Fig. 9(d)	0	n_i-1	n_j-1

$$\tfrac{1}{2}\,|\,w^{(0)}-w^*\,|\,\left|\frac{f''(w^*)}{f'(w^*)}\right|\ll 1\ . \tag{3.37b}$$

If Eq. (3.33) has several roots $w_1^*, w_2^*, \ldots$, there will be an interval around each root w_i^* within which the Newton iteration converges to that root.

Let us now proceed to the simplest case in which we encounter the iterative method which will be used to solve Eq. (3.25). We consider the discrete functional

$$L=\tfrac{1}{2}\sum_{r=1}^{N}\sum_{s=1}^{N}A_{rs}\varphi_r\varphi_s-\sum_{r=1}^{N}J_r\varphi_r\ , \tag{3.38}$$

with A_{rs} a real, symmetric matrix with positive eigenvalues. Since the matrix A_{rs} is invertible, L attains a unique minimum when the nodal variables $\varphi_r, r=1,\ldots,N$ satisfy the N linear equations

$$0=\frac{\partial L}{\partial\varphi_r}\Longrightarrow\sum_{s=1}^{N}A_{rs}\varphi_s=J_r\ . \tag{3.39}$$

An iterative method for finding this minimum can now be constructed as follows. Let us repeatedly sweep through the φ_r, proceeding from φ_1 to φ_N and then starting over again with φ_1,

$$\begin{aligned}&\varphi_1,\ldots,\varphi_N,\varphi_1,\ldots,\varphi_N,\ldots,\\ &\text{first sweep, second sweep, }\ldots,\end{aligned} \tag{3.40}$$

at each step replacing the variable φ_R being considered by the value which minimizes L when all other variables $\varphi_r, r\neq R$ are held fixed. Specifically, let $\varphi_r^{(n)}$ be the values of all the nodal variables when the sweep reaches the variable φ_R, so that at this stage L has the value

$$L^{(n)}=\tfrac{1}{2}\sum_{r=1}^{N}\sum_{s=1}^{N}A_{rs}\varphi_r^{(n)}\varphi_s^{(n)}-\sum_{r=1}^{N}J_r\varphi_r^{(n)}\ . \tag{3.41}$$

Regarding L as a function of the single variable φ_R, with the other variables fixed, we have

$$\begin{aligned}L=&\tfrac{1}{2}\varphi_R^2A_{RR}+\varphi_R\left[\sum_{s\neq R}A_{Rs}\varphi_s^{(n)}-J_R\right]\\&+\tfrac{1}{2}\sum_{r\neq R}\sum_{s\neq R}A_{rs}\varphi_r^{(n)}\varphi_s^{(n)}-\sum_{r\neq R}J_r\varphi_r^{(n)}\ .\end{aligned} \tag{3.42}$$

Choosing $\varphi_R^{(n+1)}$ to minimize Eq. (3.42) with respect to φ_R, we get

$$\begin{aligned}\varphi_R^{(n+1)}&=-\frac{1}{A_{RR}}\left[\sum_{s\neq R}A_{Rs}\varphi_s^{(n)}-J_R\right]=\varphi_R^{(n)}+\Delta\varphi_R^{(n)}\ ,\\ \Delta\varphi_R^{(n)}&=-\frac{1}{A_{RR}}\left[\sum_{s}A_{Rs}\varphi_s^{(n)}-J_R\right]\ ,\end{aligned} \tag{3.43}$$

giving as the corresponding change in the action

$$\begin{aligned}L^{(n+1)}-L^{(n)}&=\tfrac{1}{2}[(\varphi_R^{(n+1)})^2-(\varphi_R^{(n)})^2]A_{RR}\\&\quad+(\varphi_R^{(n+1)}-\varphi_R^{(n)})\left[\sum_{s\neq R}A_{Rs}\varphi_s^{(n)}-J_R\right]\\&=\tfrac{1}{2}\Delta\varphi_R^{(n)}(\Delta\varphi_R^{(n)}+2\varphi_R^{(n)})A_{RR}\\&\quad+\Delta\varphi_R^{(n)}(-A_{RR}\Delta\varphi_R^{(n)}-A_{RR}\varphi_R^{(n)})\\&=-\tfrac{1}{2}A_{RR}(\Delta\varphi_R^{(n)})^2<0\ .\end{aligned} \tag{3.44}$$

(In the final line we have used the fact that since the matrix A_{rs} has positive eigenvalues, the diagonal matrix elements A_{RR} are all positive.) Hence, under the iteration of Eq. (3.40), the Lagrangian is monotone decreasing. In problems of physical interest with positive definite A_{rs}, we expect the Lagrangian with the source term included to be bounded from below. Equations (3.44) and (3.43) then guarantee that in the limit as n becomes infinite, the $L^{(n)}$'s converge to the minimum value of L, while the $\varphi_r^{(n)}$'s converge to the solution of Eq. (3.39). This method of solving the system of Eq. (3.39) is known as the Gauss-Seidel iteration.

As we have just seen, in the Gauss-Seidel iteration each nodal variable is successively relaxed to the value which, at that stage of the iteration, minimizes L. An important variant of the basic method, called the successively over-relaxed (SOR) Gauss-Seidel iteration, is defined by the recipe

$$\begin{aligned}\varphi_R^{(n)}\to\varphi_R^{(n+1),\mathrm{SOR}}&=\varphi_R^{(n)}+\omega\Delta\varphi_R^{(n)}\\&=\omega\varphi_R^{(n+1)}+(1-\omega)\varphi_R^{(n)},\quad\omega\geq 1\ ,\end{aligned} \tag{3.45}$$

with $\varphi_R^{(n+1)}$ and $\Delta\varphi_R^{(n)}$ given by Eq. (3.43). In other words, instead of relaxing $\varphi_R^{(n)}$ to the value which minimizes L, one systematically overshoots beyond this value. Using the over-relaxed iteration, the change in the Lagrangian is

$$\begin{aligned}L^{(n+1),\mathrm{SOR}}-L^{(n)}&=\tfrac{1}{2}[(\varphi_R^{(n+1),\mathrm{SOR}})^2-(\varphi_R^{(n)})^2]A_{RR}+(\varphi_R^{(n+1),\mathrm{SOR}}-\varphi_R^{(n)})\left[\sum_{s\neq R}A_{Rs}\varphi_s^{(n)}-J_R\right]\\&=\tfrac{1}{2}\omega\Delta\varphi_R^{(n)}(\omega\Delta\varphi_R^{(n)}+2\varphi_R^{(n)})A_{RR}+\omega\Delta\varphi_R^{(n)}(-A_{RR}\Delta\varphi_R^{(n)}-A_{RR}\varphi_R^{(n)})\\&=-\tfrac{1}{2}\omega(2-\omega)A_{RR}(\Delta\varphi_R^{(n)})^2\ .\end{aligned} \tag{3.46}$$

Thus provided that

$$0<\omega<2\ , \tag{3.47}$$

the Lagrangian remains monotone decreasing, and the SOR iteration still converges to the solution of Eq. (3.39).

For a general, symmetric matrix A_{rs}, each individual iteration step in Eq. (3.43) involves evaluating a sum of N terms, which would be computationally costly for large N. However, in the specific problems to which we will apply iterative methods, r and s are composite indices

$$\begin{aligned} r&=(i,j)\ , \\ s&=(i',j')\ , \end{aligned} \tag{3.48}$$

denoting nodes of the computational lattice, and A_{rs} is a sparse matrix in which A_{Rs} is nonvanishing only for a small number of index values s for each R. Because we have followed the prescription of squaring before averaging to ensure that the discretized action contains only nearest-neighbor couplings, we find in fact that A_{Rs} is nonvanishing only for the five index values s corresponding to the node R and its four nearest neighbors. Hence each iteration step involves only a short computation which is independent of the size of the computational lattice. If the sweep is performed[28] in "typewriter ordering"

$$\begin{aligned} &(i,j):(0,0),(1,0),\ldots,(n_i,0),(0,1),(1,1),\ldots,(n_i,1)\ , \\ &\ldots,(0,n_j),(1,n_j),\ldots,(n_i,n_j)\ , \end{aligned} \tag{3.49}$$

then the over-relaxed iteration for Eq. (3.25) is

$$\begin{aligned} &\varphi_{i,j}^{(n)}\rightarrow\varphi_{i,j}^{(n+1),\mathrm{SOR}}=\omega\varphi_{i,j}^{(n+1)}+(1-\omega)\varphi_{i,j}^{(n)}\ , \\ &\varphi_{i,j}^{(n+1)}=\left[\left[\frac{\Delta z}{\Delta\rho}+\frac{\Delta\rho}{\Delta z}\right](h_{i+1/2,j+1/2}+h_{i+1/2,j-1/2}+h_{i-1/2,j+1/2}+h_{i-1/2,j-1/2})\right]^{-1} \\ &\quad\times\left[\frac{\Delta z}{\Delta\rho}(h_{i+1/2,j+1/2}+h_{i+1/2,j-1/2})\varphi_{i+1,j}^{(n)}+\frac{\Delta z}{\Delta\rho}(h_{i-1/2,j+1/2}+h_{i-1/2,j-1/2})\varphi_{i-1,j}^{(n+1)}\right. \\ &\quad+\frac{\Delta\rho}{\Delta z}(h_{i+1/2,j+1/2}+h_{i-1/2,j+1/2})\varphi_{i,j+1}^{(n)}+\frac{\Delta\rho}{\Delta z}(h_{i+1/2,j-1/2}+h_{i-1/2,j-1/2})\varphi_{i,j-1}^{(n+1)} \\ &\quad\left.+\frac{Q}{\pi}\delta_{i,0}(\delta_{j,n_Q}-\delta_{j,-n_Q})\right],\quad h_{i+1/2,j+1/2}\equiv\rho_{i+1/2}\varepsilon_{i+1/2,j+1/2}\ . \end{aligned} \tag{3.50}$$

Equation (3.50) applies to all i,j in the range $0\le i\le n_i$, $0\le j\le n_j$, since, by virtue of the "bordering" procedure discussed above in Sec. III.B, all nodal values with indices outside this range appear in Eq. (3.50) multiplied by vanishing h factors. An initial guess $\varphi_{i,j}^{(0)}$ must be supplied as an input to the iterative process. In practice, to achieve a poor-man's version of the "hierarchical" iterative schemes (see below), we follow the procedure of first iterating to convergence on a very coarse mesh starting from a specified $\varphi_{i,j}^{(0)}$, which is chosen to be reasonably close (without sacrificing simplicity)[29] to the anticipated solution of the problem. We then successively double the mesh and iterate to convergence, taking as the new initial guess after each doubling a linear interpolation of the converged $\varphi_{i,j}$ values on the preceding coarser mesh.

According to the discussion of Eqs. (3.41)—(3.47), an iteration with $\omega=1$ produces the largest possible *single-step* reduction in the Lagrangian L. Hence at the beginning of an iterative solution one always makes three to ten complete passes through the computational lattice with $\omega=1$ (or with an ω which is gradually increased starting from 1) to eliminate the largest deviations between the initial guess $\varphi_{i,j}^{(0)}$ and the fully converged solution $\varphi_{i,j}^{(\infty)}$. After these initial iterations, the optimal strategy is to use an ω value larger than 1. The reason is that a general analysis[30] of the iterative process shows that in the asymptotic large-n limit, the difference $\varphi_{i,j}^{(n)}-\varphi_{i,j}^{(\infty)}$ behaves as

$$\varphi_{i,j}^{(n)}-\varphi_{i,j}^{(\infty)}\sim ce^{-n\gamma(\omega)}\ , \tag{3.51}$$

with the decay constant $\gamma(\omega)$ attaining its maximum at an ω value $\omega=\omega_{\mathrm{opt}}$, $1<\omega_{\mathrm{opt}}<2$. Hence one clearly achieves the maximum rate of convergence by letting ω tend to ω_{opt} from below after the initial iterations. Values of ω larger than ω_{opt} should be avoided, since in general they produce slower convergence than values of ω an equivalent distance below ω_{opt}, and since they can lead to instabilities in nonlinear problems. The optimum value of ω can be estimated from the formula [Garabedian (1956)]

$$\omega_{\mathrm{opt}}\approx\frac{2}{1+Ch}\ , \tag{3.52}$$

[28]This terminology has been borrowed from Hockney and Eastwood (1981), who discuss alternative sweeps as well.

[29]In practice, there is no great gain in convergence to be achieved by using elaborate functional forms in the initial guess.

[30]See the books cited at the end of Sec. III.A for details.

with

$$h=(n_i n_j)^{-1/2} \tag{3.53}$$

a measure of the fineness of the computational lattice, and with C a constant which depends on the lattice geometry and the boundary conditions. (For the two-dimensional Laplace equation in rectangular coordinates with Dirichlet boundary conditions, $C\sim 3$.) An empirical method for estimating the value of $\omega_{\rm opt}$ is discussed below in Sec. III.G; from the general form of Eq. (3.52) we infer the useful fact that when the computational mesh is doubled, so that

$$\begin{aligned} &n_i\to 2n_i,\quad n_j\to 2n_j\ , \\ &h\to h/2\ , \end{aligned} \tag{3.54}$$

the corresponding change in $\omega_{\rm opt}$ is

$$\omega_{\rm opt}\to\frac{4\omega_{\rm opt}}{2+\omega_{\rm opt}}\ . \tag{3.55}$$

An intuitive (and mathematically correct) way to visualize the over-relaxation algorithm is to think of n as a time step and of the algorithm as a time-dependent dissipative process, with a steady-state equilibrium at the converged solution $\varphi_{i,j}^{(\infty)}$. The starting guess $\varphi_{i,j}^{(0)}$ in general deviates from $\varphi_{i,j}^{(\infty)}$ by both large localized transients and by relatively smooth errors. The initial iterations with $\omega=1$ are used to rapidly eliminate the localized transients. The later iterations with $\omega=\omega_{\rm opt}$ minimize the relatively long time constant $[\gamma(\omega)]^{-1}$ with which the smooth errors damp away. The optimal use of the over-relaxation method requires attention to eliminating both localized transients and smooth (or long-range) errors. One method of doing this in a systematic way is the "Chebyshev acceleration" method described by Hockney and Eastwood (1981), in which the lattice is scanned using an "even-odd checkerboard ordering" (as opposed to "typewriter ordering") and in which ω is incremented from $\omega=1$ to $\omega=\omega_{\rm opt}$ in a prescribed way at the beginning of each even-semilattice and each odd-semilattice sweep. A second way of accomplishing this is through various "hierarchical" schemes[31] in which the full computational lattice is scanned in only a fraction of the sweeps, with the remaining sweeps used to scan sublattices of the basic lattice, constructed by using a larger unit cell containing two, four, etc., fundamental unit cells. The Chebyshev acceleration and hierarchical schemes can be proved to be optimal ones, according to well-defined criteria, for solving elliptical partial differential equation problems based on the Laplacian (∇^2) and similar linear operators. Since for nonlinear problems it usually is not possible explicitly to construct an optimal algorithm, we use instead a simpler method which is effectively equivalent. As discussed above, what we do is to start the iteration on a very small (typically 7×7) computational lattice, iterate to convergence, and then use an interpolation of this solution as the initial guess for iteration on a computational mesh which has been doubled as in Eq. (3.54), and so forth. After each doubling, ω is reset to 1 for several iterations to eliminate transients arising from the interpolation (these are strongly evident in the unit cells along the axis of rotation) and then increased to the $\omega_{\rm opt}$ appropriate to the new mesh spacing h. This procedure gives very satisfactory convergence and automatically generates a sequence of fully converged L values on progressively finer meshes, permitting an examination of the convergence of the discrete solution as the mesh spacing h approaches zero.

Let us consider next the imposition of boundary conditions in carrying out the iterative solution. From Eqs. (3.1)—(3.3), we see that the differential equation and boundary conditions of our dielectric model are invariant, and the source current j^0 changes sign, under the reflection operation $z\to -z$. This implies that the solution φ also has odd reflection symmetry, and vanishes on the equatorial plane $z=0$. Although this symmetry emerges automatically if the boundary value problem of Eqs. (3.1)—(3.3) is solved over the full physical space $0\le\rho<\infty, -\infty<z<\infty$, we can clearly save computer time if we impose the symmetry at the outset, by solving instead a boundary value problem on the half space $0\le\rho<\infty, 0\le z<\infty$. Similarly, if the source current j^0 were replaced by

$$j'^0=Q\delta(x)\delta(y)[\delta(z-a)+\delta(z+a)]\ , \tag{3.56}$$

which is invariant under the reflection $z\to -z$, then the corresponding solution φ would have even reflection symmetry, and $\partial_z\varphi$ would vanish at $z=0$. Again, although this symmetry would emerge automatically from the full-space boundary-value problem, we can halve the computational effort by using the symmetry to reduce the computation to an equivalent half-space boundary-value problem.

When we solve the numerical problem on a half space, we introduce an inner boundary $z=0, 0\le\rho<\infty$ on which a boundary condition must be specified, together with the outer boundary condition of Eq. (3.3). On this inner boundary, the appropriate boundary conditions are, respectively, the Dirichlet or Neumann conditions,

$$\varphi=0 \text{ at } z=0,\ j^0 \text{ odd [Eq. (3.1)]}\ , \tag{3.57a}$$

$$\partial_z\varphi=0 \text{ at } z=0,\ j^0 \text{ even [Eq. (3.56)]}\ , \tag{3.57b}$$

and we must translate each of these into a corresponding updating algorithm for the lattice nodes on the line $z=0$. (The more general Robin or mixed boundary condition $\alpha\varphi+\beta\partial_z\varphi=0$ can also be implemented computationally, but will not be encountered in any of the models studied in this paper.) In addition, in either the full-space or half-space problems, there is an inner coordinate boundary

[31] Hierarchical over-relaxation methods have been discussed, for example, by Brandt (1977) and Press (1978).

(but not a physical boundary) at $\rho=0$, which must also be dealt with by an appropriate updating algorithm for the lattice nodes on the line $\rho=0$.

To infer the appropriate updating algorithms for the boundaries, let us examine the variational principle of Eq. (3.1) when restricted to the coordinate quadrant $0\le\rho<\infty, 0\le z<\infty$, keeping all surface terms which result from integrations by parts. We have

$$\begin{aligned}0=\delta L \propto \delta\int_0^\infty \rho d\rho \int_0^\infty dz\{\tfrac{1}{2}\varepsilon[(\partial_\rho\varphi)^2+(\partial_z\varphi)^2]-j^0\varphi\}\\ =-\int_0^\infty \rho d\rho\int_0^\infty dz\delta\varphi\left[\frac{1}{\rho}\frac{\partial}{\partial\rho}\left[\rho\varepsilon\frac{\partial\varphi}{\partial\rho}\right]+\frac{\partial}{\partial z}\left[\varepsilon\frac{\partial\varphi}{\partial z}\right]+j^0\right]+\int_0^\infty dz(\varepsilon\rho\partial_\rho\varphi\delta\varphi)_{\rho=\infty}+\int_0^\infty \rho d\rho(\varepsilon\partial_z\varphi\delta\varphi)_{z=\infty}\\ -\int_0^\infty \rho d\rho(\varepsilon\partial_z\varphi\delta\varphi)_{z=0}-\int_0^\infty dz(\varepsilon\rho\partial_\rho\varphi\delta\varphi)_{\rho=0}\,,\end{aligned}\tag{3.58}$$

and the differential equation of Eq. (3.2) follows when the surface terms all vanish. The surface terms at infinity vanish by virtue of the Dirichlet outer-boundary condition of Eq. (3.3), which guarantees that $\delta\varphi\,|_{\rho=\infty}=\delta\varphi\,|_{z=\infty}=0$. (All statements about a Dirichlet boundary condition $\varphi=0$ generalize immediately to a Dirichlet condition $\varphi=\psi$, with ψ a specified function.) Assuming that the computational mesh effectively extends to infinity, this condition can be imposed by equating to zero the nodal variables at the edges of the computational mesh,

$$\varphi^{(n)}_{i,n_j}=\varphi^{(n)}_{n_i,j}=0, \text{ for all } n \text{ and all } i,j\,. \tag{3.59a}$$

In the case when j^0 is an odd function of z, the surface term at $z=0$ vanishes by virtue of the Dirichlet boundary condition of Eq. (3.57a), which guarantees that $\delta\varphi\,|_{z=0}=0$, and which can be implemented by equating to zero the nodal variables on the line $z=0$,

$$\text{Eq.(3.57a)} \Longleftrightarrow \varphi^{(n)}_{i,0}=0, \text{ for all } n \text{ and all } i\,. \tag{3.59b}$$

In the case when j^0 is an even function of z, the surface term at $z=0$ vanishes by virtue of the Neumann boundary condition of Eq. (3.57b). Since $\partial_z\varphi\,|_{z=0}$ appears in Eq. (3.58) multiplied by $\delta\varphi\,|_{z=0}$, the Neumann boundary condition follows from requiring that δL be stationary with respect to all variations, including variations in the boundary value $\varphi\,|_{z=0}$.[32] Hence the boundary condition of Eq. (3.57b) can be implemented computationally by iterating the nodal variables on the line $z=0$ with the algorithm of Eq. (3.50),

$$\text{Eq. (3.57b)} \Longleftrightarrow \varphi^{(n)}_{i,0} \text{ iterated according to Eq. (3.50)}\,. \tag{3.59c}$$

Finally, let us consider the surface term at the coordinate boundary $\rho=0$. In the discretized version of Eq. (3.58), the factor ρ is evaluated at the nearest point to the axis on the half-node lattice. Hence the final term in Eq. (3.58) behaves as

$$-\int_0^\infty dz\varepsilon\tfrac{1}{2}\Delta\rho(\partial_\rho\varphi\delta\varphi)_{\rho=0}\,, \tag{3.59d}$$

and vanishes either if (i) the physics of the problem specifies a Dirichlet boundary condition $\varphi=\psi$ on the rotational axis, or if (ii) the physics of the problem leaves φ on the rotational axis to be determined by the variational principle, in which case φ is freely iterated,

$$\begin{aligned}&\text{(i)} \Longrightarrow \varphi^{(n)}_{0,j}=\psi_j, \text{ all } j \text{ and } n\,,\\ &\text{(ii)} \Longrightarrow \varphi^{(n)}_{0,j} \text{ iterated according to Eq. (3.50).}\end{aligned}\tag{3.59e}$$

The second case in Eq. (3.59e) is the alternative which applies at $\rho=0$ in the model of Eqs. (3.1)—(3.3) (and also is the alternative which always applies at the end points $\eta=0,\pi$ of the bispherical coordinates introduced in Sec. III.D below). To summarize, the boundary conditions encountered in this paper are dealt with by one of two updating algorithms for the nodal values lying on the boundaries of the computational mesh: either these nodal values are constrained by a Dirichlet boundary condition and are not iterated, or (in the "bordered" mesh scheme introduced at the end of Sec. III.B) they are updated using the same algorithm used for the interior nodes.[33]

In the discussion of relaxation methods given above, we based our convergence proof on the assumption that the matrix A_{rs} is symmetric and has positive eigenvalues. While this is a sufficient condition for the convergence of the over-relaxation algorithm, it is *not* a necessary condition, and convergence can be proved under much weaker conditions on the matrix A_{rs} [see Ames (1977), p. 101]. The practical implementation of the over-relaxation recipe in these more general cases remains the same as in Eqs. (3.43) and (3.45) above.

[32]The same result follows from considering the discrete problem in the full plane, where the condition

$$0=(\partial_z\varphi)_{i,0}=\frac{1}{2\Delta z}(\varphi_{i,1}-\varphi_{i,-1})$$

leaves the nodal value $\varphi_{i,0}$ unconstrained.

[33]In the case of Robin or mixed boundary conditions, the nodal values on the boundary would be updated using a different algorithm from that used for the interior points.

D. Use of Jacobian transformations

In reducing the Lagrangian functional L of Eq. (3.19) to discrete form, it is not necessary to use the physical coordinates ρ,z as the computational coordinates. In situations in which the Lagrangian density is sharply peaked, it is often advantageous to concentrate the mesh nodes where the Lagrangian density is largest, while at the same time preserving the convenience of working with a uniformly spaced computational mesh. This can be accomplished by making a Jacobian transformation from ρ,z to new computational variables ξ_1,ξ_2,

$$\begin{aligned} &\rho=F(\xi_1,\xi_2)\ , \\ &z=G(\xi_1,\xi_2)\ , \\ &d\rho dz=\left|\frac{\partial(F,G)}{\partial(\xi_1,\xi_2)}\right| d\xi_1 d\xi_2\ , \end{aligned} \tag{3.60}$$

with ξ_1,ξ_2 chosen to be an orthogonal coordinate family. The simplest orthogonal transformation is

$$\begin{aligned} &(\xi_1,\xi_2)=(\rho',z')\ , \\ &\rho=F(\rho')\ , \\ &z=G(z')\ , \\ &d\rho dz=J_\rho J_z d\rho' dz',\ \partial_\rho=J_\rho^{-1}\partial_{\rho'},\ \partial_z=J_z^{-1}\partial_{z'}\ , \\ &J_\rho=\left|\frac{\partial F}{\partial \rho'}\right|,\ J_z=\left|\frac{\partial F}{\partial z'}\right|\ , \end{aligned} \tag{3.61}$$

corresponding to an independent stretching (or compression) of the coordinates in the ρ,z directions. Assuming that $\rho=0,z=a$ is the image of $\rho'=0$, $z'=a'$, the Lagrangian functional in the new variables is

$$L=2\pi\int_0^\infty \rho J_\rho d\rho' \int_{-\infty}^{\infty} J_z dz' \tfrac{1}{2}\varepsilon(\rho,z)\left[\frac{1}{J_\rho^2}\left[\frac{\partial\varphi}{\partial\rho'}\right]^2+\left[\frac{1}{J_z}\right]^2\left[\frac{\partial\varphi}{\partial z'}\right]^2\right]-Q\varphi(\rho'=0,z'=a')+Q\varphi(\rho'=0,z'=-a')\ . \tag{3.62}$$

In the reduction of Eq. (3.62) to discrete form it is again convenient to use both node and half-node meshes, with φ specified on the nodes and with ρ, J_ρ, J_z, and ε specified on the half nodes. The half-node factors in each term of the action are then lumped together in the factors h of Table I, which applies with the obvious substitutions $\rho\to\rho',z\to z'$.

A second useful coordinate transformation, which will be applied to the study of the confining model of Sec. II.D, involves the introduction of bispherical coordinates μ,η [see Morse and Feshbach (1953), p. 1298],

$$\begin{aligned} &z=v^{-1}a\sinh\mu,\ \ \rho=v^{-1}a\sin\eta\ , \\ &v=\cosh\mu-\cos\eta,\ \ -\infty<\mu<\infty,\ \ 0\le\eta\le\pi\ , \\ &\rho d\rho dz=\frac{a^3}{v^3}\sin\eta d\eta d\mu, \end{aligned} \tag{3.63a}$$

$$|\nabla\varphi|=\frac{v}{a}\left[\left[\frac{\partial\varphi}{\partial\mu}\right]^2+\left[\frac{\partial\varphi}{\partial\eta}\right]^2\right]^{1/2},$$

in terms of which the Lagrangian integral becomes

$$L=2\pi\int_0^\pi \sin\eta d\eta\int_{-\infty}^{\infty} d\mu\frac{a}{v}\tfrac{1}{2}\varepsilon(\rho,z)\left[\left[\frac{\partial\varphi}{\partial\mu}\right]^2+\left[\frac{\partial\varphi}{\partial\eta}\right]^2\right]$$
$$-Q\varphi(\mu=\infty)+Q\varphi(\mu=-\infty)\ . \tag{3.63b}$$

As the name of these coordinates suggests, in the limits $\mu\to\pm\infty$ the coordinate surfaces approach concentric spheres around the charges at $\rho=0,z=\pm a$, e.g.,

$$\begin{aligned} &\mu\gg1\Rightarrow\rho=2ae^{-\mu}\sin\eta+O(e^{-2\mu})\ , \\ &z=a+2ae^{-\mu}\cos\eta+O(e^{-2\mu})\ . \end{aligned} \tag{3.63c}$$

Also, spheres of constant $\tilde{r}=(\mu^2+\eta^2)^{1/2}$ around the origin of bispherical coordinates $(\mu,\eta)=(0,0)$ correspond, in the limit $\tilde{r}\to0$, to spheres of radius $r\approx2a/\tilde{r}\to\infty$ in the physical coordinate space. To reduce Eq. (3.63b) to discrete form, we cover the μ,η plane with node and half-node meshes, with φ specified on the nodes and with $\sin\eta$ and v specified on the half nodes. The half-node factors in each term of the action are again lumped together in the factors h of Table I, which applies with the substitutions $\rho\to\eta,z\to\mu$.

E. Removal of the Coulomb singularity

In order to extract a finite static potential V_{static} from the example of Eqs. (3.1)–(3.3), and from the models of Secs. II.C and II.D, it is necessary to remove the infinite Coulomb self-energy associated with the point-charge sources at $\rho=0,z=\pm a$. One way of doing this, which we illustrate in the case of Eq. (3.1), is by explicit analytic rearrangement of the Lagrangian functional L. For simplicity, let us assume that the varying dielectric constant $\varepsilon(x)$ takes the same value ε_C at the two source charges,

$$\varepsilon_C=\varepsilon(\rho=0,z=\pm a)\ , \tag{3.64a}$$

and let us denote by φ_C the Coulomb solution

$$\varphi_C=\frac{Q}{4\pi\varepsilon_C}\left[\frac{1}{r_{(1)}}-\frac{1}{r_{(2)}}\right],\quad r_{\left[\begin{smallmatrix}1\\2\end{smallmatrix}\right]}=[\rho^2+(z\mp a)^2]^{1/2}\ , \tag{3.64b}$$

which satisfies

$$\nabla\cdot(\varepsilon_C\nabla\varphi_C)=-j^0\ . \tag{3.64c}$$

To remove the infinite Coulomb energy from Eq. (3.1), we introduce a new dependent variable ψ defined by

$$\varphi=\varphi_C+\psi\ , \tag{3.65}$$

so that after eliminating j^0 by substituting Eq. (3.64c) and integrating by parts, Eq. (3.1) becomes

$$V_{\text{static}}=-\text{ext}_\psi L_1-L_2\ , \tag{3.66a}$$

$$\begin{aligned}L_1&=\int d^3x\{\tfrac{1}{2}\varepsilon(x)(\nabla\psi)^2\\&\quad+[\varepsilon(x)-\varepsilon_C][\tfrac{1}{2}(\nabla\varphi_C)^2+\nabla\varphi_C\cdot\nabla\psi]\}\ ,\\L_2&=-\int d^3x\tfrac{1}{2}\varepsilon_C(\nabla\varphi_C)^2\ .\end{aligned} \tag{3.66b}$$

Since the functional L_2 is independent of ψ, the equation of motion for ψ is determined by the functional L_1 alone, yielding

$$\begin{aligned}&\nabla\cdot(\varepsilon\nabla\psi)=-\nabla\cdot[(\varepsilon-\varepsilon_C)\nabla\varphi_C]\ ,\\&\psi\to-\varphi_C\ \text{as}\ r\to\infty\ .\end{aligned} \tag{3.67}$$

Provided that $\varepsilon(x)$ varies slowly enough near the source charges, the functional L_1 has no Coulomb self-energy singularities. Consequently, the discretization of L_1 by the methods of the preceding sections gives a numerical determination of ψ and of $\text{ext}_\psi L_1$, which both converge to well-defined limiting values as the spacing of the computational mesh approaches zero.

Although the functional L_2 has no dependence on ψ, it cannot be omitted in calculating V_{static} because it still has a nontrivial dependence on the distance $R=2a$ between the source charges. To separate the infinite Coulomb self-energies correctly from L_2, we must split L_2 into a finite but R-dependent part $L_2(R)$, and an infinite but R-independent piece L_{2C}. This is readily accomplished by substituting Eq. (3.64b) into Eq. (3.66b) and separating off the cross term, giving

$$\begin{aligned}L_2&=L_2(R)+L_{2C}\ ,\\L_2(R)&=\int d^3x\frac{Q^2}{(4\pi)^2\varepsilon_C}\nabla\frac{1}{r_{(1)}}\cdot\nabla\frac{1}{r_{(2)}}\\&=\frac{Q^2}{4\pi R\varepsilon_C},\quad R=2a\ ,\\L_{2C}&=-\int d^3x\frac{Q^2}{(4\pi)^2}\frac{1}{2\varepsilon_C}\left[\left[\nabla\frac{1}{r_{(1)}}\right]^2+\left[\nabla\frac{1}{r_{(2)}}\right]^2\right].\end{aligned} \tag{3.68}$$

Since L_{2C} is simply an infinite constant, it can be omitted from the static potential, giving

$$V_{\text{static}}=\frac{-Q^2}{4\pi R\varepsilon_C}-\text{ext}_\psi L_1\ . \tag{3.69}$$

Equations (3.66a) and (3.69) are the basic formulas for the Coulomb-subtracted static potential when the computational mesh is infinite.

When a finite computational mesh $\rho\le\rho_{\max}$, $|z|\le z_{\max}$ is used, we must take into account the fact that because of the boundary condition $\psi\to-\varphi_C$ at infinity, the contribution to L_1 from outside the computational mesh should not be neglected. Approximating[34] $\psi\approx-\varphi_C$ when $\rho\ge\rho_{\max}$ or $|z|\ge z_{\max}$, and using reflection symmetry in the $z=0$ plane, we have

$$\begin{aligned}L_1&=L_{1\text{ inside}}+L_{1\text{ outside}}\ ,\\L_{1\text{ inside}}&=\int_{\text{inside}}\{\tfrac{1}{2}\varepsilon(\nabla\psi)^2\\&\quad+(\varepsilon-\varepsilon_C)[\tfrac{1}{2}(\nabla\varphi_C)^2+\nabla\varphi_C\cdot\nabla\psi]\}\ ,\\L_{1\text{ outside}}&=\int_{\text{outside}}\{\tfrac{1}{2}\varepsilon(\nabla\psi)^2\\&\quad+(\varepsilon-\varepsilon_C)[\tfrac{1}{2}(\nabla\varphi_C)^2+\nabla\varphi_C\cdot\nabla\psi]\}\\&\approx\int_{\text{outside}}\tfrac{1}{2}\varepsilon_C(\nabla\varphi_C)^2\ ,\\\int_{\text{inside}}&\equiv4\pi\int_0^{\rho_{\max}}\rho d\rho\int_0^{z_{\max}}dz\ ,\\\int_{\text{outside}}&\equiv4\pi\left[\int_{\rho_{\max}}^{\infty}\rho d\rho\int_0^{z_{\max}}dz+\int_0^{\rho_{\max}}\rho d\rho\int_{z_{\max}}^{\infty}dz\right.\\&\quad\left.+\int_{\rho_{\max}}^{\infty}\rho d\rho\int_{z_{\max}}^{\infty}dz\right].\end{aligned} \tag{3.70}$$

The integral for $L_{1\text{ outside}}$ either can be evaluated numerically by using the general formula

$$\begin{aligned}\int_{\text{outside}}F(\rho,z)&=4\pi\rho_{\max}^2z_{\max}\int_0^1du\int_0^1dv[v^{-3}F(v^{-1}\rho_{\max},uz_{\max})\\&\quad+u^{-2}vF(v\rho_{\max},u^{-1}z_{\max})+u^{-2}v^{-3}F(v^{-1}\rho_{\max},u^{-1}z_{\max})],\end{aligned} \tag{3.71a}$$

or it can be transformed, by using Eq. (3.68), into a numerical integral over the inside region and a simpler integral over the outside which can be evaluated analytically,

[34] In the application of the analytic rearrangement method to the Abelian Higgs model (see Appendix C), the analog of the total potential $\varphi=\psi+\varphi_C$ is the total scalar potential $A^0=B^0+A_C^0$, which vanishes exponentially at infinity. Hence in the Abelian Higgs model the analog of the approximation of replacing ψ by $-\varphi_C$ in Eq. (3.70) is the replacement of B^0 by $-A_C^0$ in the outside region in deriving Eq. (C2), and this approximation becomes very accurate for only moderately large values of $\rho_{\max}$ and $z_{\max}$.

$$
\begin{aligned}
L_{1\ \text{outside}} &= \int_{\text{outside}} \frac{Q^2}{(4\pi)^2}\frac{1}{2\varepsilon_C}\left[\left[\nabla\frac{1}{r_{(1)}}\right]^2+\left[\nabla\frac{1}{r_{(2)}}\right]^2-2\nabla\frac{1}{r_{(1)}}\cdot\nabla\frac{1}{r_{(2)}}\right] \\
&= \int_{\text{outside}} \frac{Q^2}{(4\pi)^2\varepsilon_C}\left[\nabla\frac{1}{r_{(1)}}\right]^2-\frac{Q^2}{4\pi R\varepsilon_C}+\int_{\text{inside}}\frac{Q^2}{(4\pi)^2\varepsilon_C}\nabla\frac{1}{r_{(1)}}\cdot\nabla\frac{1}{r_{(2)}} \\
&= \frac{Q^2}{4\pi}\frac{1}{2\varepsilon_C}I(\rho_{\max},z_{\max})-\frac{Q^2}{4\pi R\varepsilon_C}+\int_{\text{inside}}\frac{Q^2}{(4\pi)^2\varepsilon_C}\frac{\rho^2+z^2-a^2}{(r_1r_2)^3}\ , \qquad (3.71b) \\
I(\rho_{\max},z_{\max}) &= \frac{z_{\max}}{z_{\max}^2-a^2}+\frac{1}{2\rho_{\max}}\left[\tan^{-1}\left[\frac{z_{\max}-a}{\rho_{\max}}\right]+\tan^{-1}\left[\frac{z_{\max}+a}{\rho_{\max}}\right]\right] .
\end{aligned}
$$

Equations (3.69)—(3.71) give formulas which we can use for evaluating the Coulomb-subtracted static potential, in the example of Eqs. (3.1)—(3.3), on a finite computational mesh. The analytic rearrangement procedure which we have just described is directly applicable to the Abelian Higgs model, for which the analogous formulas are summarized in Appendix C.[34]

In the case of the leading logarithm model of Sec. II.D, the extreme nonlinearity of the action functional precludes an explicit analytic subtraction of the Coulomb self-energies. Instead, we use either of the following two numerical procedures to remove the Coulomb singularities. The first procedure is to calculate V_{static} for two different R values, say $R=R_1$ and $R=R_2$, keeping the mesh structure near the charges the same in both computations. The Coulomb self-energy contributions then cancel when we form the difference

$$\Delta V_{\text{static}} = V_{\text{static}}(R_1)-V_{\text{static}}(R_2)\ , \qquad (3.72)$$

and so ΔV_{static} approaches a limiting value as the spacing of the computational mesh approaches zero, even though $V_{\text{static}}(R_1)$ and $V_{\text{static}}(R_2)$ individually diverge in this limit. The second procedure is to use bispherical coordinates [cf. Eq. (3.63)], for which a cutoff $\mu_{\max}$ on the size of the computational mesh corresponds to a cutoff

$$r_{\min}=Re^{-\mu_{\max}} \qquad (3.73)$$

on the distance of approach to the Coulomb singularities of the solution. Finite answers for V_{static} are then obtained as the mesh spacing approaches zero for a fixed cutoff $\mu_{\max}$. By varying $\mu_{\max}$ with R so that $r_{\min}$ remains constant, and then forming differences as in Eq. (3.72), one can again get the Coulomb self-energies to drop out in measurements of ΔV_{static}. The boundary condition for the flux function which is now needed on the line $\mu=\mu_{\max}, 0\le\eta\le\pi$ can be obtained by combining Eqs. (2.62) and (3.63c), giving

$$\Phi(\mu=\mu_{\max},\eta)=Q\tfrac{1}{2}(1-\cos\eta)+O(r_{\min}^2)\ . \qquad (3.74a)$$

Although Eq. (3.74a) gives only an approximate boundary condition for Φ near the charge, the effect of the $O(r_{\min}^2)$ error on the Coulomb-subtracted static potential is of order

$$\frac{O(r_{\min}^2)}{O(1)}\times\left[E_{r_{\min}}\propto\frac{1}{r_{\min}}\right]\propto r_{\min}\propto e^{-\mu_{\max}}\ , \qquad (3.74b)$$

where $E_{r_{\min}}$ is the energy within a sphere of radius $r_{\min}$ around charge and can be made arbitrarily small by taking $\mu_{\max}$ large enough. Both of the methods just described are used in the computation of Sec. IV.C.

F. Iterative solution of nonlinear problems by quasilinearization

In describing iterative methods for the numerical solution of the example of Eqs. (3.1)—(3.3), we have had to contend with only a *linear* problem, in which the field equation is linear and in which the Lagrangian is quadratic in the field variable φ. We turn in this section to the numerical solution of *nonlinear* models, such as those of Secs. II.C.—II.E, in which the field equations contain nonlinear terms in the field variables and in which the Lagrangians are not quadratic forms. The basic method used to solve nonlinear problems numerically is *quasilinearization*, in which the nonlinear problem is replaced by a sequence of linear problems, the solutions to which converge in a limiting sense to the desired nonlinear solution. A classic example of the method of quasilinearization is provided by the Newton iteration of Eqs. (3.33)—(3.37), in which the nonlinear problem

$$0=f(w) \qquad (3.75)$$

is replaced by a sequence of linear problems

$$0=f(w^{(n)})+(w^{(n+1)}-w^{(n)})f'(w^{(n)}),\quad n=0,1,2,\ldots, \qquad (3.76)$$

the solutions of which limit to a root of Eq. (3.75). When Eq. (3.76) is solved for $w^{(n+1)}$, as in Eq. (3.35), it takes the form of an iterated map

$$w^{(n)}\to w^{(n+1)}=M(w^{(n)}),\quad n=0,1,2,\ldots \qquad (3.77a)$$

in which the map

$$M(w)=w-\frac{f(w)}{f'(w)} \qquad (3.77b)$$

reduces to the identity map $M(w)=w$ at roots of Eq. (3.75). Similarly, we have seen in Eqs. (3.43) and (3.45) that the over-relaxed Gauss-Seidel iteration is an iterated map, which reduces to the identity map at the solution of the system of linear equations of Eq. (3.39). Very generally, a quasilinear method for solving the nonlinear field equation

$$0=F[\varphi] \tag{3.78}$$

is constructed by specifying an iterated map

$$\varphi^{(n)}\rightarrow\varphi^{(n+1)}=M[\varphi^{(n)}]\ , \tag{3.79}$$

in which (i) M reduces to the identity map $M[\varphi]=\varphi$ at solutions of Eq. (3.78), and (ii) M is constructed from a finite sequence of linear operations. From the preceding discussion, it is clear that both (i) and (ii) are readily satisfied if M is constructed as a finite sequence of Newton iterations [Eq. (3.77)] and of over-relaxed Gauss-Seidel iterations [Eq. (3.45) or Eq. (3.50)].

Let us now discuss in turn the models of Secs. II.C–II.E, and describe the quasilinear iterations which we use for their numerical solution. We begin with the Abelian Higgs model of Sec. II.C, for which the Coulomb-subtracted Lagrangian functional [cf. Eq. (C2)] is

$$L_{\text{subtracted}}[B^0,\varphi]=T+4\pi\int_0^\infty\rho d\rho\int_0^\infty dz\{\tfrac{1}{2}[(\partial_\rho B^0)^2+(\partial_z B^0)^2]+e^2(B^0+A_C^0)^2\varphi^2-(\partial_\rho\varphi)^2-(\partial_z\varphi)^2-\tfrac{1}{2}C(\varphi^2-\kappa^2)^2\}\ , \tag{3.80}$$

where T represents terms independent of B^0,φ. Since Eq. (3.80) is quadratic in B^0 and quartic in φ, the derivatives of the discretized Lagrangian with respect to the nodal variables $B^0_{i,j}$ and $\varphi_{i,j}$, respectively, take the form

$$0=B^0_{i,j}C+D\ , \tag{3.81a}$$

with C, D independent of $B^0_{i,j}$, and

$$0=\varphi^3_{i,j}E+\varphi_{i,j}F+G\ , \tag{3.81b}$$

with E,F,G independent of $\varphi_{i,j}$. The quasilinearized iteration for Eq. (3.81) is composed of an over-relaxed Gauss-Seidel iteration for the linear equation $0=B^0C+D$,

$$B^{0(n)}_{i,j}\rightarrow B^{0(n+1),\text{SOR}}_{i,j}=\omega\left[\frac{-D}{C}\right]+(1-\omega)B^{0(n)}_{i,j}\ , \tag{3.82}$$

followed by some small number k of Newton iterations for the nonlinear equation[35] $0=\varphi^3E+\varphi F+G$, starting from $\varphi^{(n)}_{i,j}$ as the initial guess,

$$\begin{aligned}&\varphi^{(n)}_{i,j}\rightarrow\varphi^{(n+1)}_{i,j}\equiv\varphi^{(n,k)}_{i,j}\ ,\\ &\varphi^{(n,0)}_{i,j}\equiv\varphi^{(n)}_{i,j}\ ,\\ &\varphi^{(n,l)}_{i,j}=\varphi^{(n,l-1)}_{i,j}-\frac{f\left[\varphi^{(n,l-1)}_{i,j}\right]}{f'\left[\varphi^{(n,l-1)}_{i,j}\right]}\ ,\quad l=1,\ldots,k\ ,\\ &f(\varphi)=\varphi^3E+\varphi F+G,\quad f'(\varphi)=3\varphi^2E+F\ .\end{aligned} \tag{3.83}$$

In the iterations of both Eqs. (3.82) and (3.83), the coefficients C,D,E,F,G are understood to be computed using the most recent updates of all node variables on which they depend. In programing Eqs. (3.82) and (3.83), we choose the option of doing all the $B^0_{i,j}$ updates in one sweep of the mesh, and then doing all the $\varphi_{i,j}$ updates in the next sweep, and so forth; alternatively, we could do both the $B^0_{i,j}$ and $\varphi_{i,j}$ updates together as parts of the same sweep of the mesh.

Let us consider next the leading logarithm model, which, as shown in Sec. II.D, leads to the following nonlinear differential equation for the flux function Φ:

$$\nabla\cdot(\sigma\nabla\Phi)=0\ . \tag{3.84a}$$

The coefficient σ in Eq. (3.84a) is given as a function of $\nabla\Phi$ by

$$\sigma=\frac{2\pi\kappa}{\rho\,|\nabla\Phi|}f\left[\frac{|\nabla\Phi|}{\pi b_0\kappa\rho}\right]\ , \tag{3.84b}$$

with $f(w)$ implicitly defined by the transcendental equation

$$w=f\log f,\quad f\geq 1\ . \tag{3.84c}$$

To set up a quasilinearized iteration for Eq. (3.84), let us regard σ and Φ as dependent variables on an equal footing, and introduce the auxiliary Lagrangian

$$L[\Phi]=4\pi\int_0^\infty\rho d\rho\int_0^\infty dz\tfrac{1}{2}\sigma(\nabla\Phi)^2\ , \tag{3.85}$$

which yields Eq. (3.84a) as its variational equation when the dependence of σ on $\nabla\Phi$ is ignored. Equations (3.85) and (3.84a) have the same structure (apart from the replacements $\varphi\rightarrow\Phi,\varepsilon\rightarrow\sigma$) as Eqs. (3.1) and (3.2) of our dielectric medium example, and thus have a natural discretization corresponding to that of Sec. III.B above, in which the Φ values lie on the node lattice, and the σ values lie on the half-node lattice. In terms of this discretization, the quasilinearized iteration consists of alternating a complete sweep of the node lattice with a complete sweep of the half-node lattice. In the sweep of the node lattice, $\Phi^{(n)}_{i,j}$ is updated by the over-relaxed Gauss-Seidel iteration

[35]The same Newton iteration method can be used to solve $\nabla^2\varphi=F(\varphi)$ for a general functional form F; see, for example, Hockney and Eastwood (1981).

$$\Phi_{i,j}^{(n)} \rightarrow \Phi_{i,j}^{(n+1),\mathrm{SOR}} = \omega \Phi_{i,j}^{(n+1)} + (1-\omega)\Phi_{i,j}^{(n)} ,$$

$$\Phi_{i,j}^{(n+1)} = \left[\left[\frac{\Delta z}{\Delta \rho} + \frac{\Delta \rho}{\Delta z} \right] (h_{i+1/2,j+1/2}^{(n)} + h_{i+1/2,j-1/2}^{(n)} + h_{i-1/2,j+1/2}^{(n)} + h_{i-1/2,j-1/2}^{(n)}) \right]^{-1}$$

$$\times \left[\frac{\Delta z}{\Delta \rho} (h_{i+1/2,j+1/2}^{(n)} + h_{i+1/2,j-1/2}^{(n)}) \Phi_{i+1,j}^{(n)} + \frac{\Delta z}{\Delta \rho} (h_{i-1/2,j+1/2}^{(n)} + h_{i-1/2,j-1/2}^{(n)}) \Phi_{i-1,j}^{(n+1)} \right.$$

$$\left. + \frac{\Delta \rho}{\Delta z} (h_{i+1/2,j+1/2}^{(n)} + h_{i-1/2,j+1/2}^{(n)}) \Phi_{i,j+1}^{(n)} + \frac{\Delta \rho}{\Delta z} (h_{i+1/2,j-1/2}^{(n)} + h_{i-1/2,j-1/2}^{(n)}) \Phi_{i,j-1}^{(n+1)} \right] , \tag{3.86a}$$

$$h_{i+1/2,j+1/2}^{(n)} \equiv \rho_{i+1/2} \sigma_{i+1/2,j+1/2}^{(n)} ,$$

while in the subsequent sweep of the half-node lattice, $\sigma_{i+1/2,j+1/2}^{(n)}$ is updated by the replacement

$$\sigma_{i+1/2,j+1/2}^{(n)} \rightarrow \sigma_{i+1/2,j+1/2}^{(n+1)} = \frac{2\pi\kappa}{\rho_{i+1/2} \, | \nabla \Phi |_{i+1/2,j+1/2}^{(n+1)}} f \left[\frac{| \nabla \Phi |_{i+1/2,j+1/2}^{(n+1)}}{\pi b_0 \kappa \rho_{i+1/2}} \right] ,$$

$$| \nabla \Phi |_{i+1/2,j+1/2}^{(n+1)} = \left[\tfrac{1}{2} \left[\frac{\Phi_{i+1,j}^{(n+1)} - \Phi_{i,j}^{(n+1)}}{\Delta \rho} \right]^2 + \tfrac{1}{2} \left[\frac{\Phi_{i+1,j+1}^{(n+1)} - \Phi_{i,j+1}^{(n+1)}}{\Delta \rho} \right]^2 \right.$$

$$\left. + \tfrac{1}{2} \left[\frac{\Phi_{i,j+1}^{(n+1)} - \Phi_{i,j}^{(n+1)}}{\Delta z} \right]^2 + \tfrac{1}{2} \left[\frac{\Phi_{i+1,j+1}^{(n+1)} - \Phi_{i+1,j}^{(n+1)}}{\Delta z} \right]^2 \right]^{1/2} , \tag{3.86b}$$

with the formulas just given the ones which apply when there is no Jacobian transformation, so that the physical coordinates ρ,z are also the computational coordinates. At each point of the half-node lattice, the replacement of Eq. (3.86b) requires an evaluation of the transcendental function f for the indicated argument w. This is readily accomplished by the Newton iteration

$$f^{(0)} = \frac{w}{\log(1+w)} ,$$

$$f^{(l)} = f^{(l-1)} + \frac{w - f^{(l-1)} \log f^{(l-1)}}{1 + \log f^{(l-1)}} , \quad l = 1,2,\ldots , \tag{3.87}$$

which can be shown to give $f(w)$ to 16-place accuracy, for all w, in four or fewer iterations.

We turn finally to the axially symmetric monopoles of Sec. II.E and Appendix B, for which the Hamiltonian H is given in Eq. (B2) and the gauge-fixing term H_{gf} is given in Eqs. (B5) and (B6). If we divide the potentials of the six-function ansatz into three groups as follows (groups 1, 2, and 3, respectively):

$$h_1, f_1 ,$$
$$h_2, f_2 , \tag{3.88}$$
$$a_1, a_2 ,$$

then an examination of Eqs. (B2) and (B6) shows that $H + H_{\mathrm{gf}}$ can be rewritten as a positive definite quadratic form in the potentials of any one of the three groups, with coefficients which depend on the potentials of the other two groups [Adler and Piran (1980)]. The explanation for this feature is that the three groups in Eq. (3.88) correspond, respectively, to the internal symmetry $\hat{z}, \hat{\rho}_n$, and $\hat{\phi}_n$ components of the gauge potential, which appear at most quadratically in H, because nonlinearities in the classical Yang-Mills action arise only from internal-symmetry outer products. As a result of the multiquadratic structure of $H + H_{\mathrm{gf}}$, the discussion of the over-relaxed Gauss-Seidel iteration given for quadratic forms in Sec. III.C applies directly to the nonlinear monopole problem, provided that in any one iteration we relax only the potential components in a single group. In other words, a suitable quasilinearized iteration for the monopole problem is

relax h_1, f_1 using Eq. (3.45) with h_2, f_2, a_1, a_2 fixed

↓

relax h_2, f_2 using Eq. (3.45) with h_1, f_1, a_1, a_2 fixed

↓

relax a_1, a_2 using Eq. (3.45) with h_1, f_1, h_2, f_2 fixed

↓

relax h_1, f_1, etc., (3.89)

and the analysis of Eqs. (3.45)—(3.47) guarantees that at each update of this iteration, the Hamiltonian $H + H_{\mathrm{gf}}$ is monotone decreasing. Since in Sec. II.E we saw that H is bounded from below by $4\pi\kappa \, | n |$ in the sector with topological quantum number n, and since H_{gf} is bounded from below by 0, the monotonicity of the iteration of Eq. (3.89) gives a formal proof that the iteration converges in each topological sector. The fact that one can give a simple convergence proof for the quasilinearized iteration is an unusual special feature of the monopole problem (and more generally, of the problem of minimizing Euclidean Yang-Mills action functionals, of which the Bogomol'nyi-Prasad-Sommerfield monopoles are a special case). The analogous iterations given above for the Abelian Higgs and leading logarithm models do in fact con-

verge, but (as is typically the case in nonlinear problems) we cannot give an *a priori* proof of convergence. It is thus important in solving nonlinear problems numerically to make *a posteriori* tests of convergence, both by monitoring the convergence of the iterative process at fixed mesh size h, and by checking that physical quantities computed on meshes of progressively decreasing size approach a limit as $h \to 0$.

G. Programming considerations

Writing computer programs is a highly individualized skill; given the same algorithm, two different programmers are likely to produce very different looking codes. Nonetheless, there are some general principles and some specific ideas which we have found useful in writing programs for the models of Sec. II, and which we discuss briefly in items (1)—(6) below. A very useful list of further recommendations for programming, testing, and information processing is given in Chap. VII of Roache (1976). In particular, Roache points out the importance of doing all program development work on a coarse mesh, stating that "stability and convergence of the. . .iterations usually can be tested in a ridiculously coarse mesh." Our experience in solving the nonlinear models of Sec. II is completely consistent with this recommendation; all important qualitative features of the solutions obtained in Sec. IV can be seen on a 7×7 mesh. In further emphasis of this point, Roache asserts "If all users at a major computing center would adopt the policy of testing in as coarse a mesh as possible, the reduction in computing load would probably be comparable to the installation of a later-generation computer."

Our own specific recommendations follow. [Points (1)—(4), which may seem trivial, are included because we believe they will be useful for readers without prior programming experience who wish to pursue relaxation calculations.]

(1) Delineation of program segments. There are five distinct tasks which must be performed by a program to solve a partial differential equation system numerically. It must *initialize* by reading in parameter values and by setting up the mesh geometry and the initial guess which begins the iteration. It must then *iterate* according to one of the algorithms discussed in detail above. At the end of the iteration, it must *measure* various attributes of the converged (or partially converged) solution. Finally, it must have provisions for *control* of the iterative process and for displaying and/or writing into files selected numerical *output*. Writing, debugging, and rereading or modifying a program are facilitated if the program is clearly divided into segments with the functions described above.

(2) Use of a control integer. In developing or testing a program it is desirable to work interactively (using very coarse meshes), while in production work it is more efficient to run in batch mode. A simple way of structuring a program so that it is very flexible, can easily be run interactively, and can be run without modification in batch mode, is to use the device of a *control integer*. The program is constructed to begin by reading a control integer I, and to return to the READ I statement after performing any task. By using the IF THEN, ELSE IF THEN, ELSE construct, one sets up a correspondence between different I values and different program actions, e.g.,

I value	function
0	stop execution
$99 > I > 0$	iterate I steps
-1	unformatted dump into file
-2	unformatted retrieval from file
-3	mesh doubling: halve the mesh spacing h at fixed ρ_{max}, z_{max} and interpolate the last iterate to get a new starting guess
-4	mesh extension or reduction: change ρ_{max}, z_{max} at fixed mesh spacing h and (for extension) extrapolate the last iterate to get a new starting guess
-10 to -20	miscellaneous parameter reads for initialization
-20 to -40	miscellaneous output options
all others	read new control integer value

(3.90)

For convenience in interactive running, all input reads should be in the UNFORMATTED mode, with the ERROR = N option producing a return to the READ I statement, so that the program does not crash when keying errors are made. To run in batch mode, one simply submits a job consisting of the RUN command for the program followed by the string of I values which produce the desired sequence of program operations.

(3) Organization of input and output. The most convenient way of reading input parameter values is by use of the NAMELIST statement, available on IBM and CDC machines. This statement permits one to change any subset of the parameters specified in the NAMELIST declaration, leaving all unchanged parameters with their previous values. On machines for which NAMELIST is not available (such as the DEC VAX 11/780 used for the computations of this paper), a convenient alternative method is to group the parameters in an *input file*, which can be edited before program execution to set up the desired parameter values, and which is then automatically accessed by the program. In constructing the output options, the use of histogram-type terminal displays should play an important role. For a discussion of these with examples, see Roache (1976), Chap. VII C2, and McCracken (1972), Sec. 6.14.

(4) Optimization of the innermost DO *loop.* The running time of an iterative program is determined largely by the time required to execute the innermost DO loop of the iteration. Thus, within the innermost loop, the number of operations should be reduced by intelligent grouping of factors, library function or subroutine calls should be avoided if possible, and numerical constants should al-

ways be introduced as parameters which are declared by a PARAMETER statement at the beginning of the program. In virtual memory machines, particular attention must be paid to the avoidance of page faults (transfers from virtual disk memory to fast semiconductor memory). Specifically, the statements

```
DO   10   I=1,100
DO   10   J=1,100
A(I,J)=.25*(A(I+1,J)+A(I-1,J)+A(I,J+1)
          +A(I,J-1))
10   CONTINUE                                    (3.91a)
```

will produce many more page faults than the statements

```
DO   10   J=1,100
DO   10   I=1,100
A(I,J)=.25*(A(I+1,J)+A(I-1,J)+A(I,J+1)
          +A(I,J-1))
10   CONTINUE .                                  (3.91b)
```

The reason for this is that the array A is stored in machine memory with the first index changing most rapidly, A(1,1),A(2,1), . . . , A(100,1),A(1,2),A(2,2),. . . . Hence the program of Eq. (3.91a), which increments the second index in the innermost DO loop, steps through machine memory with a "velocity" roughly 100 times greater than that characterizing the program of Eq. (3.91b).

(5) Estimation of the optimum ω. A reliable way to estimate the optimum value of ω is to use a coarse (say, 10×10) mesh and to plot an indicator of the error after a fixed number n_0 of iterations versus the ω value used. A good error measure for this purpose is the square root of the change in the Lagrangian functional in the final sweep of the mesh, which according to Eq. (3.44) measures the root-mean-square residual error. Care must be taken that n_0 is large enough for the iterative process to have entered the asymptotic regime governed by Eq. (3.51). Typical plots obtained this way are shown in Fig. 11; in Fig. 11(a), n_0 is not large enough for $\omega_{\rm opt}$ to be determined, while in Figs. 11(b) and 11(c), obtained with larger values of n_0, one gets essentially the same value of $\omega_{\rm opt}$. Once $\omega_{\rm opt}$ has been determined for a coarse mesh, it can be estimated for finer meshes by using Eqs. (3.52)—(3.55).

(6) Convergence criteria. The number of iterations needed for convergence is a function of the physical quantity which one wants to measure. For example, since the static potential $V_{\rm static}$ is stationary at the solution of the equations of motion [cf. Eqs. (2.3), (3.19), etc.], the error in the static potential is quadratic in the errors in the field variables. Hence far fewer iterations are needed to achieve a given accuracy in measuring the static potential than are needed to measure quantities which are not stationary around the equilibrium solution (such as the field variables, energy densities, or the geometry of the free boundary in the leading logarithm model). The choice of indicators of convergence which are monitored during iteration and the convergence criteria used to terminate

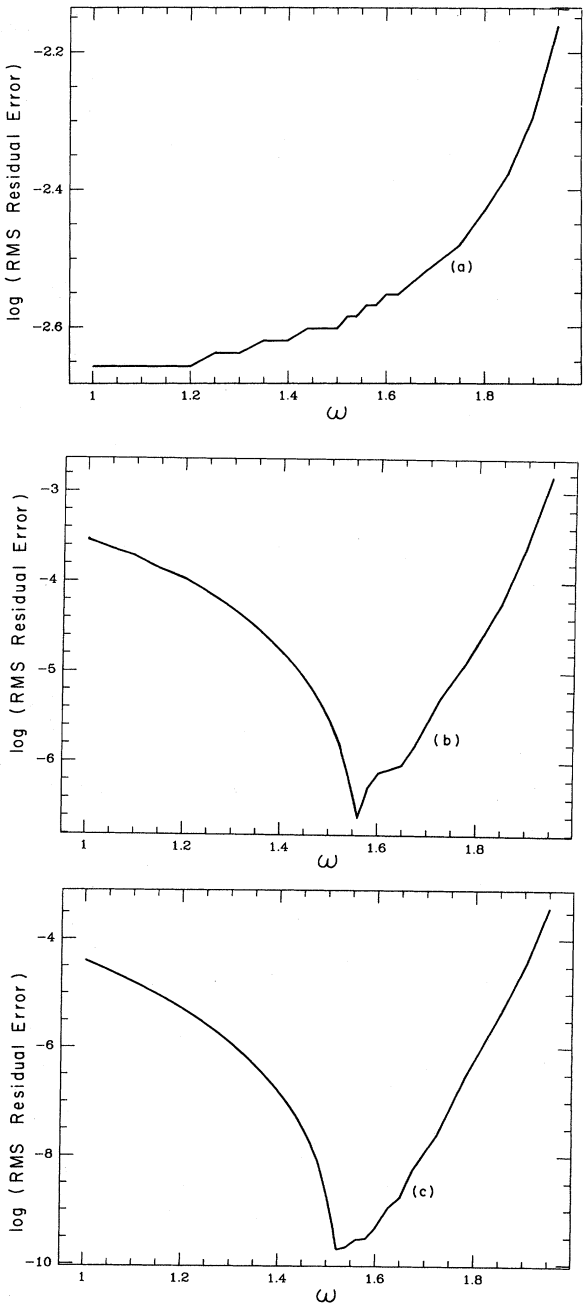

FIG. 11. Plot of the root mean-square residual error after a fixed number n_0 of complete mesh sweeps, vs the over-relaxation parameter ω (computed for the topological $n=1$ monopole example of Secs. II.E and IV.D). (a) $n_0=10$ iterations at $\omega=1$ followed by 30 iterations at variable ω. The asymptotic regime has not yet been reached. (b) $n_0=10$ iterations at $\omega=1$ followed by 60 iterations at variable ω. (c) $n_0=10$ iterations at $\omega=1$ followed by 90 iterations at variable ω. Plots (b) and (c) indicate $\omega_{\rm opt}\approx 1.54-1.56$.

the iteration will depend strongly on what is being measured at the end of the iterative process.

IV. NUMERICAL SOLUTION OF THE MODELS OF SEC. II

A. Introduction

Let us proceed now to apply the numerical methods described in Sec. III to the nonlinear models formulated in Sec. II. In Table III we summarize which dependent variables in the three models are discretized on the node lattice, and which are discretized on the half-node lattice, together with the boundary conditions which are imposed during iteration. In the brief sections which follow we discuss aspects of the numerical analysis which are specific to the three models and give sample numerical results.

B. The Abelian Higgs model

Following the analysis of Sec. III.E and Appendix C, we explicitly subtract off the Coulomb self-energy from L by making the substitution

$$A^0=A_C^0+B^0 , \tag{4.1}$$

with A_C^0 the Coulomb potential of Eq. (C1) and with B^0 a new dependent variable. Because A_C^0 and φ are both singular at the charges [cf. Eq. (2.17)], the charge coordinate $z=a$ is taken to lie midway between nodes of the computational lattice:

$$a=(n_Q+\tfrac{1}{2})\Delta z , \tag{4.2}$$

with n_Q an integer. We choose the unit of length so that $\kappa=1$, giving $\varphi\to 1$ as the boundary condition on φ at infinity. Since this boundary condition follows from requiring L to be extremal (L is infinite if $\varphi\not\to 1$ at infinity), it can be enforced computationally by simply iterating the nodal values for φ which lie on the outer boundary of the computational mesh. An alternative procedure would be to set $\varphi=1$ on the outer boundary; the two methods give the same result in the limit as $\rho_{\max}\to\infty, z_{\max}\to\infty$, but the iterative boundary condition is preferable for finite meshes.[36] To get a good approximation to the infinite volume solution, $\rho_{\max}$ and $z_{\max}$ must be chosen large compared with the characteristic exponential decay lengths appearing in Eq. (2.17), requiring (for $\kappa=1$) that

$$\min(\rho_{\max},z_{\max})\gg\max[(2C)^{-1/2},(2e^2)^{-1/2}] . \tag{4.3}$$

Sample results for the Abelian Higgs model, calculated with

$$\kappa=C=e=Q^2/(4\pi)=1 , \qquad \rho_{\max}=z_{\max}=3,\ \ a=1.625 , \tag{4.4}$$

are shown in Figs. 12(a)—12(d). These figures give values of φ and A^0 (plotted vertically) on a plane passing through the axis of rotation (represented by the horizontal plane in the figures). One can see clearly the peaks in φ and A^0 at the charges, as well as the exponential decay of φ towards 1 and of A^0 towards 0 at infinity. In Figs. 12(c) and 12(d), in which the vertical scale has been magnified by a factor of 10, one can also see that the structure of the solution extends to the computational boundary, in marked contrast to the behavior found below in the solution of the leading logarithm model.

C. The leading logarithm model

In discretizing the leading logarithm model, we put the charge coordinate $z=a$ on a node of the computational lattice,

$$a=n_Q\Delta z , \tag{4.5}$$

with n_Q an integer, and enforce the step function boundary condition of Eq. (2.50) by requiring

$$\Phi_{0,j}=Q,\ \ 0\le j<n_Q , \qquad \Phi_{0,j}=\tfrac{1}{2}Q,\ \ j=n_Q , \qquad \Phi_{0,j}=0,\ \ n_Q<j\le n_j . \tag{4.6}$$

[An alternative procedure would be to put the charge coordinate midway between lattice nodes by taking $a=(n_Q+\frac{1}{2})\Delta z$, giving the boundary condition $\Phi_{0,j}=Q, 0\le j\le n_Q$ and $\Phi_{0,j}=0, n_Q+1\le j\le n_j$.] Because the solution for Φ is confined within a finite free boundary, the numerical solution is independent of $\rho_{\max},z_{\max}$, provided that these are large enough for the fully converged free boundary to lie entirely within the computational mesh. To facilitate picking values of $\rho_{\max},z_{\max}$ which are large enough to contain the free boundary but are not excessively so, we have included a control parameter option in the program which permits the adjustment of the limits of the computational mesh during iteration.

In carrying out the iteration we do not let the dielectric function ε assume the value 0, but rather impose a minimum value $\varepsilon_{\min}$ by computing ε and σ from the formulas

[36] In general, for solutions with r^{-n} asymptotic behavior at infinity, using an iterated boundary condition on the computational outer boundary gives greater accuracy than using a Dirichlet boundary condition (York and Piran, 1982). For linear problems, for example, Cantor (1983) has proved that a sequence of solutions with the iterated boundary condition and with increasing $(\rho_{\max},z_{\max})$ will converge to the true solution with $(\rho_{\max},z_{\max})=(\infty,\infty)$, and this sequence can even be used to study the asymptotic behavior of the true solution at $r=\infty$. Such strong statements cannot in general be made when a Dirichlet boundary condition is used on the outer boundary. In the Abelian Higgs model, where φ approaches its asymptotic value exponentially at infinity, the difference between the two types of boundary conditions is not expected to be as marked as in the case of power-law asymptotic behavior.

TABLE III. Node and half-node assignments and boundary conditions for the models of Sec. II.

Model	Defined on node lattice	Defined on half-node lattice	Boundary conditions (or remarks) $\rho = 0$	$z = 0$	Outer boundary $\rho = \rho_{max}$ or $z = z_{max}$
Abelian Higgs Sec. II.C	B^0 (cf. Appendix C; $A^0 = A_C^0 + B^0$)		(charge coordinate $z = a$ midway between nodes) B^0 iterated	$B^0 = 0$	B^0 iterated
	φ		φ iterated	φ iterated	φ iterated (could also use $\varphi = 1$)
Leading logarithm Sec. II.D	Φ		(charge coordinate $z = a$ on node) $\Phi = Q$, $z < a$; $\Phi = \frac{1}{2}Q$, $z = a$; $\Phi = 0$, $z > a$	Φ iterated	$\Phi = 0$
		σ	σ determined at all half-node points within computational mesh by updating from Φ		
Axially symmetric monopole Sec. II.E	h_1		h_1 iterated	$h_1 = 0$	$h_1 = (1 - n/r)\cos\vartheta$
	h_2		$h_2 = 0$	h_2 iterated	$h_2 = (1 - n/r)\sin\vartheta$
	f_1		$f_1 = n$	f_1 iterated	$f_1 = n\cos^2\vartheta$
	f_2		$f_2 = 0$	$f_2 = 0$	$f_2 = n\sin\vartheta\cos\vartheta$
	a_1		$a_1 = 0$	a_1 iterated	$a_1 = -(1/r)\sin\vartheta$
	a_2		a_2 iterated	$a_2 = 0$	$a_2 = (1/r)\cos\vartheta$

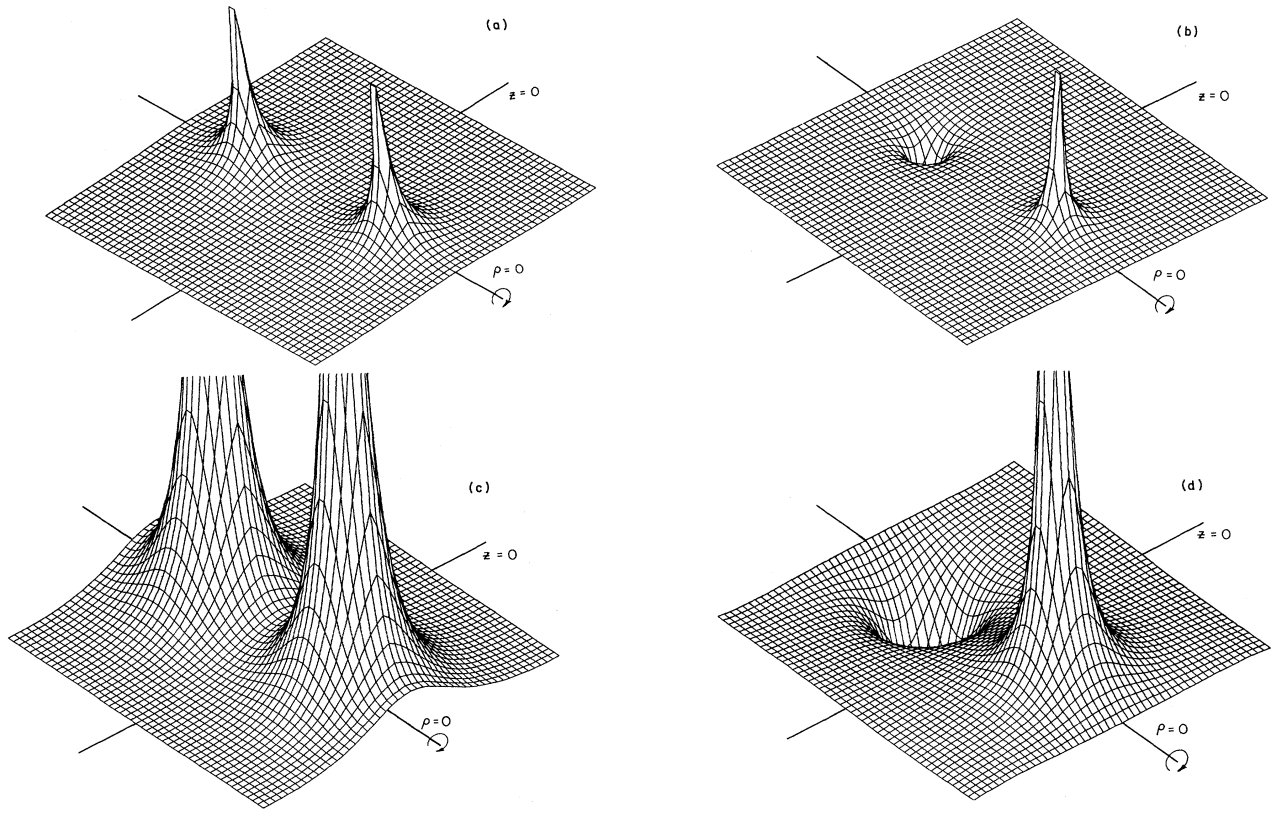

FIG. 12. Sample results for the Abelian Higgs model, calculated for the parameter values in Eq. (4.4). The graphs show (a) φ, (b) A^0, (c) φ with the vertical scale magnified by a factor of 10, and (d) A^0 with the same vertical scale magnification, all plotted vertically over a horizontal plane through the rotation axis. The values of φ and A^0 at the base of the figures are $\varphi = 1$ and $A^0 = 0$, respectively.

$$\varepsilon=\max\left[\tfrac{1}{4}b_0\log(E^2/\kappa^2),\varepsilon_{\min}\right],$$
$$\sigma=\min\left[\frac{2\pi\kappa}{\rho\,|\nabla\Phi|}f\left[\frac{|\nabla\Phi|}{\pi b_0\kappa\rho}\right],\frac{1}{\rho^2\varepsilon_{\min}}\right]. \tag{4.7}$$

This procedure avoids floating point underflows and overflows, and corresponds to keeping the differential equation for Φ just barely elliptic even outside the free boundary. Provided that $\varepsilon_{\min}$ is chosen to be very small (we have used values ranging from 10^{-15} to 10^{-35} with equally satisfactory results), the results for V_{static} are essentially independent of $\varepsilon_{\min}$. Although convergence of the iteration is improved by over-relaxation, we have found that the nonlinearity of the combined iteration of Eqs. (3.86a) and (3.86b) leads to instabilities in the free boundary shape, if one attempts to use ω values as large as the optimum ω appropriate to the linear subiteration of Eq. (3.86a). These instabilities are avoided by limiting ω to at most $\omega=1.7$ when iterating on meshes larger than 25×25. Full convergence within the free boundary requires about 1–2 min of CPU time on a VAX 11/780 computer for a 25×25 mesh, and around 1 h for a 100×100 mesh. Sample results on a 25×25 mesh [Adler and Piran (1982a)], computed for the parameter values

$$\kappa=1,\quad Q=(\tfrac{4}{3})^{1/2},\quad b_0=9/(8\pi^2),$$
$$\rho_{\max}=z_{\max}=8,\quad \tfrac{1}{2}R=a=4, \tag{4.8}$$

are given in Figs. 13(a)–13(d). These figures show, respectively, the flux function Φ, the field energy density $\mathscr{H}$, $\mathscr{H}$ with a vertical scale magnification of 100, and the *logarithm* of the dielectric constant ε, all plotted vertically over a horizontal plane through the rotation axis. In the plot of Φ the $\rho=0$ boundary condition of Eq. (4.6) is clearly visible, and in both plots of $\mathscr{H}$ one can see the Coulomb energy peaks. The plot of Φ and the magnified plot of $\mathscr{H}$ show that the flux and energy are confined within an oval curve, approximating the continuum limit free boundary, which is also clearly visible in the contour plots of Φ and $\mathscr{H}$ shown in Figs. 14(a) and 14(b). Both because we have imposed a cutoff $\varepsilon>\varepsilon_{\min}=10^{-15}$, and because of finite mesh-spacing effects, the computational problem has low-level residual structure extending outside the continuum free boundary (but lying within a second, computational, free boundary), as can be seen in the plot of $\log\varepsilon$ in Fig. 13(d). This residual structure, together with the fact that the location of the free boundary is not stationary under small variations around the equilibrium

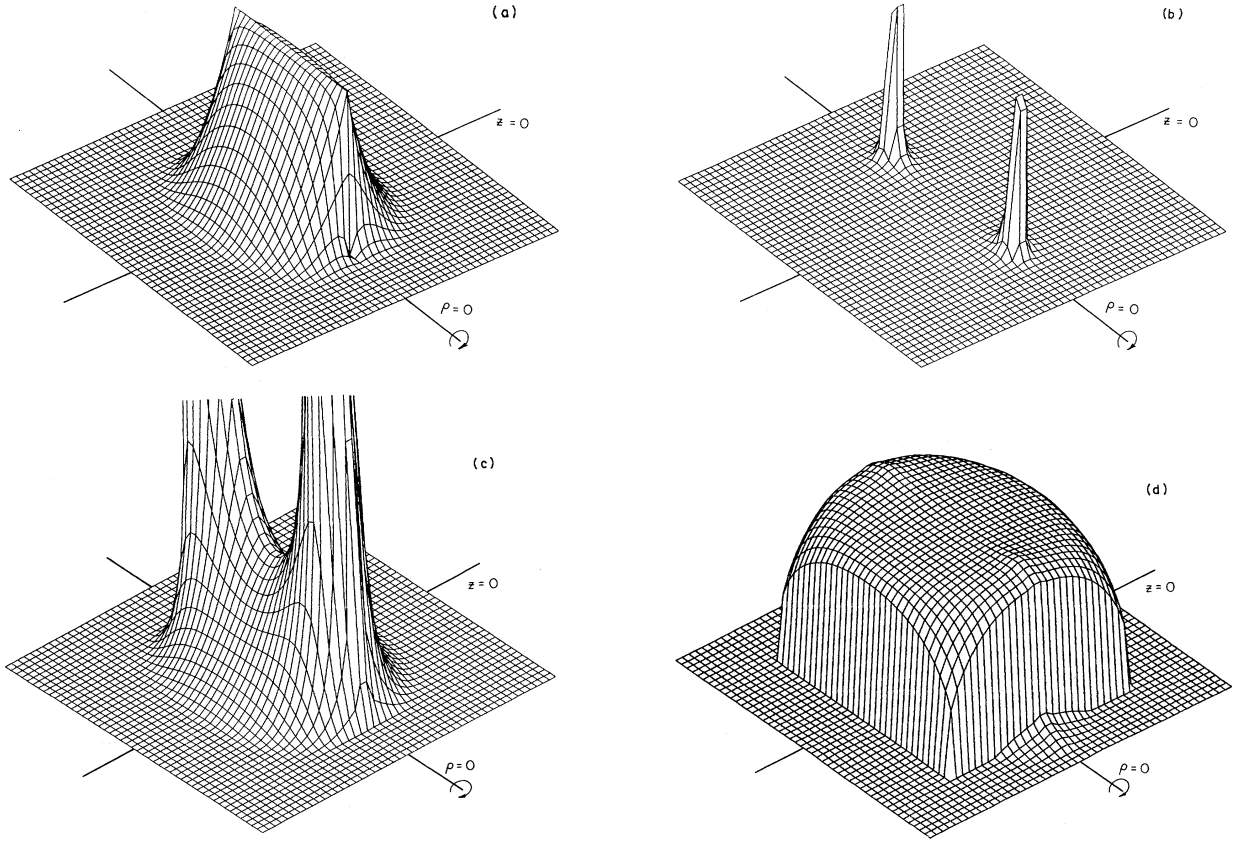

FIG. 13. Sample results for the leading logarithm model, calculated for the parameter values in Eq. (4.8). The graphs show (a) the flux function Φ, (b) the field energy density $\mathscr{H}$, (c) $\mathscr{H}$ with the vertical scale magnified by a factor of 100, and (d) the logarithm of the dielectric constant ε, all plotted vertically over a horizontal plane through the rotation axis. The values of Φ, $\mathscr{H}$, and ε at the base of the figures are 0, 0, and $\varepsilon_{\min}=10^{-15}$, respectively, with ε falling 14 decades from the top of (d) to the base. [When $\varepsilon_{\min}$ is reduced to 10^{-35}, the residual structure along the axis at the base of (d) is eliminated.]

solution Φ, makes an accurate determination of the free boundary location more difficult computationally than an accurate measurement of V_{static}, which is stationary around equilibrium [cf. Eq. (2.42)]. An analytic investigation by Lehmann and Wu (1983), described briefly below, shows that in the limit as $R \to \infty$, the continuum free boundary approaches an ellipsoid of revolution. Rigorous proofs of the existence of a continuum free boundary have been given by Lieb (1983) and by Gidas and Caffarelli (1983).

As described above in Sec. III.E, to measure $V_{\text{static}}(R)$ we make a sequence of measurements of $V_{\text{static}}(R) - V_{\text{static}}(R/2)$, with mesh geometries at the separations R, $R/2$ chosen so that the Coulomb self-energies cancel. For R values between 128 and 1, the calculation can be done in the original ρ,z coordinates, with uniform mesh spacings $\Delta\rho,\Delta z$ in the ρ and z directions. For R values smaller than 1, a Jacobian transformation as described in Sec. III.D is necessary. A simple "stretching"-type transformation which gives good results down to the smallest R values is given by

$$\rho = H(\rho', 0.8a) ,$$
$$z = H(z', a) , \tag{4.9}$$
$$H(z',a) = \begin{cases} z', & z' \le 3a \\ \dfrac{3a}{\left[4 - \dfrac{z'}{a}\right]^{1/3}}, & 3a \le z' < 4a , \end{cases}$$

to be used with $z'_{\max} = 4a, \rho'_{\max} = 3.2a$. This transformation has continuous first derivatives, leaves the mesh uniform near the source charges (so that Coulomb self-energies still cancel), and has an outer region in which mesh points are distributed so as to sample in a roughly uniform way the field energy of a dipole source, as indicated by the following estimate,

$$\mathscr{H}_{\text{dipole}} d^3x \propto \frac{(1+3\cos^2\vartheta)}{r^6} r^2 dr$$
$$= \begin{cases} \dfrac{4}{3}\left| d\left[\dfrac{1}{z^3}\right]\right| = 0.05\dfrac{dz'}{a^4} , & \vartheta = 0 \\ \dfrac{1}{3}\left| d\left[\dfrac{1}{\rho^3}\right]\right| = 0.03\dfrac{d\rho'}{a^4} , & \vartheta = \pi/2 . \end{cases} \tag{4.10}$$

In the calculations for R values much smaller than 1 the free boundary cannot be resolved even on a 100×100 mesh, but at small separations the infrared contributions to the static potential are no longer dominant, and so there is no difficulty in making an accurate determination of V_{static} by using the transformation of Eq. (4.9). An alternative method for doing the calculation at short distances is to use the transformation to bispherical coordinates given in Eq. (3.63). [This transformation is in fact useful at large distances as well; in Fig. 14(c) we show a contour plot of the flux function Φ in bispherical coordi-

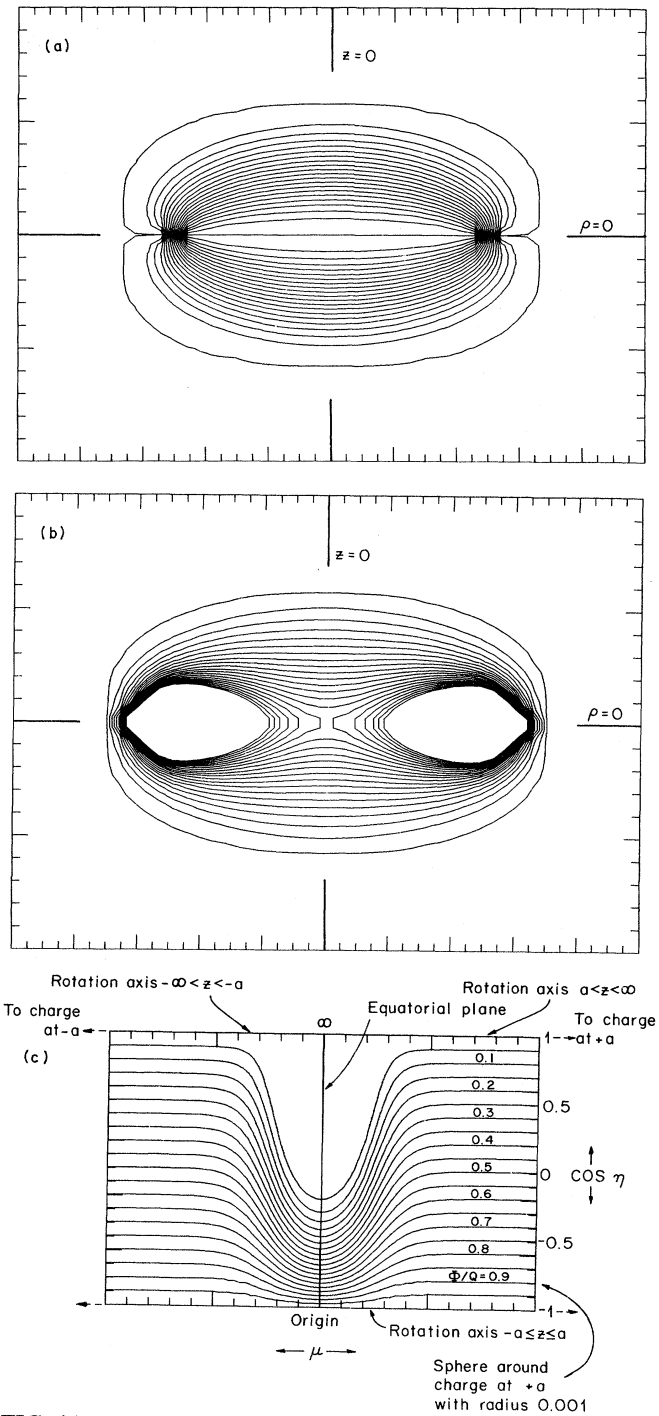

FIG. 14. Contour plots obtained from the numerical solution of the leading logarithm model, with the parameter values of Eq. (4.8). The plots (a) and (b) show contours of the flux function Φ and the energy density $\mathscr{H}$ in uniform Cartesian coordinates, corresponding to the elevation plots of Figs. 13(a) and 13(c), respectively. Specifically, (a) contains 21 equally spaced contours ranging from 0.001 to 1, while (b) contains 21 equally spaced contours ranging from 0.0001 to 0.01 (with the maximum of $\mathscr{H}$ scaled to 1). The plot (c) shows contours of the flux function Φ obtained on a bispherical grid. The coordinates are μ and $\cos\eta$, and the charges are located at $\mu = \pm\infty$. The free boundary is just inside the contour line $\Phi/Q = 0.05$.

nates, calculated for the distance $a=4$ at which the free boundary is clearly resolved.] The results of the calculations using "stretched" cylindrical coordinates and using bispherical coordinates agree to better than 1% at all distances, and are presented in the form of a parametrized analytic fit to V_{static} in Adler and Piran (1982b).

In solving a complicated problem numerically, it is important to check the computer program, wherever possible, against analytic expressions which are available in limiting cases. In the case of the leading logarithm model, systematic analytic approximations can be developed in the small-R limit (Adler, 1983) and in the large-R limit (Lehmann and Wu, 1983). At small R a perturbation analysis in powers of an appropriately defined running coupling $\zeta(R)$ gives

$$V_{\text{static}}(R) \underset{R\to 0}{=} \frac{-Q^2}{4\pi R \frac{1}{2} b_0}[\zeta(R)+O(\zeta^3)] ,$$

$$\zeta(R)=\frac{f(w_R)}{w_R}$$

$$=\frac{1}{\log w_R}+O\left[\frac{\log\log w_R}{(\log w_R)^2}\right]+O\left[\frac{1}{(\log w_R)^3}\right] , \quad (4.11)$$

$$w_R=\frac{1}{\Lambda_P^2 R^2} , \quad \Lambda_P=2.52\kappa^{1/2} .$$

When the numerical results for V_{static} in the range $\kappa^{1/2}R\sim 10^{-6}-10^{-8}$ are fit to the functional form of Eq. (4.11) with Λ_P adjustable, we find $\Lambda_P\approx 2.49$, in excellent agreement with the analytic result. At large R, a systematic expansion of the differential equation for Φ in powers of $1/R$ gives[37]

$$\Phi=\Phi^{(0)}(\rho/R^{1/2},z/R)+\frac{1}{R}\Phi^{(1)}(\rho/R^{1/2},z/R)+\cdots , \quad (4.12)$$

$$\Phi^{(0)}=Q\left[1-\tfrac{1}{2}\left[\frac{\pi b_0}{2Q}\right]^{1/2}\frac{a\rho^2\kappa^{1/2}}{a^2-z^2}\right]^2 , \quad a=\tfrac{1}{2}R ,$$

permitting the determination[37] of the leading two terms in the large-distance behavior of the static potential,

$$V_{\text{static}}(R) \underset{R\to\infty}{=} \kappa QR+Q^{3/2}\frac{2}{3}\left[\frac{2}{\pi b_0}\right]^{1/2}\kappa^{1/2}\log(\kappa^{1/2}R)$$

$$+\cdots . \quad (4.13)$$

This formula shows that the large R bound on the linear potential derived by Adler (1981a) is saturated. The numerical results for V_{static} in the range $R\sim 10-100$ yield coefficients of the R and $\log(\kappa^{1/2}R)$ terms which agree with the analytic results of Eq. (4.13) to better than 1%. According to Eq. (4.12), at large R the limiting behavior of the free boundary is an ellipsoid of revolution

$$1=\frac{z^2}{a^2}+\tfrac{1}{2}\left[\frac{\pi b_0}{2Q}\right]^{1/2}\left[\frac{\rho\kappa^{1/2}}{a^{1/2}}\right]^2 , \quad (4.14)$$

with the major axis along the axis of rotation growing as R, and with the minor axis growing as $R^{1/2}$. A study of the structure of the free boundary using the numerical solutions for $R\sim 50-10^3$ shows that the outer contours of Φ have a shape agreeing well with this formula. Hence in both limiting cases in which analytic approximations are available, they are in excellent agreement with the results of the numerical solution for Φ.

D. Axially symmetric monopoles

In solving numerically for the axially symmetric monopoles, we use the leading terms of the asymptotic formulas of Eq. (2.99) as Dirichlet boundary conditions on the outer boundary, without including the $l=2$ or higher terms in the expansion. Consequently, the potentials obtained computationally will contain errors of order $1/\rho_{\max}^3, 1/z_{\max}^3$, which can be made small by choosing $\rho_{\max}$ and $z_{\max}$ large enough. An important check on convergence is to verify that the bound

$$H=4\pi\kappa\,|\,n\,| \quad (4.15)$$

is attained. Since the leading terms which are retained in Eq. (2.99) make a contribution to the energy density given by

$$\mathscr{H}_{\text{asymptotic}}=\frac{n^2}{(\rho^2+z^2)^2} , \quad (4.16)$$

we must include an analytic correction for the energy lying outside the boundary of the computational mesh when we test Eq. (4.15). Following the notation of Eq. (3.70), we do this by writing

$$H=H_{\text{inside}}+H_{\text{outside}} , \quad (4.17a)$$

with

$$H_{\text{inside}}=4\pi\int_0^{\rho_{\max}}\rho d\rho\int_0^{z_{\max}}dz\,\mathscr{H} \quad (4.17b)$$

determined computationally, and with a simple integration giving

[37]The solution $\Phi^{(0)}$ positions the charges on the free boundary, reflecting the fact that the distance between the charges and the free boundary (z_A-a in Fig. 6) vanishes relative to R as $R\to\infty$. The derivation of the logarithmic coefficient in Eq. (4.13) assumes the stronger statement that $(z_A-a)/R$ vanishes faster than $R^{-1}\log R$ as $R\to\infty$. The agreement of Eq. (4.13) with the numerical results gives *a posteriori* evidence for the validity of this assumption; for an analytic investigation of this issue see Lehmann and Wu (1983).

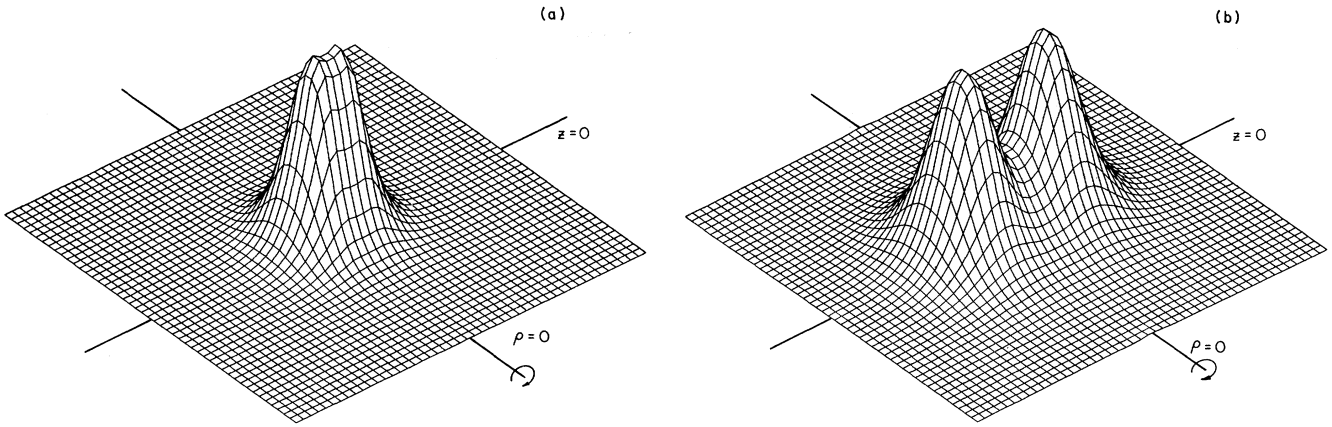

FIG. 15. Sample results for the axially symmetric Bogomol'nyi-Prasad-Sommerfield monopole problem. The graphs show the field energy density $\mathscr{H}$ (a) for $n=1$ and (b) for $n=2$, plotted vertically over a horizontal plane through the rotation axis. The two cases can be characterized, respectively, as a fuzzy "ball" and a fuzzy "doughnut" of energy.

$$H_{\text{outside}} = \int_{\text{outside}} \mathscr{H} \approx \int_{\text{outside}} \mathscr{H}_{\text{asymptotic}} = n^2 \left[\frac{2\pi}{z_{\max}} + \frac{2\pi}{\rho_{\max}} \sin^{-1} \left[\frac{z_{\max}}{(\rho_{\max}^2 + z_{\max}^2)^{1/2}} \right] \right] . \tag{4.17c}$$

As illustrations of the solution of the monopole equations, we have solved the $n=1,2$ cases on a mesh with $\rho_{\max}=z_{\max}=10$, in units in which $\kappa=1$ (and with the gauge function ψ of Appendix B taken as 0).[38] For the total energy H calculated from Eq. (4.17), we get (on the relatively coarse mesh plotted in Fig. 15)

$$\begin{aligned} n&=1, \quad H=12.88 , \\ n&=2, \quad H=25.22 , \end{aligned} \tag{4.18}$$

in good agreement with the values of 12.57, 25.13 expected from Eq. (4.15). In Fig. 15 we give plots of the energy density $\mathscr{H}$ for the solutions. The $n=1$ solution shows, in the large, the expected spherical symmetry, while the $n=2$ solution has the form of a fuzzy "doughnut," in agreement with a variational calculation of Rebbi and Rossi (1980) and with the recently found analytic solution for this case.[39] However, we also observe that the $n=1$ numerical solution has a dip in $\mathscr{H}$ along the rotation axis, whereas in the exact $n=1$ monopole solution given in Eq. (2.96) above, $\mathscr{H}$ decreases monotonically away from the axis. This dip is a remnant of the second-order errors in the discretization procedure which, in the present instance, weight too heavily the lattice cells along the axis, and thus lead to a reduction in the $\mathscr{H}$ value of the converged discrete solution at the axis. When the lattice spacing is made finer, the dip becomes smaller, but the correct monotinicity properties of $\mathscr{H}$ at $\rho=0$ appear only in the limit of zero mesh spacing.

ACKNOWLEDGMENTS

We wish to thank many colleagues in Princeton and elsewhere for their helpful questions and comments, and to thank Valerie Nowak for her beautiful work in computer composition of the manuscript. This work was supported by the U.S. Department of Energy under Grant No. DE-ACO2-76ERO2220 and the National Science Foundation under Grant No. PHY-82-17352. Tsvi Piran acknowledges a grant from the Revson foundation.

APPENDIX A: MATHEMATICAL FEATURES OF THE LEADING LOGARITHM MODEL

We discuss in this appendix a number of mathematical features of the leading logarithm model. We begin by analyzing the structure of the real characteristic (the free boundary) of the differential equation

[38] As a check on the computer code, we have verified that the energy H of the numerical solution is unchanged when a choice $\psi \neq 0$ is used.

[39] For a discussion of the axially symmetric solutions realizable within the six-function ansatz, see, for example, Prasad and Rossi (1981).

$$\nabla\cdot[\sigma(\rho,|\nabla\Phi|)\nabla\Phi]=0\ , \tag{A1}$$

with σ defined in Eqs. (2.59) and (2.60) of the text. Using the chain rule and dividing by σ, we see that Eq. (A1) becomes

$$\nabla^2\Phi+\frac{\partial\log\sigma}{\partial\log|\nabla\Phi|}\nabla(\log|\nabla\Phi|)\cdot\nabla\Phi+\frac{\partial\log\sigma}{\partial\rho}\partial_\rho\Phi=0\ . \tag{A2}$$

This can be further rewritten by substituting

$$\begin{aligned}\nabla^2&=\partial_\rho^2+\partial_z^2+\rho^{-1}\partial_\rho\ ,\\ \nabla(\log|\nabla\Phi|)\cdot\nabla\Phi&=\frac{\partial_i\Phi\partial_j\Phi}{|\nabla\Phi|^2}(\partial_i\partial_j\Phi)\\ &=\hat n_i\hat n_j\partial_i\partial_j\Phi\\ &=\hat n_i\partial_i\hat n_j\partial_j\Phi-|\nabla\Phi|\hat n_i\hat n_j\partial_i\hat n_j\\ &=\partial_n^2\Phi\ ,\end{aligned} \tag{A3}$$

with $\hat n$ the unit normal defined by

$$\hat n=\frac{\nabla\Phi}{|\nabla\Phi|},\quad \hat n\cdot\hat n=1\ , \tag{A4}$$

thus giving

$$\left[(\partial_\rho^2+\partial_z^2-\partial_n^2)+\left[1+\frac{\partial\log\sigma}{\partial\log|\nabla\Phi|}\right]\partial_n^2\right]\Phi+\left[1+\frac{\partial\log\sigma}{\partial\log\rho}\right]\rho^{-1}\partial_\rho\Phi=0\ . \tag{A5}$$

Now from Eq. (2.59) we have

$$\begin{aligned}\log\sigma&=\log(2\pi\kappa)-\log\rho-\log|\nabla\Phi|+\log f(w)\ ,\\ w&=\frac{|\nabla\Phi|}{\pi b_0\kappa\rho}=\frac{\partial_n\Phi}{\pi b_0\kappa\rho}\ ,\end{aligned} \tag{A6}$$

and so the derivatives of σ appearing in Eq. (A5) can be expressed in terms of $f(w)$,

$$\begin{aligned}1+\frac{\partial\log\sigma}{\partial\log|\nabla\Phi|}&=\frac{\partial\log f}{\partial\log|\nabla\Phi|}=\frac{wf'(w)}{f(w)}\ ,\\ 1+\frac{\partial\log\sigma}{\partial\log\rho}&=\frac{\partial\log f}{\partial\log\rho}=-\frac{wf'(w)}{f(w)}\ ,\end{aligned} \tag{A7}$$

yielding Eqs. (2.72) and (2.73) of the text,

$$\begin{aligned}&[(\partial_\rho^2+\partial_z^2-\partial_n^2)+\alpha\partial_n^2]\Phi-\alpha\rho^{-1}\partial_\rho\Phi=0\ ,\\ &\alpha=\frac{wf'(w)}{f(w)}=\frac{w}{w+f(w)}\ .\end{aligned} \tag{A8}$$

In the vicinity of a general, off-axis point B with coordinates x_B on the free boundary, we have

$$-\alpha\rho^{-1}\partial_\rho\Phi\approx-w\rho^{-1}\partial_\rho\Phi\sim|\nabla\Phi|^2\ , \tag{A9}$$

so to first order in $|\nabla\Phi|$, Eq. (A8) can be approximated by

$$\left[\partial_l^2+\frac{\partial_n\Phi}{\pi b_0\kappa\rho_B}\partial_n^2\right]\Phi=0\ , \tag{A10}$$

with l and n, respectively, tangential and normal Cartesian coordinates at the free boundary, as shown in Fig. 7. When the radius of curvature of the free boundary (and of the nearby level surfaces of Φ) is R_B, then to the needed accuracy the behavior of Φ near the free boundary has the form

$$\Phi=F\left[n-\tfrac{1}{2}\frac{l^2}{R_B}\right],\quad F(0)=0\ . \tag{A11}$$

Substituting Eq. (A11) into Eq. (A10) determines the function $F(z)$ to be

$$F(z)=\tfrac{1}{2}\frac{\pi b_0\kappa\rho_B}{R_B}z^2\ , \tag{A12}$$

giving Eq. (2.75) of the text.

Let us consider next the point $\rho=0,z=z_A$, where the free boundary intersects the axis of rotation. From Eq. (2.62) we know that $A^0=+\infty$ at the source charge Q, and A^0 is arbitrarily large within a sufficiently small neighborhood of the point $\rho=0,z=a$. On the other hand, since A^0 can be determined along the free boundary by integrating $\partial_l A^0=\kappa$ out from the plane $z=0$, where A^0 vanishes, we have

$$A^0(\rho=0,z=z_A)=\kappa L\ , \tag{A13}$$

with L the (finite) length of the segment of the free boundary lying within the quadrant drawn in Fig. 6. Hence A^0 is finite at $\rho=0,z=z_A$, and so we must have $z_A>a$, with the possibility $z_A=a$ excluded.

Let us suppose now that we have solved Eq. (2.56) or (A8), and hence know $\varepsilon=(\rho^2\sigma)^{-1}$ as a function of x. As mentioned in the text, one way (not the simplest way!) to determine A^0 is to solve the linear differential equation

$$\nabla\cdot(\varepsilon\nabla A^0)=-j^0 \tag{A14}$$

within the free boundary. Since Eq. (A14) is the Euler-Lagrange equation corresponding to minimization (for fixed $\varepsilon\geq0$) of the functional

$$\int d^3x[\tfrac{1}{2}\varepsilon(\nabla A^0)^2-j^0A^0]\ , \tag{A15}$$

solutions will exist. To see that the solution is unique, even without the imposition of a boundary condition on the free boundary, let us suppose that Eq. (A14) has two C^1 solutions A_1^0 and A_2^0, so that $\delta A^0=A_1^0-A_2^0$ satisfies

$$\nabla\cdot(\varepsilon\nabla\delta A^0)=0\ . \tag{A16}$$

Multiplying by δA^0 and integrating over the interior of

the free boundary, we have

$$0=\int d^3x\,\delta A^0\nabla\cdot(\varepsilon\nabla\delta A^0)$$
$$=\int d^3x\,\nabla\cdot(\delta A^0\varepsilon\nabla\delta A^0)-\int d^3x\,\varepsilon(\nabla\delta A^0)^2$$
$$=\int_{\text{free boundary}} d\mathbf{S}\cdot(\delta A^0\varepsilon\nabla\delta A^0)-\int d^3x\,\varepsilon(\nabla\delta A^0)^2 . \tag{A17}$$

The first term in the final line of Eq. (A17) vanishes, because ε vanishes on the free boundary, and so Eq. (A17) implies that $\nabla\delta A^0=0$ in the interior. This, together with the requirement that δA^0 be an odd function of z, implies the vanishing of δA^0 within the free boundary.

The seemingly paradoxical fact that Eq. (A5) requires a Dirichlet condition $\Phi=0$ on the free boundary, while Eq. (A14) requires no boundary condition for A^0 on the free boundary, has an interpretation in terms of the general boundary-value problem for second-order equations with non-negative characteristic form, given by Fichera (1956). The generalized Dirichlet problem takes the form[17]

$$L(u)=a^{kj}(x)\partial_k\partial_j u+b^k(x)\partial_k u+c(x)u=f(x)\text{ in }\Omega ,$$
$$u=g\text{ on }\Sigma_2\cup\Sigma_3 , \tag{A18}$$

with f and g functions defined on Ω and on $\Sigma_2\cup\Sigma_3$, respectively. The sets Σ_2 and Σ_3 are subsets of the boundary Σ of the domain Ω, specified as follows. Let n_k be the inward directed normal to the boundary. The set Σ_3 is defined to be the noncharacteristic part of the boundary, where $a^{kj}n_kn_j>0$. The characteristic part of the boundary, where $a^{kj}n_kn_j=0$, is divided into sets $\Sigma_0,\Sigma_1,\Sigma_2$, defined by

$$b=0\text{ on }\Sigma_0 ,$$
$$b>0\text{ on }\Sigma_1 ,$$
$$b<0\text{ on }\Sigma_2 , \tag{A19}$$
$$b=n_k(b^k-\partial_j a^{kj}) .$$

According to Eq. (A18), a Dirichlet boundary condition is required on Σ_2 and Σ_3, while no boundary condition is needed on the subsets Σ_0 and Σ_1 of the boundary.

Let us now analyze Eqs. (A8) and (A14) using this formalism. In discussing Eq. (A8) it suffices to use the approximate form of Eq. (A10), with l and n fixed Cartesian axes as in Fig. 7, giving

$$a^{ll}=1,\quad a^{ln}=0,\quad a^{nn}=\frac{\partial_n\Phi}{\pi b_0\kappa\rho_B},\quad b^l=b^n=c=0 , \tag{A20}$$

so that

$$b=-\frac{\partial}{\partial n}a^{nn}=-\frac{1}{\pi b_0\kappa\rho_B}\partial_n^2\Phi=-\frac{1}{R_B}<0 . \tag{A21}$$

Thus for Eq. (A8) the free boundary is in Σ_2, and the imposition of a Dirichlet condition $\Phi=0$ on the free boundary is required. [Note that this condition, together with the discontinuity of Φ at the source charges given by Eq. (2.50), then implies that $\Phi=Q$ on the interior line segment $\rho=0$, $|z|<a$.] In Eq. (A14), we have

$$a^{ij}=\varepsilon\delta^{ij},\quad b^k=\partial_k\varepsilon,\quad c=0$$
$$\Rightarrow b^k-\partial_j a^{kj}=0 , \tag{A22}$$

so that the free boundary is in Σ_0. Hence no boundary condition for A^0 on the free boundary is needed when ε has been determined as a function of x by first solving the equation for Φ.

Suppose, on the other hand, that we attempt to solve the full nonlinear problem for A^0 given by Eqs. (2.41) and (2.46) directly, with ε not known *a priori*. These equations, when recast in the standard quasilinear form of Eq. (2.70), yield

$$\varepsilon_{ij}\partial_i\partial_j A^0=-j^0 , \tag{A23a}$$

with ε_{ij} the field-strength dependent dielectric tensor

$$\varepsilon_{ij}=\delta_{ij}\tfrac{1}{4}b_0\log[(\nabla A^0)^2/\kappa^2]+\tfrac{1}{2}b_0\hat{l}_i\hat{l}_j . \tag{A23b}$$

The unit vector $\hat{l}_i$ is defined by

$$\hat{l}_i=\frac{\partial_i A^0}{|\nabla A^0|} , \tag{A24a}$$

and since

$$\hat{l}\cdot\nabla\Phi\propto\mathbf{D}\cdot\nabla\Phi\propto(\hat{\phi}\times\nabla\Phi)\cdot\nabla\Phi=0 , \tag{A24b}$$

$\hat{l}$ is orthogonal to the unit vector $\hat{n}$ of Eq. (A4). Comparing Eq. (A23) with Eq. (A18), we see that

$$a^{ij}=\varepsilon_{ij},\quad b^i=c=0 , \tag{A25}$$

and so Eq. (A23) is elliptic in the interior region and degenerates on the characteristic, with

$$b=-\partial_n[\tfrac{1}{4}b_0\log(E^2/\kappa^2)]-\tfrac{1}{2}b_0\hat{n}_i\partial_j(\hat{l}_i\hat{l}_j)$$
$$=-\tfrac{1}{2}b_0(E^{-1}\partial_n E+\hat{n}_i\partial_l\hat{l}_i) . \tag{A26}$$

At a point B on the free boundary where the radius of curvature is R_B, we see from Fig. 7 that

$$\hat{n}_i\partial_l\hat{l}_i=\frac{1}{R_B} , \tag{A27a}$$

while from Eqs. (2.61), (2.75), and (A6) we get the leading behavior of E in the vicinity of the free boundary,

$$E\approx\kappa(1+w)=\kappa\left[1+\frac{\partial_n\Phi}{\pi b_0\kappa\rho_B}\right]\approx\kappa\left[1+\frac{n}{R_B}\right]$$
$$\Rightarrow E^{-1}\partial_n E=\frac{1}{R_B} , \tag{A27b}$$

giving

$$b=-\frac{b_0}{R_B}<0 . \tag{A28}$$

Hence according to the Fichera criterion of Eq. (A19), a Dirichlet boundary condition for A^0 is required at all points x_B on the free boundary. This boundary condition is implicitly available in the form

$$A^0(x_B)=\int_{z=0\text{ plane}}^{x_B} dl\,\partial_l A^0=\int_{z=0\text{ plane}}^{x_B} dl\,\kappa\ , \qquad \text{(A29)}$$

with $\int dl$ a line integral along the characteristic, but since $A^0(x_B)$ thus becomes a function of the geometry of the free boundary (which is not known *a priori*), this condition is difficult to implement in a numerical calculation. An important advantage of the flux function reformulation is that it replaces Eq. (A29) by the explicit Dirichlet boundary condition $\Phi(x_B)=0$.

APPENDIX B: STRUCTURE AND PROPERTIES OF THE SIX-FUNCTION ANSATZ

Substituting the six-function ansatz of Eq. (2.97) into the field-potential relations of Eq. (2.80), we get the following expressions for the various field-strength components (with $\partial_z=\partial/\partial z, \partial_\rho=\partial/\partial\rho$):

$$\begin{aligned}
&(\mathscr{D}_j\varphi^a)\hat{z}^a\hat{z}^j=\partial_z h_1+a_1 h_2,\quad B^{aj}\hat{z}^a\hat{z}^j=\rho^{-1}(\partial_\rho f_1+a_2 f_2)\ ,\\
&(\mathscr{D}_j\varphi^a)\hat{\rho}_n^a\hat{z}^j=\partial_z h_2-a_1 h_1,\quad B^{aj}\hat{\rho}_n^a\hat{z}^j=\rho^{-1}(\partial_\rho f_2-a_2 f_1)\ ,\\
&(\mathscr{D}_j\varphi^a)\hat{z}^a\hat{\rho}^j=\partial_\rho h_1+a_2 h_2,\quad B^{aj}\hat{z}^a\hat{\rho}^j=-\rho^{-1}(\partial_z f_1+a_1 f_2)\ ,\\
&(\mathscr{D}_j\varphi^a)\hat{\rho}_n^a\hat{\rho}^j=\partial_\rho h_2-a_2 h_1,\quad B^{aj}\hat{\rho}_n^a\hat{\rho}^j=-\rho^{-1}(\partial_z f_2-a_1 f_1)\ ,\\
&(\mathscr{D}_j\varphi^a)\hat{\phi}_n^a\hat{\phi}^j=\rho^{-1}(h_2 f_1-h_1 f_2),\quad B^{aj}\hat{\phi}_n^a\hat{\phi}^j=\partial_\rho a_1-\partial_z a_2\ .
\end{aligned} \qquad \text{(B1)}$$

Substituting these expressions into Eq. (2.86) gives a formula for the Hamiltonian H directly in terms of $h_{1,2},\ldots,$

$$\begin{aligned}
H&=4\pi\int_0^\infty \rho d\rho\int_0^\infty dz\,\mathscr{H}\ ,\\
\mathscr{H}&=\tfrac{1}{2}[(\partial_z h_1+a_1 h_2)^2+(\partial_z h_2-a_1 h_1)^2+(\partial_\rho h_1+a_2 h_2)^2+(\partial_\rho h_2-a_2 h_1)^2]\\
&\quad+\frac{1}{2\rho^2}[(\partial_z f_1+a_1 f_2)^2+(\partial_z f_2-a_1 f_1)^2+(\partial_\rho f_1+a_2 f_2)^2+(\partial_\rho f_2-a_2 f_1)^2]\\
&\quad+\tfrac{1}{2}(\partial_z a_2-\partial_\rho a_1)^2+\frac{1}{2\rho^2}(h_1 f_2-h_2 f_1)^2\ .
\end{aligned} \qquad \text{(B2)}$$

Equations (B1) and (B2) and the boundary conditions at $\rho=0$, $z=0$, and $r=\infty$ given in Eqs. (2.98) and (2.99) have a residual Abelian gauge invariance of the form

$$\begin{aligned}
&h_1\to h_1\cos\delta-h_2\sin\delta\ ,\\
&h_2\to h_2\cos\delta+h_1\sin\delta\ ,\\
&f_1\to f_1\cos\delta-f_2\sin\delta\ ,\\
&f_2\to f_2\cos\delta+f_1\sin\delta\ ,\\
&a_1\to a_1+\partial_z\delta\ ,\\
&a_2\to a_2+\partial_\rho\delta\ ,
\end{aligned} \qquad \text{(B3)}$$

with δ a function of ρ,z satisfying

$$\delta=0 \text{ at } z=0,\ \rho=0,\ r\to\infty\ . \qquad \text{(B4)}$$

Hence in order for H to have a unique minimum, it is necessary to add to it a gauge-fixing term

$$H_{\rm gf}=4\pi\int_0^\infty \rho d\rho\int_0^\infty dz\,\mathscr{H}_{\rm gf}\ . \qquad \text{(B5)}$$

In the numerical work of Sec. IV.D, we shall use the following choice of gauge-fixing:

$$\mathscr{H}_{\rm gf}=\tfrac{1}{2}(\partial_z a_1+\partial_\rho a_2-\psi)^2\ , \qquad \text{(B6)}$$

with ψ an arbitrary function which vanishes at the boundaries. Minimization of $H+H_{\rm gf}$ then picks out the member of the gauge-equivalence class of minima of H which satisfies

$$\partial_z a_1+\partial_\rho a_2-\psi=0\ . \qquad \text{(B7)}$$

Since the differential equation for δ,

$$(\partial_z^2+\partial_\rho^2)\delta=\psi-(\partial_z a_1+\partial_\rho a_2),\quad 0<z<\infty,\quad 0<\rho<\infty\ , \qquad \text{(B8)}$$

with the boundary conditions of Eq. (B4), gives a well-posed Dirichlet problem, the gauge condition of Eq. (B7) is always attainable and completely breaks the gauge degeneracy.

Adding Eq. (B6) to the kinetic term for $a_{1,2}$ in $\mathscr{H}$ gives

$$\begin{aligned}
&\tfrac{1}{2}(\partial_z a_2-\partial_\rho a_1)^2+\tfrac{1}{2}(\partial_z a_1+\partial_\rho a_2-\psi)^2\\
&\quad=\tfrac{1}{2}[(\partial_z a_1)^2+(\partial_\rho a_1)^2+(\partial_z a_2)^2+(\partial_\rho a_2)^2+\psi^2]\\
&\qquad-\psi(\partial_z a_1+\partial_\rho a_2)+\partial_z a_1\partial_\rho a_2-\partial_z a_2\partial_\rho a_1\ .
\end{aligned} \qquad \text{(B9)}$$

Although the final term in Eq. (B9) is a total derivative, it does not vanish when integrated over a finite domain $0\le z\le z_{\max}, 0\le\rho\le\rho_{\max}$, and so should not be dropped in the numerical work.

As discussed in the text, the minima of H in the sector with topological quantum number n are self-dual or anti-self-dual gauge fields. In the self-dual case, where $-\mathscr{D}_j\varphi^a=B^{aj}$, the use of Eq. (B1) gives the differential equations

$$
\begin{aligned}
&\partial_z h_1 + a_1 h_2 = -\rho^{-1}(\partial_\rho f_1 + a_2 f_2)\ , \\
&\partial_z h_2 - a_1 h_1 = -\rho^{-1}(\partial_\rho f_2 - a_2 f_1)\ , \\
&\partial_\rho h_1 + a_2 h_2 = \rho^{-1}(\partial_z f_1 + a_1 f_2)\ , \\
&\partial_\rho h_2 - a_2 h_1 = \rho^{-1}(\partial_z f_2 - a_1 f_1)\ , \\
&\rho^{-1}(h_2 f_1 - h_1 f_2) = -(\partial_\rho a_1 - \partial_z a_2)\ .
\end{aligned}
\tag{B10}
$$

At large r, substituting a spherical harmonic expansion into Eq. (B10) gives Eq. (2.99) as the form of the power-law terms in the potentials. A similar analysis for small r shows that the leading behavior at $r=0$ [omitting terms $O(r^{2n+1})$ in $h_1, f_1/\rho$ and $O(r^{n+1})$ in $h_2, a_{1,2}, f_2/\rho$] is given by

$$
\begin{aligned}
&h_1 = \sum_{\substack{l=1 \\ l\ \text{odd}}}^{2n-1} r^l C_l P_l(\cos\vartheta)\ , \\
&-a_1 = h_2 = b\rho^n\ ,
\end{aligned}
\tag{B11}
$$

$$
a_2 = f_2 = 0\ ,
$$

$$
f_1 = n + \sum_{\substack{l=1 \\ l\ \text{odd}}}^{2n-1} \frac{lC_l}{2l+1} r^{l+1}[P_{l+1}(\cos\vartheta) - P_{l-1}(\cos\vartheta)]\ .
$$

APPENDIX C: COULOMB-SUBTRACTED FUNCTIONAL FOR THE ABELIAN HIGGS MODEL

We give here the results of removing Coulomb self-energies from the Lagrangian functional $L[A^0,\varphi]$ of Eq. (2.14) by the analytic-rearrangement method of Sec. III.E. Defining

$$
\begin{aligned}
&A_C^0 = \frac{Q}{4\pi}\left[\frac{1}{r_{(1)}} - \frac{1}{r_{(2)}}\right],\quad r_{\left[\begin{smallmatrix}1\\2\end{smallmatrix}\right]} = [\rho^2 + (z \mp a)^2]^{1/2}\ , \\
&A^0 = B^0 + A_C^0\ ,
\end{aligned}
\tag{C1}
$$

and dropping an infinite constant which is independent of $R=2a$, we get

$$
\begin{aligned}
L_{\text{subtracted}}[B^0,\varphi] = {}& \tfrac{1}{2}\frac{Q^2}{4\pi} I(\rho_{\max}, z_{\max}) \\
&+ 4\pi \int_0^{\rho_{\max}} \rho d\rho \int_0^{z_{\max}} dz \{ \tfrac{1}{2}[(\partial_\rho B^0)^2 + (\partial_z B^0)^2] + e^2 (B^0 + A_C^0)^2 \varphi^2 - (\partial_\rho \varphi)^2 \\
&- (\partial_z \varphi)^2 - \tfrac{1}{2} C(\varphi^2 - \kappa^2)^2 + \psi \}\ ,
\end{aligned}
\tag{C2}
$$

$$
\psi = \frac{Q^2}{(4\pi)^2} \frac{\rho^2 + z^2 - a^2}{(r_1 r_2)^3}\ ,
$$

with $I(\rho_{\max}, z_{\max})$ given by Eq. (3.71b) of the text.

REFERENCES

Abbott, L.F., 1981, Nucl. Phys. B **185**, 189.
Abers, E.S., and B.W. Lee, 1973, Phys. Rep. **9**, 1.
Actor, A., 1979, Rev. Mod. Phys. **51**, 461.
Adler, S.L., 1978a, Phys. Rev. D **18**, 411.
Adler, S.L., 1978b, Phys. Rev. D **17**, 3212.
Adler, S.L., 1979, Phys. Rev. D **20**, 3273.
Adler, S.L., 1980, "Nonlocal gauge theories," in *The High Energy Limit* (the 1980 Erice Lectures), edited by A. Zichichi (Plenum, New York), p. 29.
Adler, S.L., 1981a, Phys. Rev. D **23**, 2905.
Adler, S.L., 1981b, "The mechanism for confinement in massive quark QCD," in *The Fifth Johns Hopkins Workshop on Current Problems in High Energy Theory,* edited by G. Domokos and S. Kövesi-Domokos (Johns Hopkins University, Baltimore), p. 43.
Adler, S.L., 1982, Phys. Lett. B **110**, 302.
Adler, S.L., 1983, Nucl. Phys. B **217**, 381.
Adler, S.L., and R.B. Pearson, 1978, Phys. Rev. D **18**, 2798.
Adler, S.L., and T. Piran, 1980, in *High Energy Physics—1980,* edited by L. Durand and L.G. Pondrum (AIP Conference Proceedings No. 68, Particles and Fields Subseries No. 22), V2, p. 958.
Adler, S.L., and T. Piran, 1982a, Phys. Lett. B **113**, 405.
Adler, S.L., and T. Piran, 1982b, Phys. Lett. B **117**, 91.
Ames, W.F., 1977, *Numerical Methods for Partial Differential Equations* (Academic, New York).
Anishetty, R., 1982, Phys. Lett. B **108**, 295.
Batalin, I.A., S.G. Matinyan, and G.K. Savvidy, 1977, Yad. Fiz. **26**, 407 [Sov. J. Nucl. Phys. **26**, 214 (1977)].
Bauer, F., O. Betancourt, and P. Garabedian, 1978, *A Computational Method in Plasma Physics* (Springer, New York).
Bender, I., D. Gromes, and H.J. Rothe, 1980, Z. Phys. C **5**, 151.
Bernstein, J., 1974, Rev. Mod. Phys. **46**, 7.
Bogomol'nyi, E.B., 1976, Yad. Fiz. **24**, 861 [Sov. J. Nucl. Phys. **24**, 449 (1976)].
Boulware, D.G., 1981, Phys. Rev. D **23**, 389.
Brandt, A., 1977, Math. Comput. **31**, 333.
Cabo, A., and A.E. Shabad, 1980, "Quantum theory of gauge field with external source," Academia de Ciencas de Cuba pub. No. 167.
Callan, C.G., Jr., R.F. Dashen, and D.J. Gross, 1979, Phys. Rev. D **19**, 1826.
Cantor, M., 1983, SIAM J. Num. Anal. **20**, 72.
Chodos, A., R.L. Jaffe, K. Johnson, C.B. Thorne, and V.F. Weisskopf, 1974, Phys. Rev. D **9**, 3471.
Coleman, S., S. Parke, A. Neveu, and C.M. Sommerfield, 1977, Phys. Rev. D **15**, 544.

Creutz, M., 1978, Rev. Mod. Phys. **50**, 561.
Cvitanović, P., R.J. Gonsalves, and D.E. Neville, 1978, Phys. Rev. D **18**, 3881.
DeWitt, B.S., 1981, "A gauge invariant effective action," in *Quantum Gravity II,* edited by C.J. Isham, R. Penrose, and D.W. Sciama (Oxford University, Oxford).
Fichera, G., 1956, Atti Accad. Naz. Lincei, Mem. Cl. Sci. Fis. Mat. Nat. Sez. 1 (8) **5**, 1.
Friedberg, R., and T.D. Lee, 1978, Phys. Rev. D **18**, 2623.
Garabedian, P., 1956, Math. Tables Aids Comput. **10**, 183.
Gidas, B., and L. Caffarelli, 1983, in preparation.
Giles, R., and L. McLerran, 1978, Phys. Lett. B **79**, 447.
Hasenfratz, P., and J. Kuti, 1978, Phys. Rep. **40**, 76.
Hilf, E.R., and L. Polley, 1981, "Stability and Screening Solutions in a Semi-Classical Yang Mills Theory Proposed by Pagels and Tomboulis," TH Darmstadt report IKDA 81/8.
Hockney, R.W., and J.W. Eastwood, 1981, *Computer Simulation Using Particles* (McGraw-Hill, New York).
't Hooft, G., 1974, Nucl. Phys. B **79**, 276.
't Hooft, G., 1975a, in *Functional and Probabilistic Methods in Quantum Field Theory,* edited by Bernard Jancewicz, Acta Universitatis Wratislavensis No. 368, XIIth Winter School of Theoretical Physics in Karpacz, February 17—March 2, 1975, Vol. I, p. 345.
't Hooft, G., 1975b, in *Recent Progress in Lagrangian Field Theory and Applications,* proceedings of the Marseille Colloquium, 1974, edited by C.P. Korthes-Altes *et al.* (Centre de Physique, Marseille).
Houston, P., and L. O'Raifeartaigh, 1981, Z. Phys. C **6**, 1.
Jackiw, R., and P. Rossi, 1980, Phys. Rev. D **21**, 426.
Jaffe, A., and C. Taubes, 1980, *Vortices and Monopoles,* Progress in Physics, Vol. 2 (Birkhäuser, Boston).
Johnson, K., 1978, Phys. Lett. B **78**, 259.
Khriplovich, I.B., 1978, Zh. Eksp. Teor. Fiz. **74**, 37 [Sov. Phys.—JETP **47**, 18 (1978)].
Kiskis, J., 1980a, Phys. Rev. D **21**, 421.
Kiskis, J., 1980b, Phys. Rev. D **21**, 1074.
Kogut, J., and L. Susskind, 1974, Phys. Rev. D **9**, 3501.
Lee, S.-C., 1979, Phys. Rev. D **20**, 1951.
Lee, S.-C., 1980, Phys. Rev. D **21**, 466.
Lehmann, H., and T. T. Wu, 1983, "Classical Models of Confinement," Universität Hamburg and DESY preprint.
Lieb, E., 1983, in preparation.
Mandula, J., 1976, Phys. Rev. D **14**, 3447.
Matinyan, S.G., and G.K. Savvidy, 1978, Nucl. Phys. B **134**, 539.
McCracken, D.D., 1972, *A Guide to Fortran IV Programming* (Wiley, New York).
Mills, R. 1979, Phys. Rev. Lett. **43**, 549.
Milton, K.A., W.F. Palmer, and S.S. Pinsky, 1982, Phys. Rev. D **25**, 1718.
Milton, K.A., W. Wilcox, W.F. Palmer, and S.S. Pinsky, 1982, Phys. Rev. D **27**, 1348.
Morse, P.M., and H. Feshbach, 1953, *Methods of Theoretical Physics* (McGraw-Hill, New York).
Nambu, Y., 1981, Phys. Lett. B **102**, 149.
Nielsen, H.B., 1981, in *Particle Physics 1980* (Proceedings of the 3rd Adriatic Summer Meeting on Particle Physics, Dubrovnik, Yugoslavia), edited by I. Andrić, I. Dadić and N. Zovko (North-Holland, Amsterdam), p. 67.
Oleĭnik, O.A., and E.V. Radkevič, 1973, *Second Order Equations with Nonnegative Characteristic Form* (American Mathematical Society, Providence-Plenum, New York).
O'Raifeartaigh, L., and S. Rouhani, 1981, "Recent Developments in Finite Energy (Topological) Monopole Theory" (lectures at the 1981 Winter School, Schladming, Austria) Acta Physica Austriaca Supplementum XXIII; also in *New Developments in Mathematical Physics,* edited by H. Mitter and L. Piltner (Springer, New York).
Pagels, H., and E. Tomboulis, 1978, Nucl. Phys. B **143**, 485.
Polyakov, A.M., 1974, Zh. Eksp. Teor. Fiz. Pis'ma Red. **20**, 430 [JETP Lett. **20**, 194 (1974)].
Prasad, M.K., and P. Rossi, 1981, Phys. Rev. D **24**, 2182.
Prasad, M.K., and C.M. Sommerfield, 1975, Phys. Rev. Lett. **35**, 760.
Press, W., 1978, "Hierarchical Modification of Successive Over-Relaxation for 'Fast' Convergence of Elliptic Systems with General Boundaries," Harvard-Smithsonian Center for Astrophysics preprint No. 971.
Rebbi, C., and P. Rossi, 1980, Phys. Rev. D **22**, 2010.
Rittenberg, V., and D. Wyler, 1978, Phys. Rev. D **18**, 4806.
Roache, P.J., 1976, *Computational Fluid Dynamics* (Hermosa, Albuquerque).
Savvidy, G.K., 1977, Phys. Lett. B **71**, 133.
Schanbacher, V., 1982, Phys. Rev. D **26**, 489.
Sikivie, P., and N. Weiss, 1978, Phys. Rev. D **18**, 3809.
Sikivie, P., and N. Weiss, 1979, Phys. Rev. D **20**, 487.
York, J.W., Jr., and T. Piran, 1982, in *Spacetime and Geometry,* edited by L.C. Shepley and R. Matzner (University of Texas, Austin), p. 147.